



Megacity Istanbul Project Reports

Municipality Disaster Management Center (AKOM), Istanbul, Turkey

22 October, 2008



Universität Karlsruhe (TH)
Forschungsuniversität • gegründet 1825

Contents

Introduction	IV
M. Erdik, and J. Zschau	
1. Disaster Prevention Mitigation Studies for a Safer Urban Life. Measures for Preventing Disaster of Istanbul Metropolitan Municipality	1
M. Bas, and M. O. Yagci	
2. Megacity Indicators System for Disaster Risk Management - Implementation in Istanbul	8
B. Khazai, O. Kilic, A. Basmaci, B. Konukcu, B. Sungay, A. Zeidan, and F. Wenzel	
3. Preparation for an Expected Disaster - The Contribution of Remote Sensing and Civil Engineering to Support Risk Management at Mega City Istanbul, Turkey	14
H. Taubenböck, C. Münich, A. Roth, L. Stempniewski, H. Mehl, and S. Dech	
4. Stress Field Modelling in the Marmara Sea Region	20
O. Heidbach, F. Wenzel, and T. Hergert	
5. Crustal Attenuation, Empirical Ground Motion Prediction Equations and Source Parameters for Northwestern Turkey	28
D. Bindi, S. Parolai, H. Grosser, C. Milkereit, E. Durukal, S. Karakisa, S. Zünbül, and J. Zschau	
6. The Application of Persistent Scatterer Interferometry to Analyze Interseismic Deformation at Ganos Fault	36
M. Motagh, and J. Zschau	
7. Armutlu - A Key Region to Understand the Evolution of Seismicity at the Western End of the 1999 Izmit Earthquake Rupture	42
Ş. Bariş, S. Sandberg, H. Grosser, S. Irmak, H. Woith, M. F. Özer, B. G. Lühr, D. Çaka, and J. Zschau	
8. Attenuation of Macroseismic Intensity in the Marmara Sea Region, NW Turkey	48
M. B. Sørensen, D. Stromeyer, and G. Grünthal	
9. Site Characterization by Seismic Noise in Istanbul, Turkey	54
S. Parolai, M. Picozzi, A. Strollo, E. Durukal, O. Özel, S. Karabulut, M. Erdik, and J. Zschau	
10. The Ataköy Vertical Array, Turkey: Preliminary Results	64
S. Parolai, A. Ansal, A. Kurtulus, A. Strollo, and J. Zschau	

11.	Karlsruhe-Istanbul Mobile Network - The Kimnet Experiment.....	72
	J. Ritter, and the KIMNET Research Group	
12.	Test Installation of the Self-Organising Seismic Early Warning Information Network in the Ataköy District, Istanbul, Turkey.....	74
	C. Milkereit, M. Picozzi, I. Veit, K.-H. Jäckel, K. Fleming, J. Zschau, F. Kühnlenz, B. Lichtblau, J.-P. Redlich, J. Fischer, C. Zulfikar, and M. Erdik	
13.	Realities of and Expectations from Compulsory Earthquake Insurance.....	82
	A. Taylan	
14.	Effects of the Marmara Earthquake of 1999 on Micro and Small Businesses.....	90
	C. Menny, and U. Werner	
15.	Economic Assessment of Indirect Earthquake Losses on the Macro and Micro Scale.....	96
	D. Borst, R. Mechler, and U. Werner	

Introduction

Megacities, as large urban agglomerations of people and infrastructure, are at the same time sites of rapid development and places of high risk. Growing cities and, therefore, growing risk potential will become a major feature of human development over the next decades.

Because of the speed of change in large cities, the key challenge for risk reduction is a dynamic approach that takes into account temporal changes of hazards, vulnerability and exposure appropriately. Megacities must be especially understood as entities where everything is highly variable in time and everything is interacting in a complex non-linear manner. Understanding and managing risks in megacities has, therefore, become a key challenge to governments and society in general.

In order to assist in addressing this challenge, GFZ German Research Centre for Geosciences and the Kandilli Observatory and Earthquake Research Institute of Bogazici University Istanbul (KOERI), in association with the Istanbul Metropolitan Municipality (IMM) began a co-operation in 2005 with the aim to further develop the scientific basis for the assessment and mitigation of earthquake risk in the megacity of Istanbul.

GFZ is represented in this co-operation by section:

- 2.1 “Earthquake Risk and Early Warning”

with contributions from the sections

- 1.4 “Remote Sensing”
- 3.2 “ Deformation and Rheology”
- 5.3 “ Engineering Seismology”.

KOERI is represented by the:

- Department of Earthquake Engineering

with contributions from the

- Department of Geophysics.

IMM is represented by the:

- Directorate of Earthquake & Soils Investigations

with contributions from the

- Istanbul Gas Distribution Co.

Further contributions came from a number of other institutions which include on the Turkish side:

- Center of Disaster Management (CENDIM), Bogazici University, Istanbul
- Istanbul University, Faculty of Engineering, Geophysical Engineering Department, Istanbul

- Kocaeli University, Earthquake and Space Sciences Research Planning Department, Kocaeli
- Ministry of Public Works and Settlement, General Directorate of Disaster Affairs, Earthquake Research Department, Ankara.

On the German side, contributions have been made by:

- Centre of Disaster Management and Risk Reduction Technology (CEDIM), Karlsruhe and Potsdam
- German Aerospace Center (DLR), Oberpfaffenhofen
- Heidelberg Academy of Sciences and Humanities, Heidelberg
- Humboldt University of Berlin, Department of Computer Science, Berlin
- University of Karlsruhe, Karlsruhe
 - ❑ Geophysical Institute
 - ❑ Institute for Finance, Banking and Insurance
 - ❑ Institute of Reinforced Concrete Structures and Building Material Technology
- University of Potsdam, Institute of Geosciences, Potsdam

Outside of Turkey and Germany, the following parties have been involved:

- Earthquake and Megacity Initiative (EMI)
- International Institute for Applied System Analysis (IIASA), Laxenburg, Austria
- Istituto Nazionale di Geofisica e Vulcanologia, Milano, Italy

It was mutually agreed by GFZ and KOERI, in association with IMM, to jointly prepare and conduct projects on the following nine subjects:

1. Probabilistic Hazard Assessment for Istanbul
2. Stress Field and Crustal Deformation Modelling
3. Site Effects
4. Use of Remote Sensing for the Assessment of Urban Elements, Vulnerability and Risk
5. Inundation Risk due to Dam Failure
6. Indirect Economic Losses
7. Geophysical and Geological Investigations of the Marmara Region
8. Study on Seismicity and Pore Pressure
9. Data Management

Except for task N° 5, which could not be undertaken for various reasons, all of the other subjects have been successfully worked on, providing basic results on earthquake hazard, risk and early warning all of which are important for risk reduction in the metropolitan area of Istanbul.

The project has gained a great deal from close cooperation with other initiatives, such as

- the Integrated Earth Observing System (EOS) of the Helmholtz Association of German Research Centres (HGF)
- the Geotechnology-project EDIM (Earthquake Disaster Information System for the Marmara Region, Turkey) of Germany together with Turkey
- the ICDP (International Continental Drilling Program) – Initiative on “Drilling the North Anatolian Fault”, and
- the European FP6-project SAFER (Seismic Early Warning for Europe).

The following 15 articles are considered as the final project report. They provide a representative overview of the broad range of activities undertaken within the project, covering important aspects of earthquake hazard assessment, complex risk analysis and seismic early warning in the rapidly growing region of Istanbul. The project was financially supported by the Helmholtz-Association of German Research Centres, GFZ German Research Centre for Geosciences and the University of Karlsruhe within the framework of their common CEDIM-Institute, the Kandilli Observatory and Earthquake Research Institute and the Istanbul Metropolitan Municipality. Additional support came from the other participating institutions. We are grateful to all these organisations. We would also like to thank all colleagues who contributed to this project with their scientific expertise and, in particular, our colleagues from the Istanbul Metropolitan Municipality for their steady and constructive accompaniment and support of the project and their always active and fruitful co-operation.

The coordinators

Mustafa Erdik
KOERI

Jochen Zschau
GFZ

1. **Disaster Prevention Mitigation Studies for a Safer Urban Life Measures for Preventing Disaster of Istanbul Metropolitan Municipality**

M. Bař¹ and M.Özhan Yağcı²

¹ Istanbul Metropolitan Municipality Directorate of Earthquake & Ground Analysis, Director

² Istanbul Metropolitan Municipality, Istanbul Gas Distribution Co., Project Coordinator

Introduction

Istanbul City locates on the west edge of North Anatolia Fault, and characterized as high seismic activity area. Current population of Istanbul City exceeds 10 million and the city is still growing as center of commerce, tourism and culture in Turkey.

Two big earthquakes occurred in 1999 alongside of the North Anatolian Fault. The Earthquake struck urban area of Kocaeli City in August and also urban area of Duzce City in November. The phenomena of strong earthquake migrating from east to west along the North Anatolian Fault (NAF) continue to be observed therefore it is likely that sometime in the future another large earthquake will strike Istanbul.

Disaster prevention studies of Istanbul Metropolitan Municipality focuses on risk mitigation and are being carried out under two basic topics;

- Risk Management: Scientific and Technical Studies
- Disaster management: Emergency Response Studies

To reach the ultimate goal of having a disaster resistant city, Istanbul Municipality has been conducting remarkably unique national and international projects and ready to cooperate with international organizations committed to decrease vulnerabilities globally.

In this document some of the studies will be mentioned.

Emergency Response Studies

Experiences during these natural disasters showed that establishment of a disaster coordination center is inevitable to ensure coordination of disaster related activities (pre-during and post) and to use limited resources much more efficiently. In this regard AKOM (Disaster Coordination Center) was established in 2001 (design of the building is same as the disaster management center of Los Angles / USA) in order to organize disaster preparedness activities of IMM. All the related departments of IMM come together regularly to share information about their activities to mitigate the risk and to manage any emergency situation regularly.



Photo-1-2: Disaster Coordination Center (AKOM) of Istanbul Metropolitan Municipality (IMM)

A seismic resistance diagnosis for AKOM building was conducted which showed that it has a resistance to 8.3 M earthquake. Beside being structurally a high resistant building it is a self diagnostic building. Any malfunction in any part of the system can be detected by warning signal and can be fixed easily. Latest technologies are being used for hardware and software of AKOM.



Photo-4-5-6: Meeting room and hardwares of AKOM

During the past years emergency response capacity of IMM has been increased by establishing new ones and increasing the numbers of existing fully equipped search and rescue and first aid teams.

Scientific and Technical Studies

Urban Geology Studies: 1/5000 scale land-use suitability, geological and geo-technical maps have been prepared. 1/25000 and 1/5000 scale geological studies for the whole city area (boundaries by law: 5216) have been completed. Soil investigation reports are being reviewed by IMM's Earthquake and Ground Analysis Department and technical and official judicious are delivered. All the data collected from studies are compiled and stored in a geo-database system.

Monitoring Stations: In order to monitor micro seismic activities IMM has established monitoring stations in cooperation with Bogazici University Kandilli Research Institute(KOERI). Other monitoring stations were established together with TUBITAK in order to observe and monitor physical and chemical changes in ground water and radon gas and to correlate these changes with seismic activities.

Damage Estimation Studies: At the beginning in order to define the hazard and to estimate possible dimensions of an earthquake disaster; “Disaster Prevention /Mitigation Basic Plan” was conducted together with Japan International Cooperation Agency (JICA). Study was concluded in 2002. Several different scenario earthquakes were studied and two of them (Most probable one with M:7.5 and worst case with M:7.7) were used in order to estimate the damages. Summary of estimated earthquake losses were as follows:

Heavily Damaged Buildings	50.000-60.000
Homeless	500.000-600.000
Death Toll	70.000-90.000
Injured	135.000
Water-pipe Damages	1.000-2.000
Natural Gas SB Damages	30.000
Power Lines Damages	%3
Public Facility Damages	%8 (Heavily)
Bridges Damages(460)	20 (Heavily)
Tent requirement	300.000
TOTAL ECONOMIC LOST	40 BILION USA\$

After defining the hazard Study concluded with proposals of short, medium and long term measures. IMM took those proposals seriously and with following years those proposals started to be implemented.

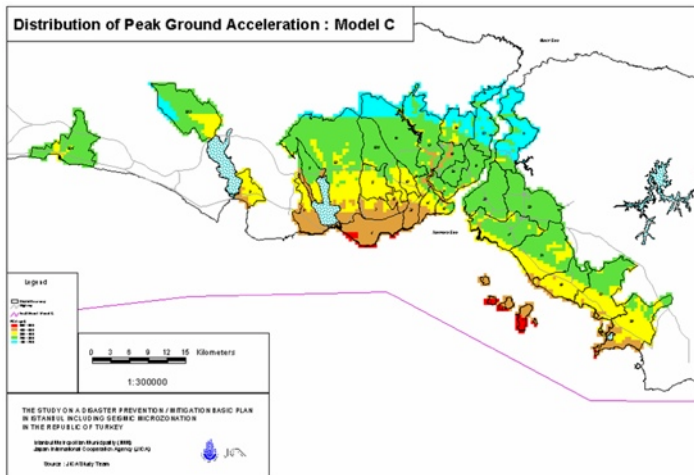


Figure: 1: Distribution of Peak Ground Acceleration (Model C: worst case)

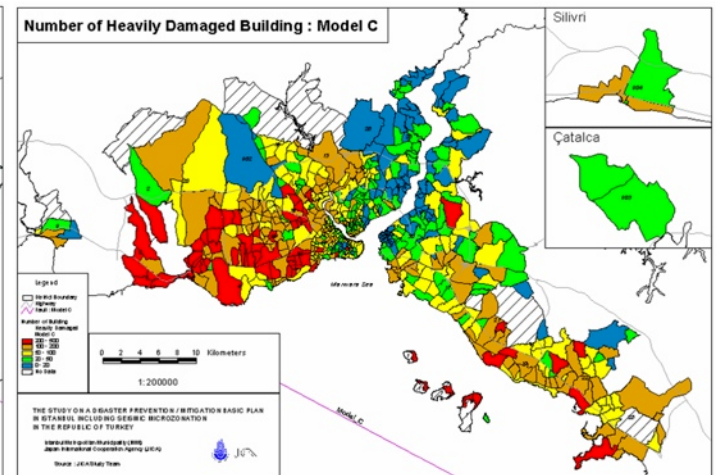


Figure: 2: Number of Heavily Damaged Buildings (Model C: worst case)

After defining the hazard IMM authorized four leading universities of Turkey (Bogazici University, Istanbul Technical University, Yildiz Technical university, Middle East Technical University) to conduct an Earthquake Master Plan study which became a road map to a safer urban environment and completed in 2003. Istanbul Earthquake Master Plan (IEMP) is a multi-disciplinary study and a kind of social contract between governorship, IMM, district municipalities, public organizations, private entrepreneurs, NGOs. Content of the master plan can be listed as fallow;

Financial Studies	Defining Current Situation
Educational Studies	CE Studies (Structural Diagnosis & Retrofitting)
Social Studies	Urban Planning Studies (Construction Plans)
Disaster & Risk Management Studies	Legislative Studies

Results of IEMP showed that 10 districts are having high disaster risk so that the total risk of these ten districts is equal to %50 of all earthquake risk of Istanbul. Below is the list of these ten districts which were considered as having priority for the next implementation stages.

Districts having High Disaster Risk	Pilot Projects
Eminonu	
Fatih	38.580 building / under screening
Beyoglu	
Zeytinburnu	16.030 building / screening completed
Bakirkoy	
Bahcelievler	
Avcilar	
Bayrampasa	
K.Cekmece	60.938 building / under screening
Adalar	

Implementation stage started from these priority districts and aimed to be expended to whole city in the future. First Pilot project was Zeytinburnu district pilot project in which 16.030 building was screened one by one. Screening methodology was described in IEMP which is consisting of three stages from general one to more detail ones. Fatih and K.Cekmece pilot projects are continuing and expected to be completed in a year. Following to the completion of building screening in each district; Mahalle (smallest administrative unit) based ‘Urban Transformation Projects’ are planned to be started. For these transformation projects temporary housing; resettlement plans, new urban design with open spaces, recreation areas and green corridors, etc all designed with many alternatives and ready to be implemented.

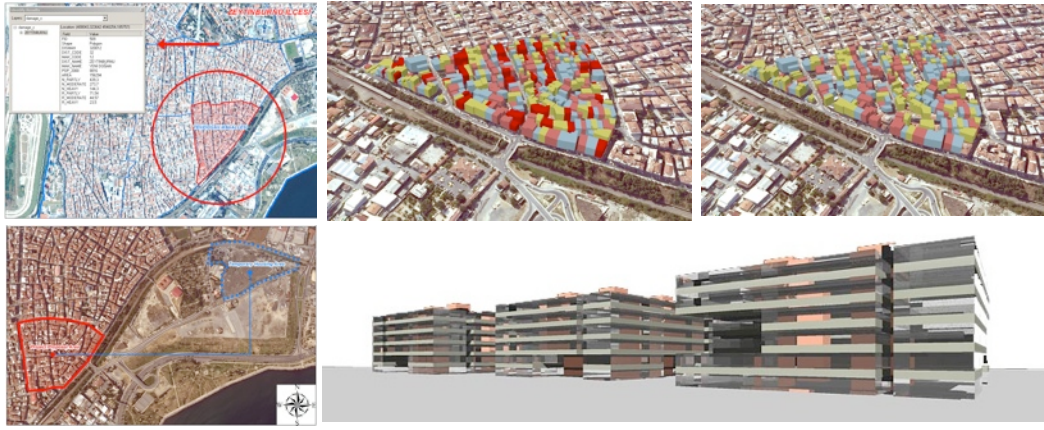


Figure: 3: Mahalle Base Urban Transformation Projects

Microzonation Project

Project was proposed by previous studies like IMM/JICA, IEMP, Housing & Construction Ministry Earthquake Council, etc. Microzonation is identification of separate areas having different hazardous potential. It is an efficient tool to mitigate risks for hazard related land use management.

Below map shows first three project stages with information like coverage area, finishing date and financial source of the stages. It is planned that microzonation study which will be used to revise all kind of construction plans with all scales will cover whole Istanbul in the future.

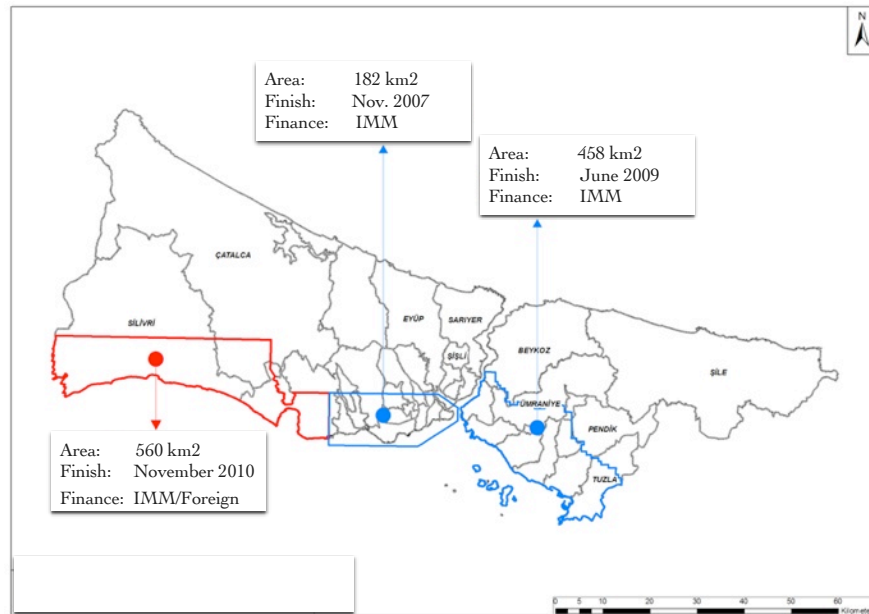
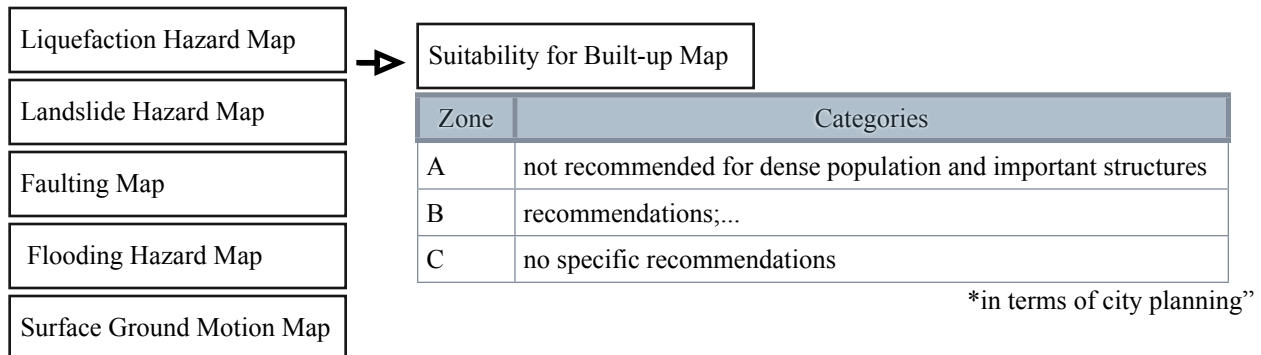


Figure: 4: Microzonation Project Phases

Grid size for all kind of site surveys and works (geological, geophysical, etc) and analysis is 250mx250m. Below tables shows work items and their volumes for the first phase of microzonation projects namely Microzonation project for European Side South. Below tables show work items with volumes and produced maps with scales as results of analysis:

WORK ITEMS	Volume	MAPS	SCALE
Drilling for 250m cells	2912 wells	Earthquake Hazard Map (whole istanbul)	1/25000
Deep Well drilling	25 wells	Tsunami Hazard Map (whole istanbul)	1/2000
Drilling for Liquefaction Analysis	~874 wells(%15)	Inclination Map	1/2000
Drilling for Landslide Analysis	~699 wells(%8)	Geology and Engineering Geology Map	1/2000
Seismic Refraction & REMi	2912 cells	Groundwater Level Map	1/5000
Electric resistivity Measurements	2912 cells	Microtremor Map	1/5000
PS-Logging	207 wells	FAULTING (Tectonic) MAP	1/5000
Microtremor Array Measurement	30 points	Ground Shaking (Intensity) Map	1/5000
Seismic Reflection	20 km	Liquefaction & Landslide Hazard Map	1/2000
		Earthquake-related Flooding Map	1/2000
		Vs (0-30m) Average Shear Wave Velocity Map	1/5000
		Soil Classification Map	1/2000
		URBAN LAND USE PLANNING MAP	1/2000

Produced hazard maps and as a result map land suitability map in terms of city planning.



As a result all kind of risks from tsunami effect to coasts to liquefaction are defined in 250mx250m grids and after detailed analysis procedure related maps are prepared showing the hazards and as a final map land suitability maps are produced which will be based for city planning activities like construction plans to urban rehabilitation and transformation projects.

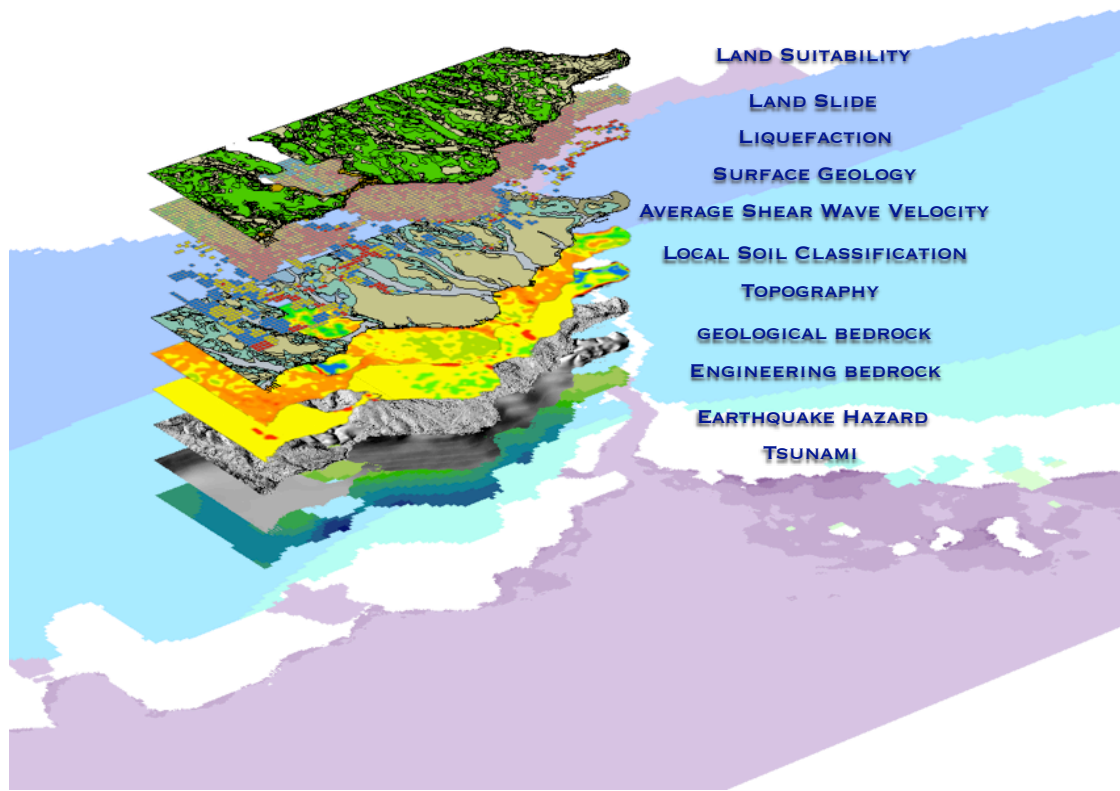


Figure: 5: Analysis Layers

Closure

To reach the ultimate goal of having a disaster resistant city, Istanbul Municipality has been conducting remarkably unique national and international projects and ready to cooperate with international organizations committed to decrease vulnerabilities globally.

The main objective of Istanbul Metropolitan Municipality is not to rescue people from the debris but not let them to stuck under it. In this regard beside increasing capacity for disaster management many technical and scientific studies are being carried out to mitigate the risk by risk management oriented projects of which only very limited are briefed in this document.

2. Megacity Indicators System for Disaster Risk Management - Implementation in Istanbul

B. Khazai¹, O. Kilic², A. Basmaci², B. Konukcu², B. Sungay³, A. Zeidan⁴ and F. Wenzel¹

¹Center for Disaster Management and Risk Reduction (CEDIM), Universität Karlsruhe (TH), Germany

²Istanbul Metropolitan Municipality, Earthquake and Ground Research Directorate, Istanbul Turkey

³Center for Disaster Management (CENDIM), Bogazici University, Istanbul, Turkey

⁴Earthquake and Megacities Initiative (EMI)

Background

City officials need tools to understand the priorities and to set up benchmarks and track progress in their disaster management systems, so that they can justify decisions and investments in disaster risk reduction. The “Megacity Indicators System” (MIS) is a tool to communicate risk and promote discussion around relevant local-level risk parameters that would enable DRM professionals and decision-makers to develop appropriate Disaster Risk Management (DRM) strategies and take concrete actions to reduce disaster risk. It also sets up benchmarks and enables tracking progress on these benchmarks, thus providing a possibility to correct, review and decide on where to invest resources. The models and methodology referred to here as the “Megacity Indicators System” (MIS) approach was originally developed for the Inter-American Development Bank through the IDB-IDEA Indicators Program (Cardona et al, 2005). Together with the original developers of the methodology, the Earthquakes and Megacities Initiative (EMI) undertook a preliminary application of the MIS approach to megacities in Metro Manila where it was used as an innovative risk communication tool to engage stakeholders in understanding their involvement and taking ownership of the risk factors in the city. Besides the implementation in Metro Manila, many other related applications of the model have been undertaken, and the methodology has been tested and evaluated in other cities and sub-national regions in Latin America and Europe, including Manizales (Colombia) Quito (Ecuador), Barcelona (Spain) and Lombardy region (Italy). The present work conducted at the Center of Disaster Management and Risk Reduction Technologies (CEDIM) at Karlsruhe University is intended to adapt the methodology to reflect the risk conditions of the megacity of Istanbul. The objective is also to focus on the implementation of the MIS methodology so that the Istanbul Metropolitan Municipality (IMM) can use it as a planning tool to measure their own DRM state-of-practice and evaluate progress in DRR objectives of Istanbul. Thus, delivering a tool to the Municipality and other stakeholders, which they use and find pertinent and relevant to their DRM agenda is one of the primary goals of this work. The project is a joint scientific activity between Karlsruhe University (CEDIM), EMI, IMM and Bogazici University (CENDIM). The project is undertaken within the Directorate of Ground and Earthquake Research of the IMM.

Approach

Building on prior methodology Cardona et al. (2005), the MIS provides an overview of not only the expected physical damage, through a Physical Risk index, but also looks into the social fragility and lack of resilience in the different districts in Istanbul through a Social Vulnerability index. Furthermore, a Disaster Risk Management index is used as a “control system” in this framework, for the Municipality to measure performance and effectiveness of different operational and organizational policies and their effect on the total Urban Seismic Risk in the different districts of Istanbul. Figure 1 provides an overview of the MIS and how the different indices combine together. Evaluation of the potential physical damage (hard

approach) as the result of the convolution of hazard and physical vulnerability of buildings and infrastructure is the first step of this method. Subsequently, a set of social context conditions that aggravate the physical effects are also considered (soft approach). According to this approach, a final step is to capture the potential for disaster risk management through a set of descriptive indicators and track progress (or lack of progress) on pre-defined benchmarks of corrective and prospective intervention, by considering them as an additional factor in aggravating the physical effects or direct damages.

According to this procedure, a physical risk index is obtained, for each unit of analysis, from existing loss scenarios, whereas the total risk index is obtained by factoring the risk index by an impact factor, based on variables associated with the socio-economic conditions and the disaster risk management potential of each unit of analysis. In the Istanbul implementation, the above framework combines the direct impact of expected physical damage, “physical” risk factors, and indirect “impact” factors that account for the socio-economic fragility and resilience within the city’s population; and the capacity of the Municipality to respond to, reduce and manage risk.

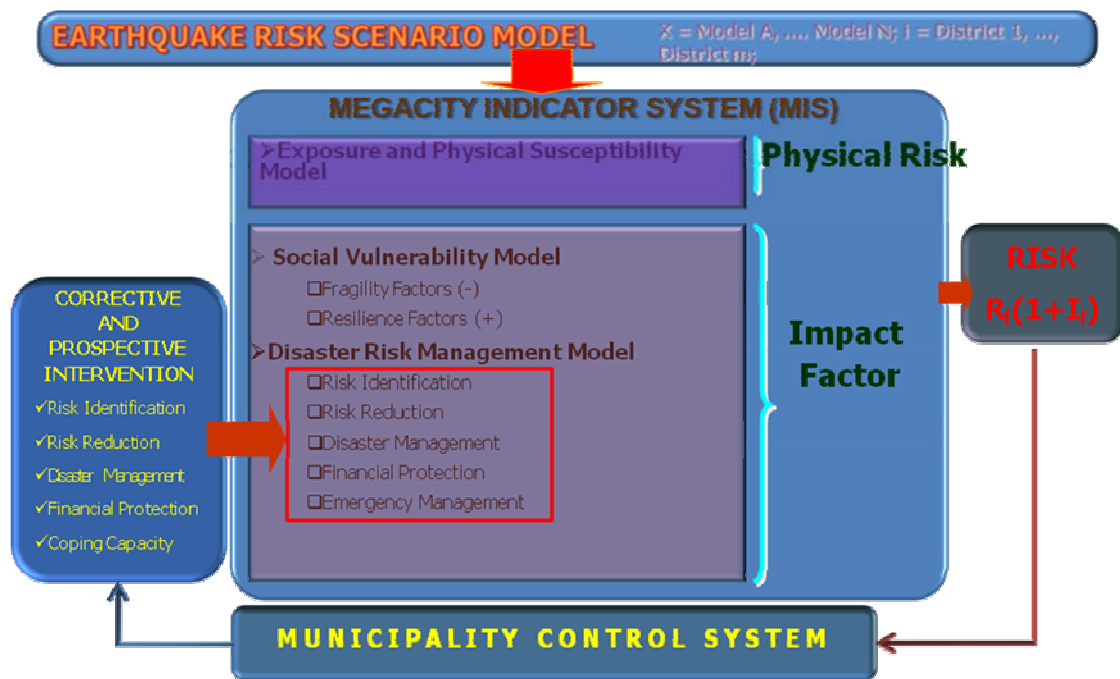


Fig. 1: Conceptual Model for MIS showing how the physical risk, social vulnerability and disaster risk management model combine together (after Cardona et al., 2005)

The potential direct impact of an earthquake, for example, is denoted as Physical Risk, R_F . The indirect effects are given by and impact factor $(1+F)$, which is based on an aggravating coefficient, F . The aggravating coefficient, F , is in turn the aggregate sum of Social Vulnerability, SV , and Disaster Risk Management potential, DRM . Thus the total Urban Seismic Risk Index is given by:

$$USR_i = \text{Physical Risk} * \text{Impact Factor} = R_F (1+F) = R_F (1+ SV + DRM)$$

Physical Risk Index

The physical risk indicators in this study are derived entirely from the 2002 “Study on Disaster Prevention / Mitigation Basic Plan in Istanbul including Seismic Microzonation in the Republic of Turkey” conducted by the Japan International Cooperation Agency (JICA).

The loss damage distributions in Istanbul are derived from for two scenario earthquakes proposed by JICA. The physical risk indicators suggested here can then be easily updated and upgraded as new studies are completed and the data for them becomes available. These indicators include: 1) Ratio of heavily damaged buildings; 2) Casualty; 3) Fire outbreak possibility; 4) Electricity cable damage; 5 Water pipe damage; 6) Sewage pipe damage; 7) Natural gas pipe damage; 8) Telecom/fiberoptics damage; 9) Bridge damage

Social Vulnerability Index

Social vulnerability is defined as “the characteristics of a person or group and their situation that influence their capacity to anticipate, cope with, resist and recover from the impact of a natural hazard” (At Risk, Wisner et al., 2004). The definition above implies that social vulnerability is affected by inherent factors of fragility of a person or group (i.e. personal attributes, living situations, finances). At the same time it is implied, that overcoming vulnerability (that is building capacity in the face of hazards) requires factors of resilience, such as available means of disaster preparedness and risk mitigation, solidarity and social networks, savings and other buffers and resources for reconstruction and recovery. The indicators for social vulnerability were developed through an iterative process with the local core investigators and reviewed in several workshops and meetings with experts. The 14 indicators shown here are consistent with previously published work on social vulnerability (Wisner, Cannon, Cardona, etc.) and complement and enrich some of those already agreed upon as core indicators. They are divided into two sets of seven each. The first category of “fragility factors” are easily “readable” from most census surveys and routinely gathered data and represent factors of inherent social and economic fragilities present within a person or group. The second group of “resilience factors” are typically not subjects of data collection, yet they represent the critical facets of resilience or capacity which are required to overcome vulnerability. The data for the “Resilience Factors” come primarily from a social structure survey conducted by the Istanbul Metropolitan Municipality.

The Planning and Strategy Department of the Municipality of Istanbul is planning to carry out a dedicated survey to determine the “Social Structure” of Istanbul. A component of the “Social Structure” survey is to determine the social vulnerability to earthquakes of the residents of Istanbul, which presents a unique opportunity to develop indicators from a direct questionnaire administered at the household level. Thus, a social vulnerability questionnaire has been developed. The survey is expected to be administered to approximately 50,000 households throughout all the districts of Istanbul. The results of the questionnaire will be collected and analyzed to derive values for the selected indicators of social vulnerability. The “Social Structure” survey provides the input to represent the spatial variability and uncertainty in the district-level indicators.

Disaster Risk Management Index

The Disaster Risk Management Index permits a systematic and



Fig. 2: Social Vulnerability Index depicted in terms of fragility factors and resilience factors

quantitative benchmarking of different operational and organizational capacities and policies at the Municipality during different periods, as well as comparisons across districts throughout different time periods. Critical to ensuring the adaptability and long-term use of the MIS by the stakeholders is that it be made compatible with Istanbul's DRM framework and that the selected indicators be immediately relevant and easily understood by policy makers and disaster management professionals. The overall goal is for the MIS to be used by the City to plan and track progress of the Municipality's operational capacities – the capacity of the Municipality to respond to emergencies and restore services – as well as functional capacities – the policies and planning measures at the Municipality which lead to reduction of risk and protection of people. The operational capacities are quantified by the emergency management and response capabilities of the Municipality. Functional capacity of the municipality is determined by quantifying four public policies, which include risk identification, risk reduction, disaster management, and financial protection.

Preliminary Results

Data has been collected for the proposed indicators of physical risk from the 2002 JICA study. With the exception of “risk perception”, “risk awareness”, “risk mitigation”, and “solidarity” (currently being obtained from the “Social Structure Survey” collected from 50,000 households) data has also been obtained from several different sources for the indicators of Social Vulnerability. For the Disaster Risk Management index, data has only been collected on three out of four of the “Emergency Management” indicators of the Municipality at this time. The evaluation survey for scoring the Risk Reduction Management indicators is still being developed and a complete evaluation of this index is pending the finalization of the survey and completion of its evaluation by a group of selected experts. The implementation of the MIS methodology involves the following five steps:

1. Collecting and analyzing data for selected indicators of Physical Risk, Social Vulnerability and Disaster Risk Management.
2. Developing transformation functions to normalize indicators and testing sensitivity and stability of transformation functions.
3. Implementation of indicators and their transformation functions with a set of “borrowed” weights in the MIS tool to compute the total Urban Seismic Risk in all districts.
4. Generating importance weights for the developed indicators, and evaluating their sensitivity and stability in a workshop with the Expert Group using the interactive MIS tool.
5. Presenting the MIS in a workshop with the Focus Group or stakeholders for risk communication, risk planning, and monitoring of different disaster risk management measures using the interactive MIS tool.

In the MIS implementation of Istanbul, to date, all physical risk indicators and all social vulnerability indicators available at the district level have been implemented in the software tool to obtain total urban risk rankings in the 30 districts of the Study Area. The analytical and interactive functionalities of the MIS tool can be used at this stage to evaluate and qualify indicators and examine the effects of their weights upon the total output. Figure 4 show the social vulnerability (SV) rankings in the district, the physical risk (R_F) rankings in the district and the Urban Seismic Risk Index (USRi).

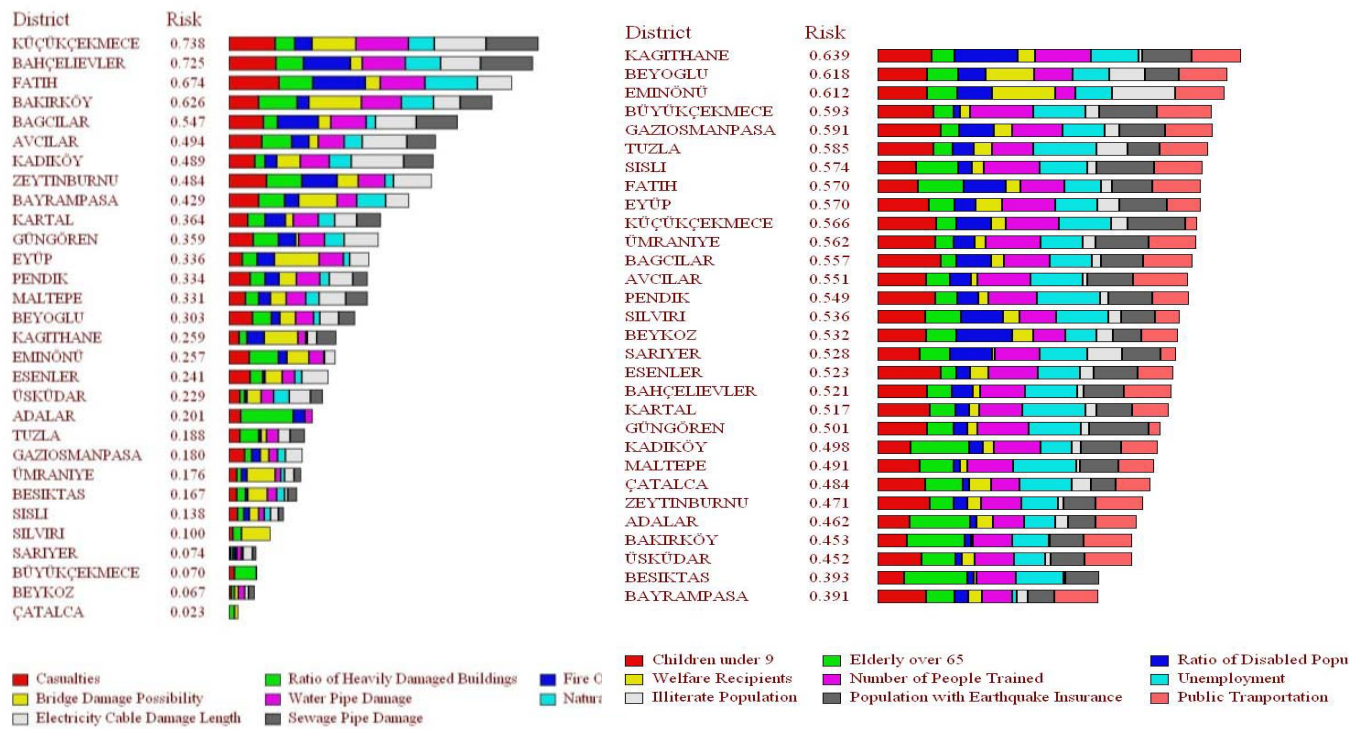


Fig. 3: Preliminary results for ranking of physical risk index (left) and social vulnerability index (right)

To aid in the implementation process an interactive software tool, Logical Decisions for Windows (LDW) is used which can be used to evaluate and qualify indicators and examine their effects upon the total output. The software supports performing sensitivity analyses, which can be used to interactively demonstrate variability of the results to different indicators. The advantage of using an MIS tool that integrates the models is that during a periodic evaluation, other indicators that may have previously not been available or simply overlooked can be integrated into the framework to obtain a new evaluation of risk and DRM practices in Istanbul.

The implementation process consists of organizing and working with the expert group in evaluating the indicators, generating their importance weights and discussing the outcomes of the MIS. The MIS application in Istanbul will rely on pre-defining the importance weights and scores of the DRM indicators with a group of experts. This allows the workshop with the stakeholders to focus on communication of the results, and translating them into specific policy recommendations. A one-day expert workshop will be used to evaluate the indicators and generate weights for both the physical and social vulnerability indicators. The aim of the expert evaluation is to provide a consensus view on the subjective importance weights of the different indicators. The MIS tool allows for the interactive implementation of several weighting methodologies, and will allow the expert group to look at the sensitivity of different weighting schemes in real time. At least two iterations of the MIS implementation in Istanbul with a target group of stakeholders from the Metropolitan and District Municipalities are expected. A first stakeholder workshop with a focus group from the different departments of the Istanbul Metropolitan Municipality is conducted once the results of the “Social Structure” survey, and DRMI evaluation survey have been analyzed; the importance weights generated by the experts; the sensitivity and stability of the indicators, their weights and transformation functions are analyzed; and the indicators, software and technical documents are translated into Turkish. A second workshop is planned with key representatives of the 30 District Municipalities of Istanbul, for communication of the MIS implementation results, and translating them into specific policy recommendations.

References

- Cardona, O. D.; J. E. Hurtado; G. Duque; A. Moreno, A. C. Chardon, L. S. Velásquez, and S. D. Prieto (2005). System of Indicators for Disaster Risk Management: Main Technical Report. *IDB/IDEA Programme of Indicators for Disaster Risk Management*, Universidad Nacional de Colombia, Instituto de Estudios Ambientales, IDEA, Manizales, <http://idea.unalmz.edu.co>.
- Carreño, M. L, O. D. Cardona, and A. H. Barbat (2007). Urban Seismic Risk Evaluation: A Holistic Approach. *Natural Hazards* **40**(1), 137-172, DOI 10.1007/s11069-006-0008-8.
- Carreño, M. L, O. D. Cardona, and A. H. Barbat (2007). A Disaster Risk Management Performance Index. *Natural Hazards* **41**(1), 1-20, DOI 10.1007/s11069-006-9008-y.
- EMI (2006). Application of Indicators in Urban and Megacities Disaster Management, A Case Study for Metro Manila. *Progress Report TR-0701*, September 2006 available for download from www.emi-megacities.org
- LDW, *Logical Decision for Windows*, is a multi-criteria decision support software for evaluating choices: <http://www.logicaldecisions.com/>
- Saaty, T. (1980). *The Analytic Hierarchy Process for Decisions in a Complex World*, McGraw-Hill, 1980.

3. Preparation for an Expected Disaster

The Contribution of Remote Sensing and Civil Engineering to Support Risk Management at Mega City Istanbul, Turkey

H. Taubenböck¹, C. Münich², A. Roth¹, L. Stempniewski², H. Mehl¹, and S. Dech¹

¹German Remote Sensing Data Center (DFD) - German Aerospace Center (DLR) – Oberpfaffenhofen, D-82234, Germany.

²Institute of Reinforced Concrete Structures and Building Material Technology, Universität Karlsruhe (TH), 76128 Karlsruhe, Germany

Introduction

Extreme natural events regularly lead to catastrophes with dramatic consequences and reveal considerable deficits hindering their effective management: Needs include systematic risk identification and evaluation, a way to assess countermeasures and decision support systems to be employed before, during and after crisis situations. While the hazards are natural, disasters are not and thus man-made. For example the problem of earthquake prediction in a deterministic sense has not been solved yet (Zschau et al., 2002). Disasters result from the impact of a hazard on a vulnerable system or society at a specific location (Taubenböck et al., 2007a). On this account Birkmann (2006) stresses the need for a paradigm shift from the quantification and analysis of the hazard to the identification, assessment and ranking of vulnerabilities.

Vulnerability evolves in the dynamic urban system by complex interactions of physical, demographic, social, economic, ecologic or political factors or processes, a myriad of feedback loops and thresholds and competing ideas, mechanisms and forms (Taubenböck et al., 2008). Here, there is no simple one-way line of causality in the production of human and environmental conditions (Pelling, 2003). For example, the mega city Istanbul, Turkey, with its estimated 15 million inhabitants is threatened by a 30-70 % probability of a major earthquake (magnitude > 7), in the next 30 years (Parsons et al., 2004). The tremendous spatial concentration of people, financial values and infrastructure in combination with the earthquake threat are the basis for the high risk and vulnerability in this large and dynamic urban environment.

Disaster management can only be as good as the available spatial information. Decision-making at each stage of the disaster risk circle (DKKV, 2003) requires a substantial, up-to-date and area-wide information basis on the multiple perspectives of vulnerability and the spatial distribution of the hazard impact. In recent years satellite systems and image analysis techniques have developed to an extent where civil and commercial earth observation instruments can contribute significantly in supporting the management of major technical and natural disasters as well as humanitarian crisis situations (Voigt et al., 2007; Taubenböck et al., 2008). Especially in such dynamically changing environments like mega cities, remote sensing data and results can be a cornerstone to support comprehensive risk and vulnerability management. The study presents manifold results of remote sensing and civil engineering for an interdisciplinary value-adding approach to identify and localize risk and vulnerability.

Methodology and Results

Remote Sensing

The capabilities of remote sensing enable the generation of multi-scale products to support decision-making. Results are products on city level with complete coverage of the mega city but with limited geometric resolution or thematic detail. On building / block level the capabilities of high resolution satellite data with a spatial resolution of about 1 m enable to identify detailed urban morphology, but with limited areal coverage.

On city level, Landsat and TerraSAR-X data were utilized to monitor and analyse urbanization processes over time. Landsat, available since 1972, with its field of view of 185 km is able to survey the large metropolitan area of the study site. In return, the requirements for the

differentiation of classes are limited to the classification of built-up and non-built-up areas because of a maximum of 15 meter geometric resolution. The stripmap data from TerraSAR-X provide a geometric resolution of 3 meters and the swath of 30 km. The sensor enables the covering of large parts of Istanbul to assure area-wide classifications. The orographic condition of the urban region of Istanbul utilizing the digital elevation model (DEM) from the Shuttle Radar Topography Missions completes the modelling of the urban environment. A land cover classification was performed separately on all available multi-sensoral images to extract the classes ‘built-up areas’, ‘bare soil’, ‘vegetation’, and ‘water’. The main goal is to identify urban built-up areas to measure the changes of the time-dependent urban extension over the time interval. For that purpose, the classification methodology is based on an object-oriented hierarchical approach (Taubenböck, 2008). The object-oriented methodology was used to combine spectral features with shape, neighbourhood and texture features. Results of the change detection are the quantification of urban sprawl and densification processes, the detection of directions of growth, the type of urban growth and the analysis of built-up density pattern. In combination with the DEM the localization of settlement in inappropriate hilly areas are detected (Figure 1).

On building / block level the capabilities of high resolution satellite data (Ikonos) with a spatial resolution of 1 m enable to identify urban morphology very detailed, and thus opens the possibility to generate multiple products supporting vulnerability and risk management. An object-oriented urban land cover classification provides information on seven land cover classes – buildings, streets, grassland, trees/bushes, bare soil, shadows and water – to map basically ‘what’ is ‘where’ (Figure 2a). The spectral and structural information on the classified buildings were used to distinguish different physical building characteristics. The shadow lengths of the buildings were used to assess three building height classes; 1 – 3 floors, 4 -7 floors and higher than 7 floors. Further parameters for the vulnerability assessment are the properties of roofs which correlate with the construction material (Münich et al., 2006).

Based on the urban land cover classification further analysis allows to detect the spatial distribution of vulnerabilities. The extracted street network was divided in three categories based on their carrying capacity to assess accessibility. Extraction of open spaces enables to localise and calculate available extents of safe areas for evacuation. In addition, the physical knowledge on building level (e.g. building height, building size, built-up density, structural

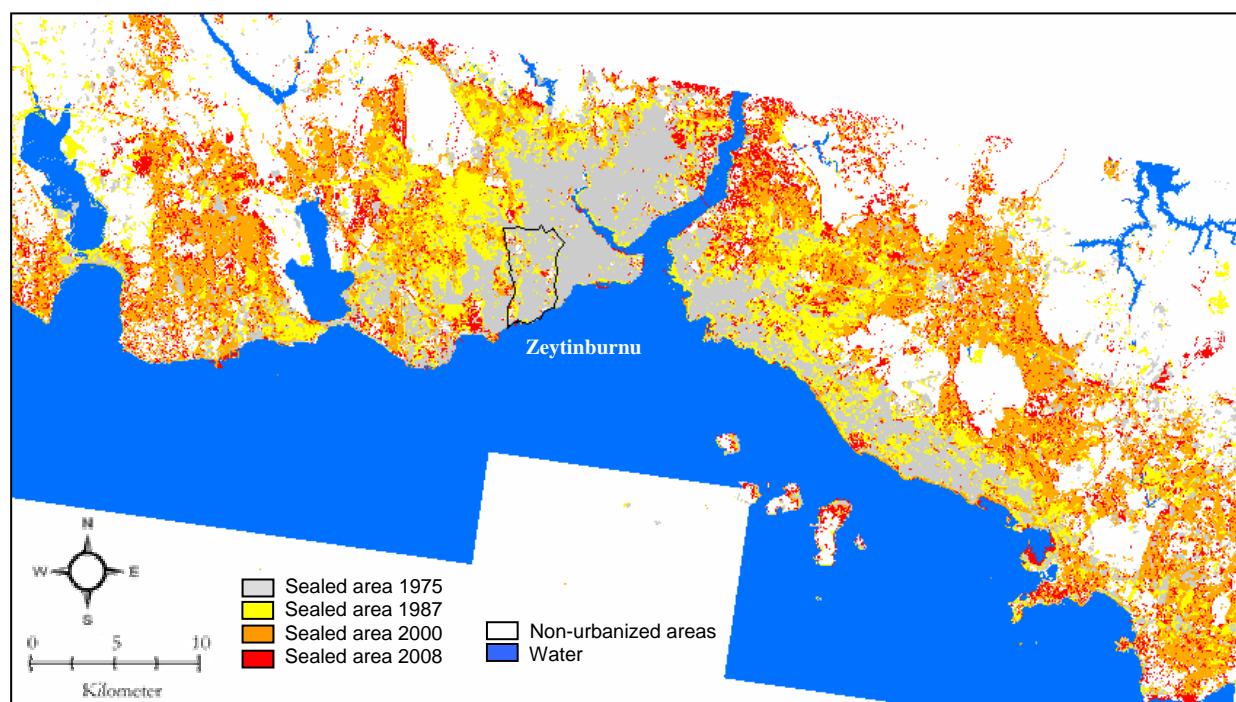


Fig. 1: Change detection of urbanized areas at mega city Istanbul utilizing multi-sensoral remote sensing data

alignment) was used to assess land use. As subsequent product, the static urban morphology and land use served to assess the population distribution. Different external input data determine the two different methodologies for calculating population distribution. On the one hand, statistical population data are based on the coarse spatial unit of administrative districts. A top-down approach distributes the total population according to urban structural characteristics derived from remote sensing data. On the other hand, punctual population information derived from a field survey is the starting point. A bottom-up extrapolation approach uses a chronologically permuted methodology using the same structural characteristics of the urban environment (Taubenböck et al., 2007b). The result is a highly detailed knowledge on the dynamic spatial behaviour and whereabouts of people within the complex urban landscape (Figure 2b).

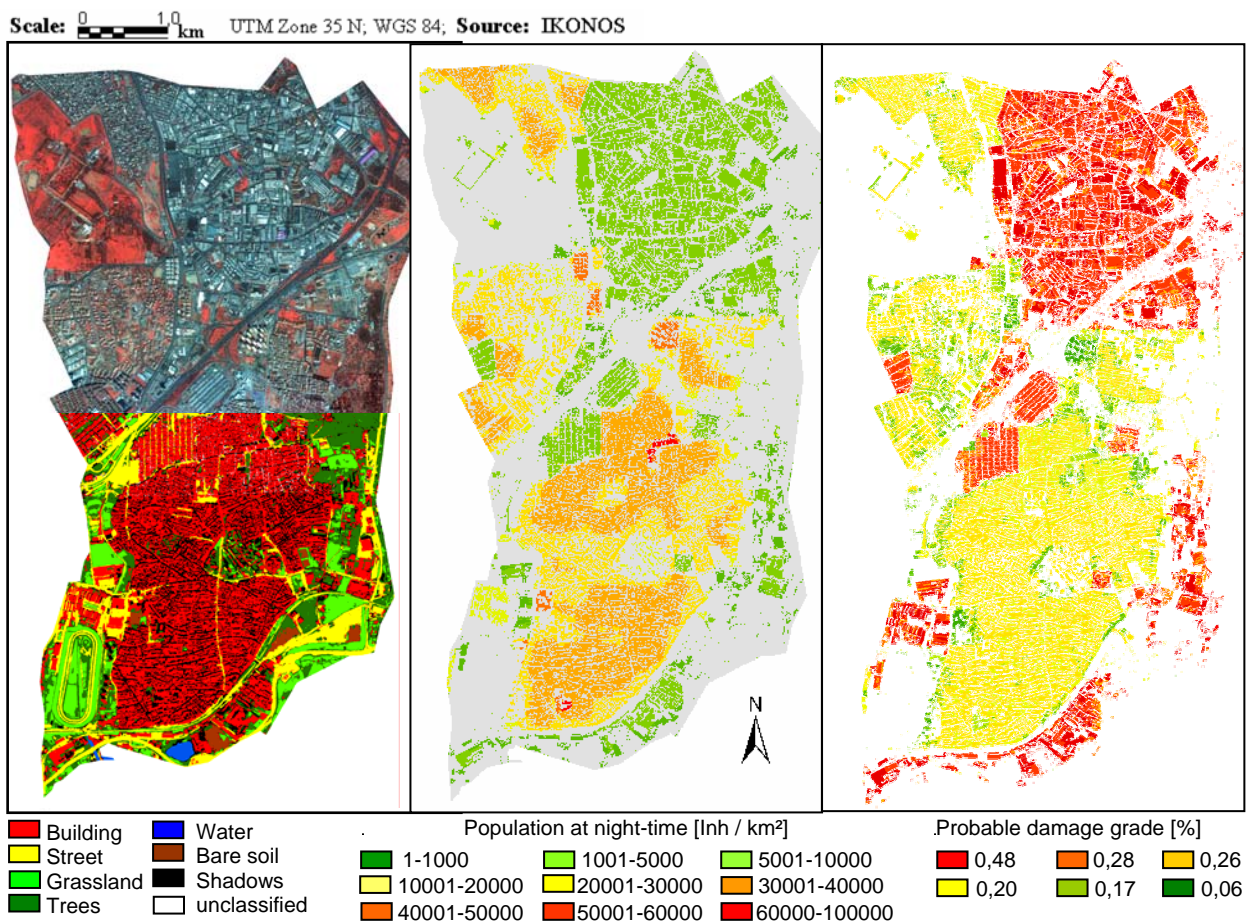


Fig. 2: Products assessing vulnerability utilizing high resolution satellite data – the example of district Zeytinburnu

Structural results using synergistically remote sensing data

Risk and loss of live emanates from the failing of structures in case of earthquakes, not by the earthquake itself. Istanbul offers a large number of buildings - partly without any civil engineering service and engineering drawing of the structural system (Metropolitan Municipality of Istanbul, 2003).

With an urban extension of about 80 km x 60 km, with an unmanageable amount of existing structures (869,444 in 2000, DIE 2005) and with an average annual growth of 300,000 new inhabitants, monitoring of the complete building stock by using street surveys is out of reach for time and cost reasons. The aim of the interdisciplinary research utilizing methods from two scientific fields – remote sensing and civil engineering – is to assess and quantify area-wide vulnerability of structures with civil engineering methods and remote sensing data for seismic scenarios.

Analysing methods exist for different modelling scales. This approach is based on building / block scaled datasets. Therefore, the accuracy of the approach depends directly on the differentiation of the building stock into separate building classes. This classification uses physical parameters of buildings derived from remote sensing data. These parameters are identified to differentiate buildings in classes with correlation to the physical performance of the structures. Parameters provided on building level by high-resolution satellite data are building height, building size, characteristics of the roof and on medium-resolution the assessment of the building age. The classification of building heights using satellite data is oriented on previous height classifications in already performed studies (ATC 40) to guarantee the compatibility. For the calculation of damage functions three height classes from 1 to 3 floors (low), 4 to 7 floors (medium) and higher than 7 floors (high) were derived by the demands of engineering – all excluding basement. To consider changes in the building code in 1975 and to follow suggestions of Aydinoglu and Erdik (2002), the buildings were classified in two age classes – pre 1980 and post 1980.

To calculate the expected physical damage two different methods were implemented. The capacity spectrum method and the use of intensity based vulnerability functions. The capacity-spectrum method is a simplified, nonlinear, static methodology. It was enhanced in the HAZUS program and standardized for California in the ATC 40 report. This study is based on the ATC 40 method and considers modifications of Aydinoglu and Erdik (2002) to adjust country-specific differences in construction styles. The calculation of expected physical damage in case of shaking can be realised by quantifying the seismological impact in a first step. Parameters are soil and underground classifications as well as seismic parameters describing the impact due to earthquakes. The capacity spectrum method uses information about the earthquake in form of response spectrums. Parameters for artificial modelled earthquake loads can be found in national and international codes (EC8). Regional fragility and capacity curves are modified to fulfil the altered demands by using remote sensing datasets (Münich et al., 2006). In a further step the correlation between the expected

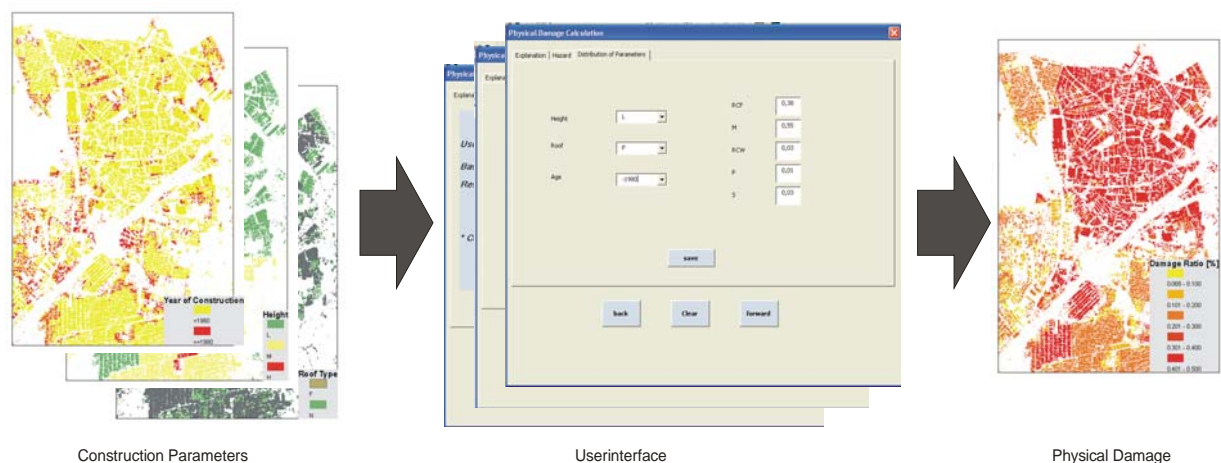


Fig. 3: Implemented GIS user interface for the process chain from remote sensing results to the damage assessment

deformation and the probability for an expected damage grade is derived (Figure 2c).

The probability of damage grades has been projected on the district Zeytinburnu on the European side of Istanbul, using the assignment of identified structures to building classes based on parameters derived by analysis of high-resolution satellite imageries. The synergistic use of remote sensing and civil engineering enables the quantitative assessment of physical damage of buildings in its spatial distribution (Figure 2c). At this validation stage, it is assumed that the earthquake impact is constant for the test site Zeytinburnu. The scenario response spectrums are based on assumptions of the eurocode (EC8). The accuracy of the interdisciplinary method depends predominantly on the accuracy of the input data, but also on

the reliability of the damage functions. The classification of building types from remote sensing shows very high accuracies (with 94.1 % accuracy for the height, 85 % for the building roof and 91.2 % for the building age). Figure 3 presents the implemented GIS user interface. The spatial distribution of building vulnerability is a basic information layer to support decision-making. The assessment of number and location of affected structures with their probable damage grades facilitates the identification and localization of areas of high priority for mitigation strategies. It complements the data basis decision makers require to decide if, where, and which preventive measures are to be done. Nevertheless, this layer serves also as information while and shortly after an earthquake struck. It enables the simulation of number and location of affected structures to assess the quantity of needed relief actions.

Conclusions and Outlook

The study has demonstrated that remotely sensed data are an independent, area-wide, and up-to-date data source for the analysis of fast changing and large areas of mega cities. A large variety of multi-scale results enables to provide information on the dimension and direction of urban sprawl over time, the derivation of physical urban morphology parameters like number of buildings, building sizes, building height, built-up density, roof types as well as the main street network or the location and extent of open spaces. In addition, these parameters were utilised to infer indirectly the land use and the population distribution with respect to the time of day. An interdisciplinary approach enables value-added results on the vulnerability of the structures.

The multiple results presented in this study produce in combination value-added information for a more holistic approximation of reality. The synergistic use of remote sensing and civil engineering enables the elimination of weaknesses of both research directions. Thus, the spatially explicit knowledge on probably affected structures, the amount of people staying there at a certain time, the possibilities of accessibility or the distance and location of safe areas supports decision making for disaster management before, during and after catastrophic events. Thus, for such complex interrelations of hazard and vulnerability in a dynamic system like mega cities research must shift from unilateral perspectives to multi-perspective analysis in the future to achieve complementary surplus value results.

References

- Applied Technology Council (ATC) (1997). 40-Report: Seismic Evaluation and Retrofit of concrete Buildings.
- Aydinoglu, N. and M. Erdik (2002). Earthquake Performance and Vulnerability in Turkey. Department of Earthquake Engineering, Kandilli Observatory an Earthquake Research Institute, Bogazici University.
- Birkmann, J. (2006). Measuring Vulnerability to Natural hazards – Towards Disaster Resilient Societies. New York, United Nations University. S. 524.
- DKKV – DEUTSCHE KOMITEE KATASTROPHENVORSORGE E. V. (2003). Lessons learned – Hochwasservorsorge in Deutschland: Kurzfassung für die Versicherungswirtschaft. <http://www.dkkv.org/DE/publications/schriftenreihe.asp?h=5> .
- Metropolitan Municipality of Istanbul (2003). Earthquake Master Plan for Istanbul, 2003.
- Münich, J., H. Taubenböck, L. Stempniewski, S. Dech, and A. Roth (2006). Remote sensing and engineering: An interdisciplinary approach to assess vulnerability in urban area. *Proceedings of the First European Conference on Earthquake Engineering and Seismology*, Geneva, Switzerland, pp.10.
- Parsons, T. (2004). Recalculated probability of $M \geq 7$ earthquakes beneath the Sea of Marmara, Turkey. *J. Geophys. Res.* **109**, B05304, doi:10.129/2003JB002667.
- Pelling, M. (2003). The Vulnerability of Cities – Natural Disasters and Social Resilience. Earthscan Publications Ltd., pp. 212, ISBN 1 85383 830 6, London.
- Taubenböck, H. (2008). Vulnerabilitätsabschätzung der Megacity Istanbul mit Methoden der Fernerkundung. PhD-Thesis. University of Würzburg; pp. 178. (Online-Publication: <http://www.opus-bayern.de/uni-wuerzburg/volltexte/2008/2804/>).

- Taubenböck, H., J. Post, A. Roth, K. Zosseder, G. Strunz, and S. Dech (2008). A conceptual vulnerability and risk framework as outline to identify capabilities of remote sensing. *Natural Hazards and Earth System Sciences* **8**(3), 409-420 (<http://www.nat-hazards-earth-syst-sci.net/8/409/2008/nhess-8-409-2008.html>).
- Taubenböck, H., A. Roth, and S. Dech (2007a). Vulnerability assessment using remote sensing: The earthquake prone megacity Istanbul, Turkey. *International Symposium on Remote Sensing and Environment*, San Jose, Costa Rica. pp. 5.
- Taubenböck, H., A. Roth, and S. Dech (2007b). Linking structural urban characteristics derived from high resolution satellite data to population distribution. Urban and Regional Data Management. In: *COORS, RUMOR, FENDEL & ZLATANOVA (Hrsg.)*. Taylor & Francis Group, London, ISBN 978-0-41544059-2. S. 35-45.
- Voigt, S, T. Kemper, T. Riedlinger, R. Kiefl, K. Scholte, and H. Mehl (2007). Satellite Image Analysis for Disaster and Crisis-Management Support. *IEEE Transactions on Geoscience and Remote Sensing* **45**(6), 1520-1528.
- Zschau, J., M. Isikara, O. Ergünay, M. N. Yalcin, and M. Erdik (2002). Towards an earthquake early warning system for the megacity Istanbul. *Early Warning Systems for Natural Disaster Reduction*, edited by J. Zschau and A. Küppers, 433-440, Springer.

4. Stress Field Modelling in the Marmara Sea Region

O. Heidbach¹, F. Wenzel¹, and T. Hergert²

¹Geophysical Institute, Universität Karlsruhe (TH), Herzstr. 16, 76187, Karlsruhe, Germany

²Heidelberg Academy of Sciences and Humanities, Heidelberg, Germany

Summary

During the last decade earthquake hazard assessment in Marmara Sea region has been investigated by several approaches based on Coulomb failure stress changes, earthquake recurrence rates, geodetic analyses, seismic moment-frequency relationships, and others. In our work we present for the first time a 4D numerical model that simulates the absolute stress state and its temporal changes. Our model results are consistent with a number of model-independent constraints such as stress observations, GPS data, fault-slip data, basin evolution, and tectonic regime. The model geometry includes the complex 3D fault system, topography, bathymetry, water load, basement, and Moho structure. The model is driven by gravity and kinematic boundary conditions to account for the tectonic loading. The results give a detailed picture of the kinematic pattern below sea level and at the fault segments. It reveals that slip-rates along the main fault in the Marmara Sea vary significantly along strike and that the displacement rates of the main fault is smaller (12.5-18 mm/a) than previously anticipated from other models (16-30 mm/a). The forward model is capable to reproduce the co-seismic slip of the Izmit 1999 that results from the modelled initial stress field and the tectonic loading of the ruptured segment. The result of this test shows a remarkably good fit between the modelled co-seismic slip and the observed one. Given this promising result the model can be used to simulate future slip-distributions on the central segment that is expected to fail next. Tobias Hergert will submit his PhD thesis on the results in Nov. 2008 at the Physics Faculty of the Karlsruhe Universität TH). Besides the presentation of the main results on a number of international workshops we currently prepare publications of the results in international journals.

Introduction

The last event within the west propagating sequence of major earthquakes along the North Anatolian Fault was the 1999 Izmit earthquake that reached the eastern Sea of Marmara. Analyses of historical earthquakes yielded a seismic gap in the Marmara Sea since 1766 or 1509 (e.g. Ambraseys, 2002) and analyses of Coulomb Failure Stress changes due to the 1999 earthquakes showed that a major earthquake beneath the Sea of Marmara has definitely to be expected (e.g. Parsons 2004). However, these numerical models were based on simplified faults structures and a homogeneous or layered rheology.

This study aims at the quantification of the contemporary absolute stress state, the displacement field and fault-slip rate, and to assess the todays seismic hazard. The 3D numerical model incorporates the 3D geometry and rheology of the Marmara Sea region with a model times of 20 ka (time-independent or steady-state model, chapter 4) and a fraction of a seismic cycle (time-dependendt model, chapter 5). Hitherto numerical models of the region addressing these goals either concentrated on the kinematics omitting the stress field or calculated stress changes. However, co-seismic stress changes do not provide information on changed probabilities without further assumptions such as e.g. fault slip rates or recurrence rates. Thus, a key aspect is to model not stress changes but the absolute stress state. A model of the absolute stress state that simultaneously accounts for the kinematics can be used to deduce the proximity of a fault towards failure by using e.g. empirical rock strength data or scaling relations. Furthermore, potential slip on a certain fault segment at a given time can be assessed.

Model setup

Modelling the absolute stress state requires incorporation of density heterogeneities such as topography/bathymetry, basement-topography, moho as well as the associated variations in elastic properties (Fig. 1). The 3D fault system of the NAF with curved and dipping faults adopted from seismics is assigned with Coulomb friction. The Marmara model is driven at its lateral boundaries by the velocity field obtained from a larger model covering northwest Anatolia and that agrees with GPS observations (see earlier report). The model consists of ~640,000 elements allowing a resolution in the subkilometer range in the most critical areas and is solved using the commercial ABAQUSTM software package.

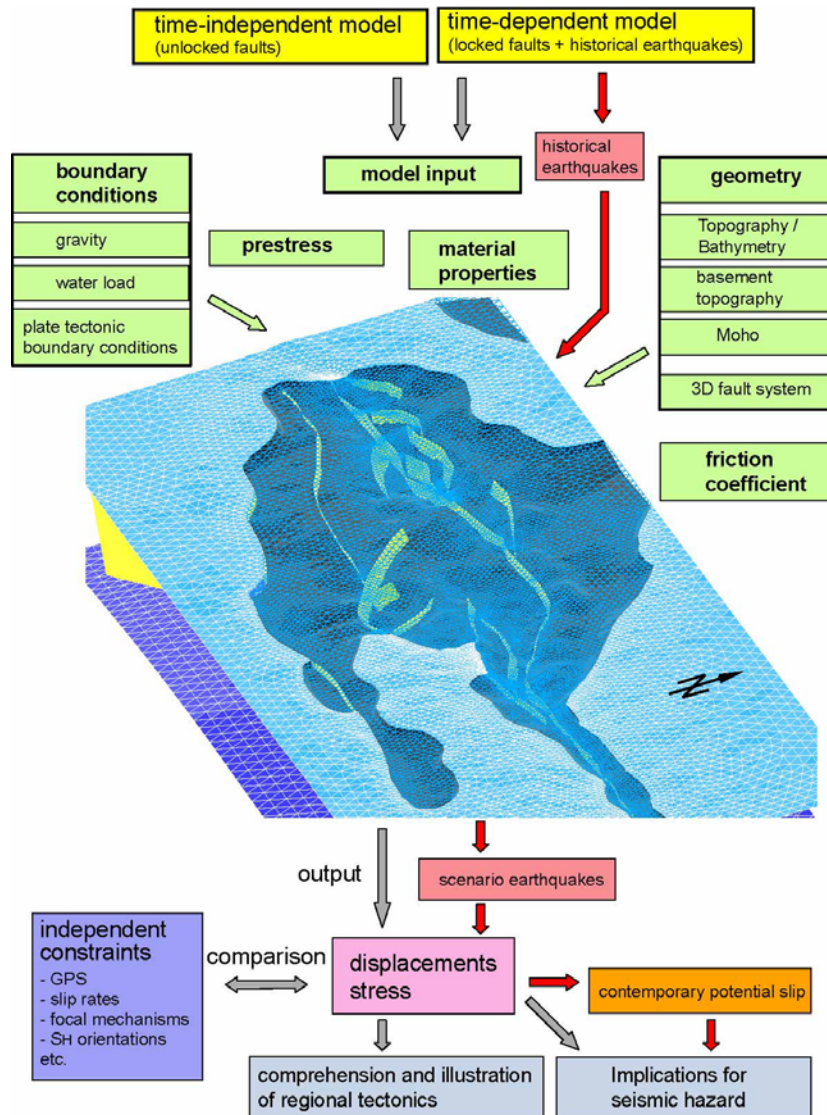


Fig. 1: Finite element mesh and modelling concept. The model incorporates the active fault system (yellow), topography and bathymetry (solid and transparent light blue, respectively), basement topography (dark grey) and the Moho (blue). Green boxes indicate the model input (geometry, boundary conditions, and material properties). Red arrows mark the additional work flow of the time-independent model with respect to the time-dependent one (grey arrows).

Two models are considered: (1) Unlocked faults simulating the long-term kinematics and stress field (time-independent model). (2) Locked faults and including historical earthquakes (time-dependent model) to determine the contemporary and temporal evolution of the state of stress (Fig. 1). The output of the model is compared with a number of model-independent constraints

such as stress observations, GPS data, fault-slip data, basin evolution, and tectonic regime (Fig. 1).

Time-independent model results

The modelled maximum horizontal stress is oriented NW-SE in the Marmara region with local deviations, e.g. EW on northern Armutlu Peninsula and in the western Marmara Sea, and NNW-SSE on the Central High in agreement to World Stress Map data (Fig. 2). Modelled principle stress orientations indicate a strike-slip to extensional stress regime with σ_1 and σ_2 either being the vertical or maximum horizontal stress axis in NW-SE orientation, whereas σ_3 is horizontal representing the minimum horizontal stress with a NE-SW orientation, which is in good agreement to inversions of earthquake focal mechanisms (Fig. 3). Fig. 4 displays the stress regime in more detail in terms of the stress regime ratio (Simpson, 1997). A transitional stress regime between strike-slip and transtension prevails. The basins are characterised by extension as well as Armutlu Peninsula, while compression is restricted to small areas east of the Central Basin, in the westernmost Izmit Bay and between Marmara Island and Ganos Bend. Fault normal stress undergoes significant lateral variations along the main Marmara Fault in the order of several hundreds of MPa (Fig. 5). This may have decisive implications for seismic hazard since a lower normal stress should require less shear stress and hence less loading time to reach the failure criterion when presupposing the validity of Mohr-Coulomb theory. Therefore, the Prince Island's segment is expectable to fail more frequently than e.g. the central segment which is under relatively high normal stress.

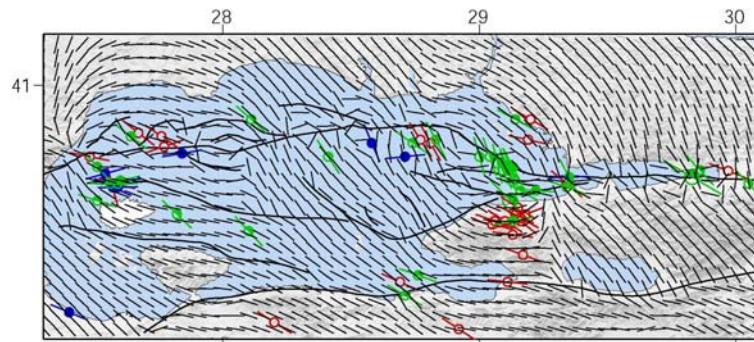


Fig. 2: Modelled maximum horizontal stress orientations at 5 km depth (black lines) in comparison to World Stress Map data (coloured lines).

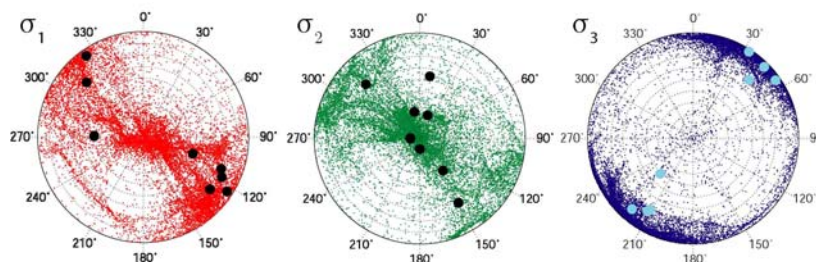


Fig. 3: Modelled principle stresses at 5 km depth on a dense grid ($0.01^\circ\text{E} \times 0.01^\circ\text{N}$) over the whole model area. Thick dots indicate reported principle stress orientations from inversion of earthquake focal mechanisms for various sub areas (Gürbüz et al. 2000; Polat et al. 2002; Pinar et al. 2003; Bohnhoff et al., 2006).

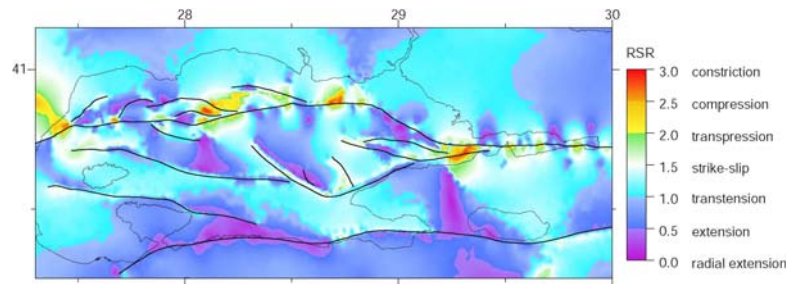


Fig. 4: Modelled stress regime at 5 km depth in terms of the stress regime ratio (Simpson, 1997).

The modelled differential stress is shown in Fig. 6 as well as its ratio with respect to a critical differential stress (called fracture potential) determined by an internal coefficient of friction $\mu_i = 0.64$, and a cohesion C_0 of 31 MPa, typical for granite (Jaeger and Cook, 1969). High differential stresses and fracture potential characterise the western Marmara Sea and eastern Cinarcik basin, whereas the Central High transected by the central segment of the Main Marmara Fault is under relatively low differential stresses and fracture potential. A comparison with seismicity reveals that the model reproduces the first order pattern of seismicity. Note that this differential stress analysis is from the time-independent model that provides the steady state characteristic of the rate in differential stress increase due to the interaction between fault geometry and plate motion. This result does not directly pertain to seismic hazard since here the fracturing of rock in the volume is addressed that locally evolves adjacent to faults, expressed by microseismicity, whereas large earthquakes normally occur on faults. However, it may be concluded that the main branch between Istanbul Bend and Central basin is capable of accumulating high levels of shear stress without reaching critical differential stresses in the surrounding of the fault.

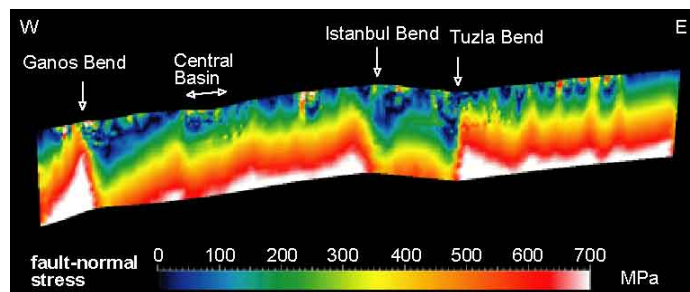


Fig. 5: Modelled normal stress on the main Marmara Fault.

The primary purpose behind the time-independent model is to quantify how relative plate motion is accommodated across the plate boundary zone, and in particular, to infer the slip rate on the main Marmara Fault. The modelled right-lateral slip rate on the main Marmara Fault is ~ 12.5 - 18 mm/yr within the model area, depending on location (Fig. 7). Slip rate on the Prince Island's segment is clearly reduced compared to the adjacent fault sections. The Ganos Fault to the west of the Marmara Sea slips at higher rates than the NAF below the Marmara Sea. These variations in slip rate should play a decisive role for seismic hazard in the Marmara Sea since the slip rate on a fault controls the rate of annual growth in shear stress. Maybe, this explains why the 1912 Ganos event did not keep to the stepwise migration of earthquakes which is typical for the NAF east of the Marmara Sea and why an unbroken segment in the Marmara Sea remains.

The inferred slip rates are lower than the commonly assumed 20 mm/yr based on geodetic observations. The lower slip rates can be well explained by the complexity of the fault system in the Marmara Sea as well as by deformable rock whereas geodetic studies commonly assume rigid block behaviour (e.g. Meade et al., 2002). Fig. 8 indicates how relative plate motion is

partitioned on the respective branches of the fault system in the Marmara Sea. Though none of the smaller faults accommodates more than 3 mm/yr, their cumulative contribution is not negligible and explains most of the reduction in the slip rate on the main branch compared to the hitherto discussed rates. The gradients in EW velocity indicate also internal deformation in the volume between the faults accounting for some fraction of relative plate motion (Fig. 8). In view of the modelled total relative motion across the width of the model (~20 mm/yr) it is important to note, that the model does not cover the whole plate boundary zone. The GPS observed relative plate motion between Uludag mountain south of the southern branch of the NAF and Istanbul is ~22 mm/yr (Straub et al., 1997). Keeping in mind that the southern branch of the NAF is beyond the southern model boundary, the inferred result can be well reconciled with GPS observations.

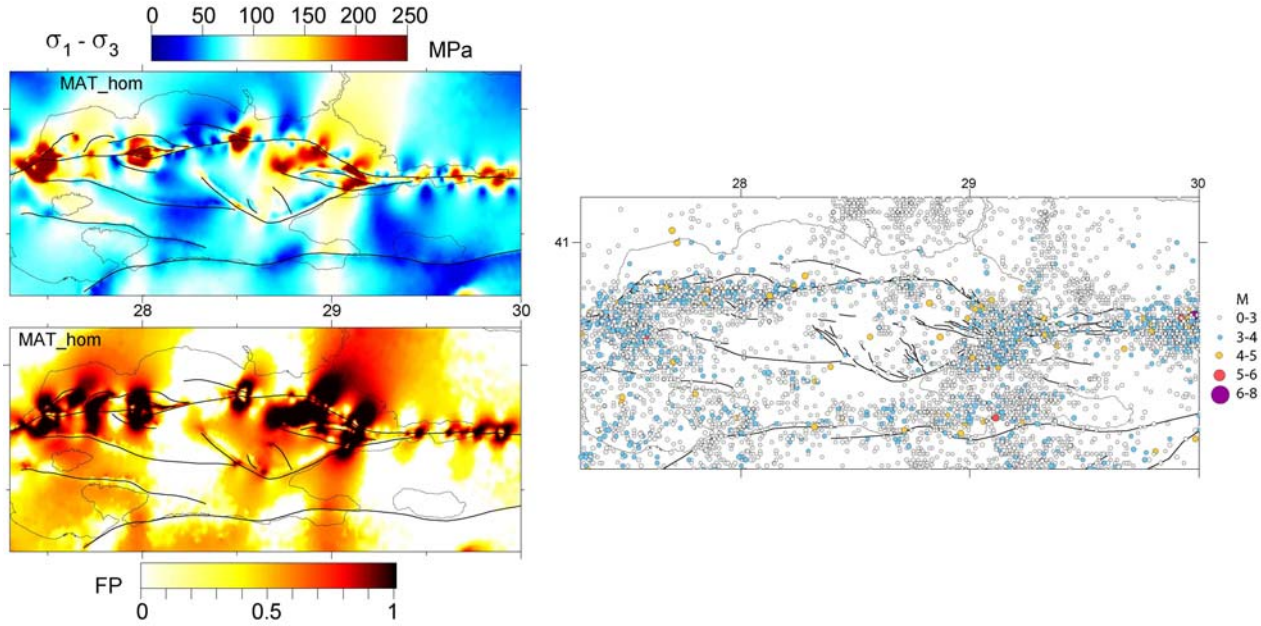


Fig. 6: Modelled differential stress $\sigma_1 - \sigma_3$ at 5 km depth (left top) and calculated fracture potential (left bottom) in comparison to seismicity (right; 1973-1989 and 2005-August 2008 from USGS NEIC catalogue and 1990-2004 from Kandilli catalogue).

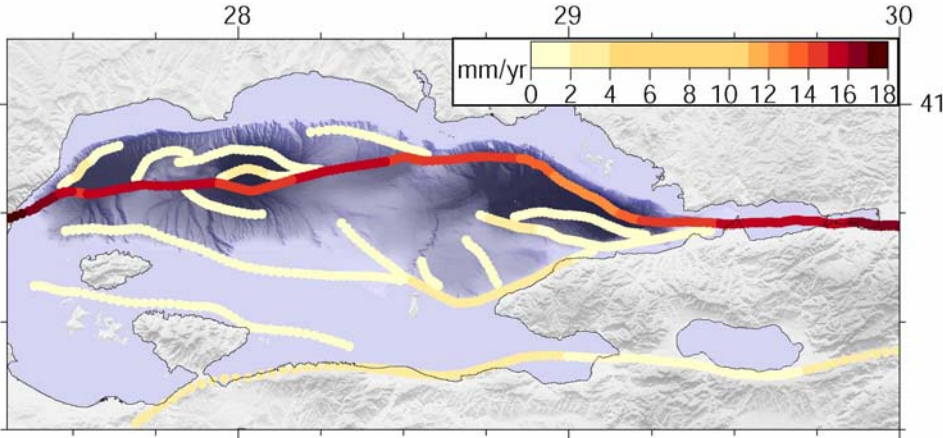


Fig. 7: Modelled right-lateral fault slip rates at the surface.

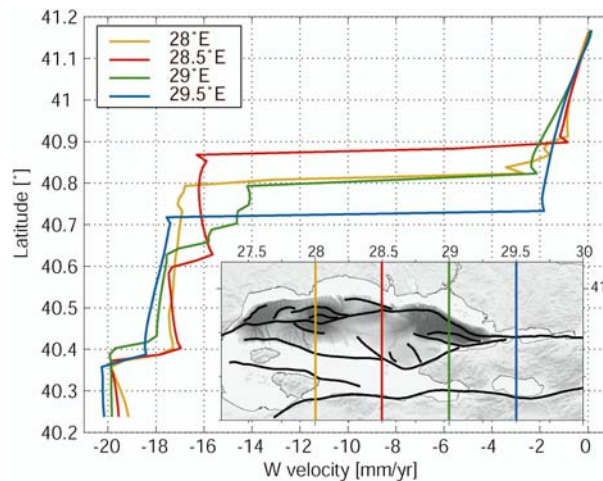


Fig. 8: Modelled EW velocities at different longitudes across the plate boundary zone.

Time-dependent Model

Unlike the time-independent model with unlocked faults, the time-dependent model considers the seismic cycle (Fig. 1). Beginning in the year 1719 the implemented faults were locked and specific fault segments were intermittently unlocked during known historical earthquakes so that the meanwhile accrued shear stresses due to the plate tectonic boundary conditions were released. The interseismic velocity field of the time-dependent model was compared with GPS observations and the modelled 1999 Izmit earthquake with reported co-seismic surface displacements, surface slip and slip at depth. The results of this comparison show that this forward model approach is capable to reproduce the co-seismic slip of the Izmit 1999 that results from the modelled initial stress field and the tectonic loading of the ruptured segment. The deviation between the modelled co-seismic slip and the observed one is remarkably small. This allows assessment of contemporary seismic hazard by modelling scenario earthquakes, i.e. a given fault segment is released at a certain time. This analysis is currently ongoing and will be finished within October/November 2008.

Acknowledgements

We would like to acknowledge the Heidelberg Academy of Sciences and Humanities for additional financial support of the project. We also would like to thank Anne Becél and Alfred Hirn from the IPG in Paris for the 3D fault data from the Seismarmara cruise, that they shared their knowledge with us, and for the very fruitful discussions.

References

- Ambraseys, N. (2002). The Seismic Activity of the Marmara Sea Region over the Last 2000 Years. *Bull. Seism. Soc. Am.* **92**, 1-18.
- Bohnhoff, M., H. Grosser, and G. Dresen (2006). Strain partitioning and stress rotation at the North Anatolian fault zone from aftershock focal mechanisms of the 1999 Izmit Mw=7.4 earthquake. *Geophys. J. Int.* **166**, 373-385, doi:310.1111/j.1365-1246X.2006.03027.x.
- Gurbuz, C., M. Aktar, H. Eyidogan, A. Cisternas, H. Haessler, A. Barka, M. Ergin, N. Türkelli, O. Polat, S. B. Üçer, S. Kuleli, S. Baris, B. Kaypak, T. Bekler, E. Zor, F. Bicmen, and A. Yoruk (2000). The seismotectonics of the Marmara region (Turkey): results from a microseismic experiment. *Tectonophysics* **316**, 1-17, PII: S0040-1951(0099)00253-X.
- Jaeger, J. C., and N. G. W. Cook (1969). *Fundamentals of Rock Mechanics*. Chapman and Hall, London.
- Meade, B. J., B. H. Hager, S. C. McClusky, R. E. Reilinger, S. Ergintav, O. Lenk, A. Barka, and H. Ozener (2002). Estimates of Seismic Potential in the Marmara Sea Region from Block Models of Secular Deformation Constrained by GPS Measurements. *Bull. Seism. Soc. Am.* **92**, 208-215.

- Parsons, T. (2004). Recalculated probability of $M \geq 7$ earthquakes beneath the Sea of Marmara, Turkey. *J. Geophys. Res.* **109**, doi:10.1029/2003JB002667.
- Pinar, A., K. Kuge, and Y. Honkura (2003). Moment tensor inversion of recent small to moderate sized earthquakes: implications for seismic hazard and active tectonics beneath the Sea of Marmara. *Geophys. J. Int.* **153**, 133-145.
- Polat, O., H. Eyidogan, H. Haessler, A. Cisternas, H. Philip (2002). Analysis and interpretation of the aftershock sequence of the August 17, 1999, Izmit (Turkey) earthquake. *J. Seism.* **6**, 287-306.
- Simpson, R. W. (1997). Quantifying Anderson's fault types. *J. Geophys. Res.* **102**, 17909-17919.
- Straub, C., H.-G. Kahle, and C. Schindler (1997). GPS and geologic estimates of the tectonic activity in the Marmara Sea region, NW Anatolia, *J. Geophys. Res.* **102**, 27,587-527,601.

5. Crustal Attenuation, Empirical Ground Motion Prediction Equations and Source Parameters for Northwestern Turkey

D. Bindi², S. Parolai¹, H. Grosser¹, C. Milkereit¹, E. Durukal³, S. Karakisa⁴, S. Zünbül⁴ and J. Zschau¹

¹Helmholtz Centre Potsdam GFZ German Research Centre for Geosciences, Section 2.1 "Earthquake Risk and Early Warning", Telegrafenberg, D-14473 Potsdam, Germany

²Istituto Nazionale di Geofisica e Vulcanologia, Via Bassini 15, 20133 Milano, Italy

³Boğaziçi Üniversitesi, Kandilli Rasathanesi ve Deprem Araştırma Enstitüsü, Department of Earthquake Engineering, 34684, Çengelköy, Istanbul, Turkey

⁴Ministry of Public Works and Settlement General Directorate of Disaster Affairs Earthquake Research Department, P.O. Box 763, Ankara, Turkey

Introduction

In this report, we collect some results provided by several seismological studies carried out in northwestern Turkey within the CEDIM project Megacity-Istanbul. In particular, the source parameters (seismic moment and stress drop) of the aftershocks of the 1999 Kocaeli earthquake were computed and their scaling laws investigated, as well as the relationship between the moment magnitude and the local magnitude computed accordingly to an ad-hoc scale calibrated for the area. The properties of the seismic attenuation in the crust were described in terms of quality factor and geometrical spreading, determining also their dependence on frequency. Finally, empirical ground motion prediction equations were developed for several strong motion parameters (peak ground acceleration, peak ground velocity, spectral ordinates), evaluated for different component of motion (maximum horizontal and vertical). The predictive models were developed considering as explanatory variables the epicentral and the hypocentral distance, the local magnitude M_l and the moment magnitude M_w , and a binary site classification (rock and soil).

Data

The aftershocks of the M_w 7.4 Kocaeli recorded between August 1999 and December 1999 were considered to compute the source parameters and to calibrate the attenuation models. Among the aftershocks recorded by the 53 stations of the German Task Force (GTF), Sapanca-Bolu (SABO) and Kandilli Observatory and Earthquake Research Institute (KOERI) networks, the recordings of 523 earthquakes with M_l values ranging between 0.5 and 5.9 were considered. GTF and SABO networks consist of 1-Hz geophones (Mark L4-3D), a 24-bit digitizer with a sampling rate of 100 sps and Global Positioning System (GPS) timing. The KOERI strong-motion network consist of GeoSys GSR-16 and Kinematics SSA-2 strong motion stations working with sampling rates of 200 samples/sec.

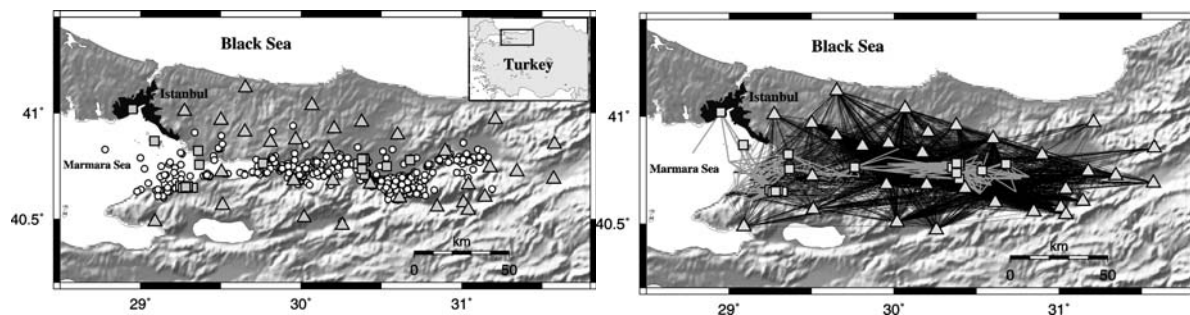


Fig. 1: (Left) epicentral location (circles), seismological GTF and SABO (triangles) and strong-motion (KOERI) stations (squares). (Right) Epicentre to seismic station ray paths (black lines)- Epicentre to strong-motion station ray paths (grey lines).

The selection of the events was carried out with the aim of obtaining satisfactory ray-path coverage of the area from well-located events (Figure 1). The hypocenter locations of the selected earthquakes, calculated using a standard procedure (Bindi et al., 2007a), lead to root mean squares (rms) values of the travel time residuals smaller than 0.5 s, with an average value of 0.13 s. The horizontal and vertical statistical errors are smaller than 1.8 and 2 km, respectively. The reader is referred to Baumbach et al. (2003), Parolai et al. (2004), Bindi et al. (2006a) and Bindi et al. (2006b) for more detailed information about the data set.

Generalized inversion technique

Source spectra and the spectral attenuation with distance were obtained by generalized spectra inversion (e.g., Castro et al., 1990), which allows the separation of the site, path, and source contributions from the observed spectra. This is achieved after having taken the logarithm of the spectra of the recordings—of several earthquakes registered by different stations—and solving the resulting linear system in a least-squares sense. A two-step nonparametric approach was adopted here for the inversion, where the attenuation with distance function $A(f,r)$ is provided by the first step. In the second step, the data corrected for the attenuation are inverted to split the source and site contributions. The distance range covered by the data set (10–190 km) was discretized into 60 bins with widths of 3 km. The inversion was performed separately for each of the 70 selected frequencies, equi-spaced in logarithmic scale between 0.4 and 25 Hz, using the least-squares algorithm (LSQR) of Paige and Saunders (1982). A detailed description of the inversion can be found in Parolai et al. (2004) and Bindi et al. (2006a).

For all recordings, the Fast Fourier Transform (FFT) of a 5 s window of signal, starting 1 second before the S-wave arrival was calculated. If the difference between S- and P-wave arrival times was smaller than 1 s the window was shifted in order to avoid the main P-wave arrival energy. Windows of maximum duration equal to 5s and encompassing the P-wave were also extracted. Trends from the chosen signal windows were removed, and a 5% cosine taper was applied at both ends before the FFT calculation. Spectra were corrected for the instrumental response of the sensors and smoothed using a Konno and Ohmachi (1998) window with $b = 20$.

Source parameters and scaling laws

Local magnitude scale

A calibrated earthquake catalogue based on M_l is of great importance for seismic hazard studies, as well pointed out in the IASPEI New Manual of Seismological Observatory Practice (Bormann, 2002). Moreover, the value of the correction for amplitude decrease with distance gives useful insights for a better understanding of seismic wave propagation in the area. Furthermore, within the framework of the project Megacity-Istanbul, new attenuation relationships for northwestern Turkey had to be derived. This required a well-constrained magnitude scale that can be applied to a data set including not only the earthquakes recorded by the seismic networks deployed in northwestern Turkey but also strong-motion data.

We calibrated a local magnitude scale following the standard nonparametric approach (e.g., Richter, 1935):

$$\log A(R) = M_l + \log A_0(R_i) + S \quad (1)$$

where A is the measured maximum horizontal amplitude in millimetres read from the synthesized Wood–Anderson seismogram, R is the hypocentral distance, $\log A_0$ is the distance dependent attenuation curve, and S is a station-dependent magnitude adjustment factor. In equation (1), R_i represents the knots of the discretization and $R_i \leq R \leq R_{i+1}$. We add several constraints to equation (1). The first, the $\log A_0$ function is constrained to assume the value -2

at 17 km and to be a smooth function with distance by constraining the second derivative to be small. To avoid the trade-off between station corrections and magnitudes, a constraint is also applied to S . In particular, we add two rows to the linear system derived from (1): in the first row, we constrain S for station 39 (i.e., the reference station) to be zero, and in the second row, we require that the station corrections for the KOERI accelerometer network sum to zero, because a reference station is not available for the accelerometer network. Details about the calibrated magnitude scale can be found in Bindi et al. (2007a).

Source parameters

The source spectra were obtained by applying the generalized inversion technique. To derive source parameters such as seismic moment (M_0), corner frequency (f_c), and the Brune stress-drop ($\Delta\sigma_B$) a two-step procedure was followed. In a first step, displacement source spectra were fitted to a ω -square source model with only one corner frequency (Brune, 1970), assuming an S-wave velocity of 3.5 km/sec, a density of 2800 kg/m³ and an average radiation pattern of 0.6. A grid search procedure was applied to $\Delta\sigma_B$ and the seismic moment M_0 in order to minimize the root-mean-square error between the logarithm of the observed and calculated spectra over the frequency range 0.4-25 Hz. In a second step, acceleration source spectra were fitted by considering not only a ω -square model, but also a high-frequency diminution function described in terms of the k parameter (Anderson and Hough, 1984; Purvance and Anderson, 2003). The high-frequency diminution function was applied from 12 Hz, which for this data set is where the high-frequency decay generally begins. The second step constrains M_0 to the value calculated in step 1, and allows for a grid search for $\Delta\sigma_B$ and k .

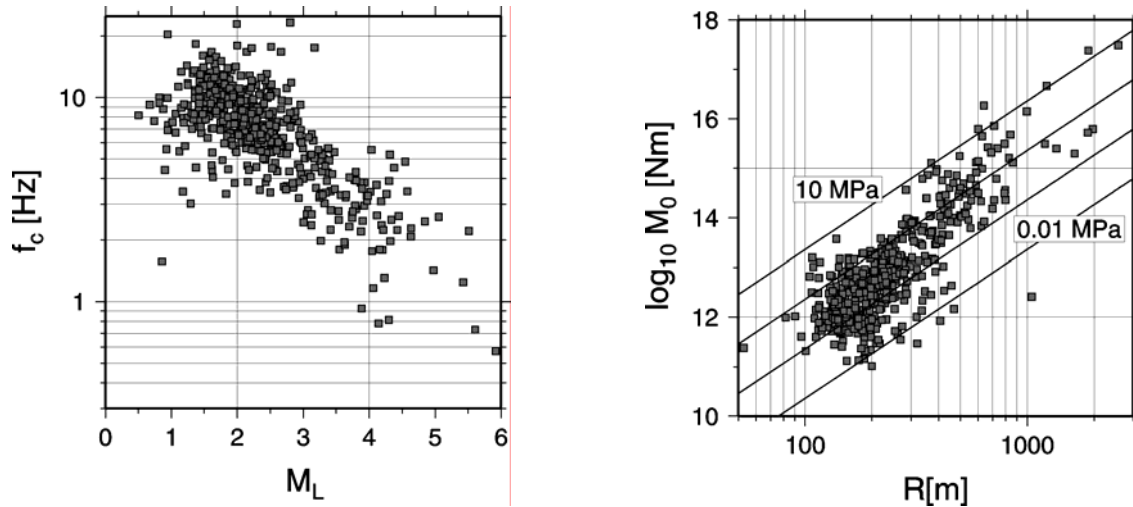


Fig. 2: (Left) f_c versus M_L . (Right) $\log_{10}M_0$ versus source radius R . Line (black) of constant $\Delta\sigma_B$ between 0.01 MPa and 10 MPa is shown.

Figure 2 shows graphically the scaling between f_c and M_L and between M_0 and the Brune source radius. A clear scaling of the corner frequency with M_L is observed within the full magnitude range considered ($0.5 \leq M_L \leq 5.9$). This is reflected in the scaling of the source radius versus the M_0 , where the source radius varies from nearly 100 m to 2.5 km. Consistent with previous studies (e.g., Abercrombie, 1995), no evidence of self-similarity breakdown is observed within the range of M_0 investigated ($1.05 \times 10^{14} \leq M_0 \leq 2.41 \times 10^{17}$ Nm). However, a tendency for $\Delta\sigma_B$ (varying between 2 kPa and 40 MPa, but with the great majority of values between 10 kPa and 10 MPa) to increase with M_0 is shown in Figure 2. The large scattering shown by the $\Delta\sigma_B$ values may be related to the hypocentral location and the focal mechanism.

In Figure 3, M_0 (left) and M_w (right), obtained using the equation of Kanamori (1977), are shown versus M_L . A linear orthogonal regression between $\log_{10}M_0$ and M_L (black line in Fig. 4, left) led to the equation:

$$\log_{10} M_0 = (1.17 \pm 0.01)M_L + (10.12 \pm 0.02) \quad (2)$$

Although this relationship is in good agreement with that of Grosser et al. (1998) (gray line) calculated from the aftershocks of the Erzican earthquake, it differs from that of Durukal and Çatalyürekli (2004) (dashed line). We think that this disagreement may be due to the use of a M_L scale with coefficients not calibrated for the area in the latter study.

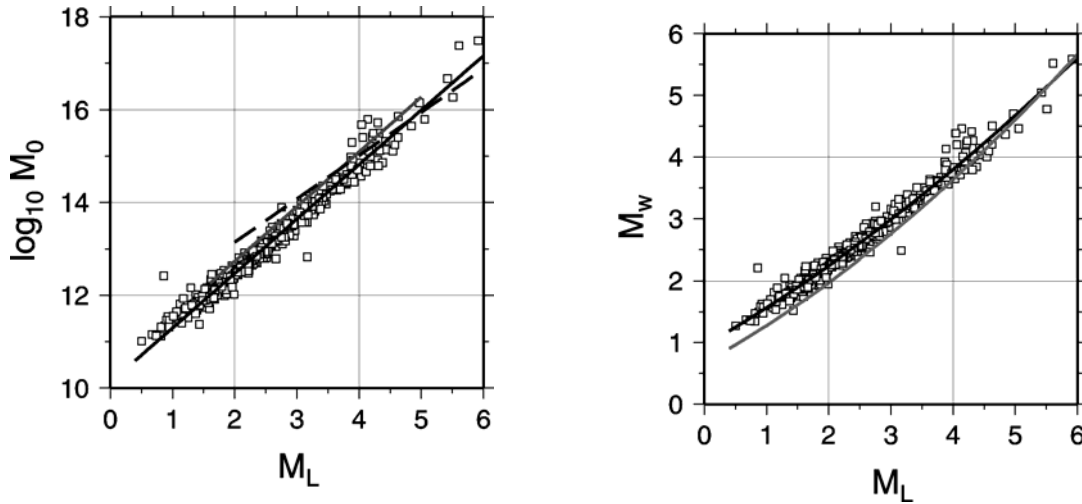


Fig. 3: (Left) $\log_{10}M_0$ versus M_L (squares). Equation (2) from this study (black line), Grosser et al. (1998) (gray line), and Durukal and Çatalyürekli (2004) (dashed line). (Bottom) M_w versus M_L (squares). Equation (4) from this study (black line) and Stromeyer et al. (2004) (grey line).

Results of the regression between M_w and M_L are shown in Figure 3 (right). In this case, a nonlinear least-squares regression was carried out considering a quadratic term. Since the regression is not orthogonal, it was carried out in two ways, considering, in one case, M_L , and in the other, M_w , as independent variables. The new relationship shows a good agreement, in general, with the chi-square regression derived by Stromeyer et al. (2004) (grey line) for continental Europe. Small discrepancies may be due to the different tectonic regimes of the areas in which the data sets have been collected. Details about the results can be found in Parolai et al. (2007).

Crustal attenuation

The generalized inversion technique was also applied to derive the spectral attenuation with distance. The nonparametric attenuation functions $A(f,r)$ provided by the first step were parameterized in terms of quality factor $Q(f)$ and geometrical spreading r^{-n} . Since the attenuation functions were computed for both P- and S-wave, an estimate of both $Q_p(f)$ and $Q_s(f)$ were obtained. Since the attenuation functions $A(f,r)$ showed a bump between 40 and 60 km, the parameterization of $A(f,r)$ was performed over two different distance ranges, one over the range 10-38 km and the other over the range 60-80 km. For distances larger than 80-90 km are characterized by the presence of critical Moho reflections.

The obtained dependence on frequency of the quality factor over the range 10-38 km was described by the following equations:

$$Q_s(f) = (17 \pm 1)f^{(0.80 \pm 0.01)} \quad \text{for } 1 \leq f \leq 10 \text{ Hz} \quad (3)$$

$$Q_p(f) = (56 \pm 4)f^{(0.25 \pm 0.05)} \quad \text{for } 2.5 \leq f \leq 10 \text{ Hz} \quad (4)$$

being the geometrical spreading exponent n close to 1, regardless the frequency.

Over the distance range 60-80 km, the propagation characteristics of P and S waves are more complex over this range than those observed in the range from 10 to 38 km. In particular, the geometrical spreading n is frequency dependent, for both S and P waves. The mean values vary between 0.95 and 1.35 for S waves and from 0.75 to 1.28 for P waves.

The multi lapse time window analysis (MLTWA) (e.g. Hoshiya, 1991) is used to estimate the contribution of scattering loss and intrinsic absorption to total attenuation. The results of MLTWA analysis indicate that the intrinsic absorption contributes equally to scattering loss in determining the total attenuation at low frequencies, but it becomes the dominant mechanism at high frequencies, suggesting that the coda could be mainly generated by a back-scattering mechanism (Menke and Chen, 1984).

Finally, the spectral amplitudes at frequencies higher than 10 Hz are analyzed to investigate the effect of local geology on seismic-wave attenuation by computing the k parameter (Anderson and Hough, 1984). The k parameter is calculated as the high-frequency asymptote of the acceleration spectrum $A(f)$:

$$A(f) = A_0 e^{-\pi k f} \quad (5)$$

where A_0 depends upon the source, epicentral distance, and other factors. Since site amplification, within the frequency range considered for evaluating k , could affect the slope of the spectrum decay (Parolai and Bindi, 2004), we discarded stations that exhibited peaks of amplification in the high frequency range (Parolai et al., 2004) and the analysis was performed on a subset of 12 stations of the GTF and SABO networks. Following Purvance and Anderson (2003), the source, site and distance contributions to the estimated k values were separated by performing a linear regression. The results showed that most of the site contributions to k are smaller than 0.01sec. Only two stations of the GTF network installed over thick sediments in the Adapazari basin and in the Yalova area showed site contribution to k greater than 0.03 sec (Bindi et al., 2006b). Furthermore, the results showed that the source contribution to k correlates with magnitude, in agreement with the results of Purvance and Anderson (2003).

Empirical Ground motion prediction equations

The aftershocks of the 1999 Kocaeli earthquake were also used to develop a set of empirical ground motion prediction equations (GrMPEs) for northwestern Turkey. The empirical GrMPEs were calibrated for peak ground acceleration (PGA), peak ground velocity (PGV) and for the spectral acceleration (SA) of a 5% critical damped oscillator, considering the maximum between the North-South and East-West components, as well as the vertical component. The inter-event and inter-station distributions of error, computed by applying the random-effects approach (e.g. Abrahamson and Youngs, 1992), were compared for different choices of the design variables. To enlarge the compatibility of the models with the seismic parametric catalogues used for hazard assessment, the empirical GrMPEs are derived for both the local (M_l) and moment (M_w) magnitudes, and for both hypocentral and epicentral distances. For the epicentral distance, the following functional form was considered (Ambraseys et al., 2005):

$$\log_{10} Y = a + bM + (c + dM) \log_{10} (R^2 + h^2)^{0.5} + s_{1,2} \quad (6)$$

where Y is the variable of interest (measured in the International System of Units), that is the PGA, PGV, or SA, M is the magnitude, and R represents either the epicentral (R_{epi}) or the hypocentral (R_{hypo}) distances (in km). The standard deviation on $\log_{10} Y$, σ_{tot} , is given by $\sigma_{tot}^2 = \sigma_{eve}^2 + \sigma_{sta}^2 + \sigma_{rec}^2$, where σ_{eve}^2 , σ_{sta}^2 , σ_{rec}^2 are the inter-event, inter-station and record-to-record components of variance, respectively. The parameter h in equation (6) (set equal to 0 when R_{hypo} is considered) represents a pseudo-depth parameter that accounts for the saturation of $\log_{10} Y$ when R_{epi} becomes small. A two-class site classification scheme (rock and soil) was considered, considering the site amplification functions provided by the generalized

inversion (Bindi et al 2007b). Table 1 exemplifies the results obtained considering M_w and R_{epi} as explanatory variables, and the maximum horizontal component, while Figure 4 shows some of the results in a graphical form.

Finally, the analysis of the error distribution showed that the record-to-record component of variance is the largest contribution to the variance of the calibrated ground-motion models. Moreover, although the contribution of the inter-event component of error to the total error is negligible, it is correlated to the stress-drop variability and it is higher when the regressions are performed considering the moment magnitude than when local magnitude is used.

f[Hz]	a	b	c	d	h	σ_2	σ_{eve}	σ_{sta}	σ_{rec}	σ_{tot}
1.00	-5.0589	1.0686	-1.6352	0.1182	3.6216	0.2763	0.0659	0.0668	0.2794	0.2947
1.35	-4.4954	0.9953	-1.9214	0.2001	4.3071	0.2578	0.0686	0.0695	0.2908	0.3068
2.00	-4.1727	1.0178	-1.8871	0.1848	4.8789	0.2762	0.0725	0.0733	0.3078	0.3246
2.50	-4.0438	1.0239	-1.8056	0.1648	4.8047	0.3018	0.0750	0.0757	0.3182	0.3356
3.33	-3.8444	1.0274	-1.7306	0.1436	4.2397	0.2926	0.0767	0.0775	0.3253	0.3431
5.00	-3.8140	1.1205	-1.4597	0.0346	3.4580	0.3839	0.0744	0.0754	0.3154	0.3327
6.25	-3.5006	1.0720	-1.4984	0.0290	3.7137	0.4467	0.1014	0.0725	0.2955	0.3207
10.0	-2.6302	0.8715	-1.7634	0.0683	3.5636	0.5390	0.1333	0.0783	0.3075	0.3442
PGV	-4.8083	0.8905	-1.9629	0.1654	3.5101	0.4405	0.0954	0.0680	0.2779	0.3016
PGA	-2.7877	0.7940	-1.9688	0.1350	3.5305	0.4670	0.1247	0.0728	0.2878	0.3220

Table 1. Regression coefficients relevant to model in equation (6), considering the moment magnitude M_w and the epicentral distance R_{epi} as explanatory variables. The coefficients are relevant to the maximum horizontal spectral acceleration at different frequencies, as well as for peak ground velocity (PGV) and acceleration (PGA).

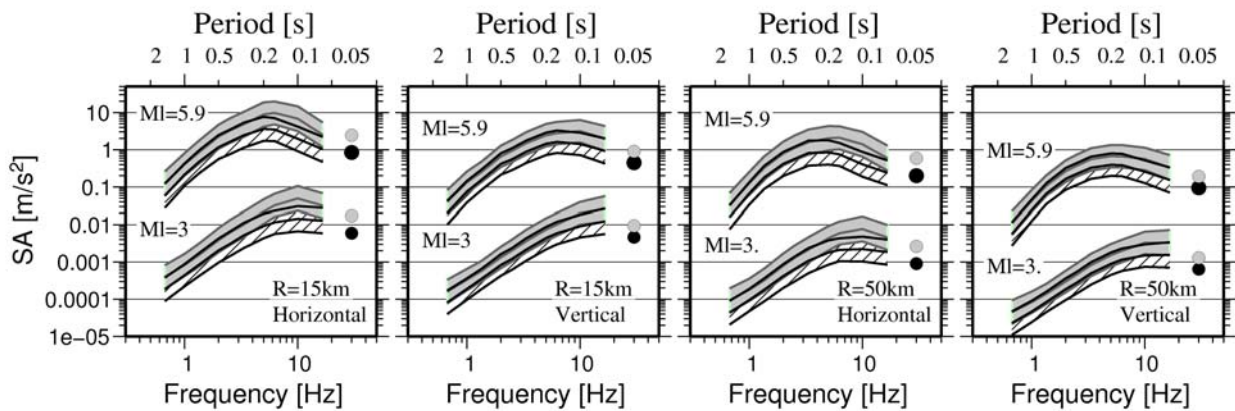


Fig. 4: Horizontal and vertical mean \pm one standard deviation spectral acceleration, for two epicentral distances (15 km and 50 km). In each panel, the results for rock (diagonal hachure pattern) and soil (gray) are compared for two different magnitudes ($M_I=3$ and 5.9). The black and gray circles represent the PGA results for soil and rock, respectively.

References

- Abercombie, R. E. (1995). Earthquake source scaling relationships from -1 to 5 M_L using seismograms recorded at 2.5 km depth. *J. Geophys. Res.* **100**, 24,015–24,036.
- Abrahamson, N. A., and R. R. Youngs (1992). A stable algorithm for regression analyses using the random effects model. *Bull. Seism. Soc. Am.* **82**, 505– 510.
- Ambraseys, N. N., J. Douglas, S. K. Sarma, and P. M. Smit (2005). Equations for estimation of strong ground motions from shallow crustal earthquakes using data from Europe and Middle East: Horizontal peak ground acceleration and spectral acceleration. *Bull. Earth. Eng.* **3**, 1– 53.
- Anderson, J. G., and S. E. Hough (1984). A model for the shape of the Fourier amplitude spectrum of acceleration at high frequencies. *Bull. Seism. Soc. Am.* **74**, 1969–1993.

- Baumbach, M., D. Bindi, H. Grosser, C. Milkereit, S. Parolai, R. Wang, S. Karakisa, S. Zümbül, and J. Zschau (2003). Calibration of an ML scale in Northwestern Turkey from 1999 Izmit aftershocks. *Bull. Seism. Soc. Am.* **93** (5), 2289–2295.
- Bindi, D., S. Parolai, H. Grosser, C. Milkereit, and S. Karakisa (2006a). Crustal attenuation characteristics in northwestern Turkey in the range from 1 to 10 Hz. *Bull. Seism. Soc. Am.* **96**, 200–214.
- Bindi, D., S. Parolai, H. Grosser, C. Milkereit, and S. Zümbül (2006b). Cumulative attenuation along source-to-receiver paths in northwestern Turkey. *Bull. Seism. Soc. Am.* **96**, 188–199.
- Bindi, D., S. Parolai, E. Görgün, H. Grosser, C. Milkereit, M. Bohnhoff, and E. Durukal (2007a). ML scale in northwestern Turkey from 1999 Izmit aftershocks: Updates. *Bull. Seism. Soc. Am.* **97**, 331–338.
- Bindi, D., S. Parolai, H. Grosser, C. Milkereit, and E. Durukal (2007b). Empirical ground-motion prediction equations for northwestern Turkey using the aftershocks of the 1999 Kocaeli earthquake. *Geophys. Res. Lett.* **34**, L08305, doi:10.1029/2007GL029222.
- Bormann, P. (2002). Magnitude of seismic events, in *IASPEI New Manual of Seismological Observatory Practice*, P. Bormann, (Editor), Vol 1, GeoForschungsZentrum, Potsdam, 16–50.
- Brune, J. N. (1970). Tectonic stress and the spectra of seismic shear waves from earthquakes. *J. Geophys. Res.* **75**, 4997–5009.
- Castro, R. R., J. G. Anderson, and S. K. Singh (1990). Site response attenuation and source spectra of S waves along the Guerrero, Mexico, subduction zone. *Bull. Seism. Soc. Am.* **80**, 1481–1503.
- Durukal, E., and Y. Çatalyürekli (2004). Spectral analysis of source parameters of the 1999 Kocaeli and Düzce earthquake aftershock sequences. Presented at the *13th World Conference on Earthquake Engineering*, Vancouver, BC, Canada, 1–6 August 2004
- Grosser, H., M. Baumbach, H. Berckhemer, B. Baier, A. Kaharan, H. Schelle, F. Krüger, A. Paulat, G. Michel, R. Demirtas, S. Gencoglu, and R. Yilmaz (1998). The Erzican (Turkey) earthquake (Ms 6.8) of March 13, 1992 and its aftershocks sequence. *Pure Appl. Geophys.* **152**, 465–505.
- Hoshiaba, M. (1991). Simulation of multiple scattered coda waves excitation based on the energy conservation law. *Phys. Earth Planet. Interiors* **67**, 123–136.
- Kanamori, H. (1977). The energy release of great earthquakes. *J. Geophys. Res.* **82**, 2981–2987.
- Konno, K., and T. Ohmachi (1998). Ground-motion characteristics estimated from spectral ratio between horizontal and vertical components of microtremors. *Bull. Seism. Soc. Am.* **88**, 228–241.
- Menke, W., and R. Chen (1984). Numerical studies of the coda falloff rate of multiply scattered waves in randomly layered media. *Bull. Seism. Soc. Am.* **74**, 1605–1621.
- Paige, C. C., and M. A. Saunders (1982). LSQR: An algorithm for sparse linear equations and sparse least squares. *ACM Trans. Math. Soft* **8**, 43–71.
- Parolai, S., and D. Bindi (2004). Influence of soil-layer properties on k evaluation. *Bull. Seism. Soc. Am.* **94**, 349–356.
- Parolai, S., D. Bindi, M. Baumbach, H. Grosser, C. Milkereit, S. Karakisa, and S. Zümbül (2004). Comparison of different site response techniques using aftershocks of the 1999 Izmit earthquake. *Bull. Seism. Soc. Am.* **94**, 1096–1108.
- Parolai, S., D. Bindi, E. Durukal, H. Grosser, and C. Milkereit (2007). Source parameters and seismic moment-magnitude scaling for northwestern Turkey. *Bull. Seism. Soc. Am.* **97**, 655–660.
- Purvance, M. D., and J. G. Anderson (2003). A comprehensive study of the observed spectral decay in strong-motion accelerations recorded in Guerrero, Mexico. *Bull. Seism. Soc. Am.* **93**, 600–611.
- Richter, C. F. (1935). An instrumental earthquake magnitude scale. *Bull. Seism. Soc. Am.* **25**, 1–32.
- Stromeyer, D., G. Grünthal, and R. Wahlström (2004). Chi-square regression for seismic strength parameter relations, and their uncertainties, with applications to an Mw based earthquake catalogue for central, northern and northwestern Europe. *J. Seism.* **8**, 143–153.

6. The Application of Persistent Scatterer Interferometry to Analyze Interseismic Deformation at Ganos Fault

Mahdi Motagh¹, and Jochen Zschau¹

¹Helmholtz Centre Potsdam GFZ German Research Centre for Geosciences, Section 2.1 "Earthquake Risk and Early Warning", Telegrafenberg, D-14473, Potsdam, Germany

Abstract

We apply the Persistent Scatterer Interferometry technique (PS-InSAR), using 38 radar images from ERS1/2 satellites in descending orbits between 1992 and 2000 to map the interseismic crustal deformation across the Gazikoy-Saros (Ganos) segment of the North Anatolian Fault (NAF), northwestern Turkey. Using earthquake cycle models incorporating elastic and viscoelastic rheology the resultant velocity field is inverted to get insight into the mechanism of deformation at the fault.

Introduction

The North Anatolian Fault (NAF), with a total length of about 1500 km, is one of the most active dextral (right-lateral) strike-slip faults in the world. It defines the tectonic boundary between the Anatolian Plate and the Eurasian Plate in northern Turkey, accommodating $\sim 14\text{-}30$ mm/yr of relative plate motion between the two plates (Ambraseys and Finkel, 1987; Straub et al., 1997). The dextral strike-slip Ganos fault is the onshore segment of the northern strand of the North Anatolian Fault (NAF) between the Marmara Sea and the Gulf of Saros (Fig. 1). The last event to have ruptured the Ganos fault occurred in 1912 ($M_s=7.4$). Other large historical earthquakes that have been attributed to the fault occurred in A.D. 824, 1343, 1509 and 1766 (Ambraseys et al., 1987).

Extensive spatial coverage provided by Interferometric Synthetic Aperture Radar (InSAR) makes it an excellent tool for measuring the interseismic crustal deformation in active tectonic regions. With centimeter wavelengths InSAR observations are sensitive to surface displacements of only a few millimeters. Successful interferometric processing requires two conditions: The spatial orbital separation between SAR acquisitions must be small, and the surface must not have been unduly changed during the time between observations. If the surface is perturbed too much, for example due to vegetation growth, erosion, cultivation or irrigation, coherence will be lost.

Areas with dense vegetation cover or rugged topography, characterizing most of the western end of the NAF, cause significant decorrelation between SAR images spanning long time interval. This makes it difficult to discern the small scale interseismic signal in such areas using conventional interferometry techniques. In this study we apply the persistent scatterer interferometry (PS-InSAR) technique (Kampes, 2006), using data from ERS1/2 satellites, to map interseismic line-of-sight (LOS) velocities across the Ganos segment of the North Anatolian Fault (NAF), northwestern Turkey. Conditions at the west end of the NAF are not optimal for interferometry. The interferograms are highly decorrelated. Thus, we use PS technique to get a full picture of the deformation field at the fault.

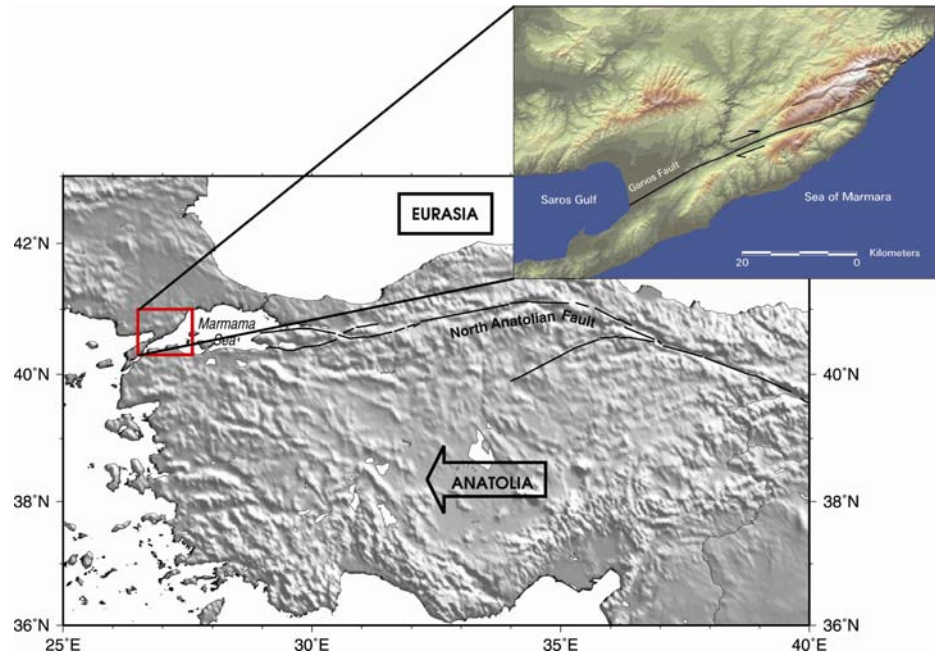


Fig. 1: Simplified map Turkey and Ganos fault between the Marmara Sea and Gulf of Saros.

Observations

The persistent scatterer (PS) processing is done using the PSI-GENESIS interferometry package developed at the German Aerospace Center (DLR) (Kampes, 2006; Adam et al., 2004). The data include 38 ERS1 and ERS2 radar images (Track 150; frame: 2781) acquired from a descending orbit over the Ganos fault during the time period 1992-2000. Fig. 2 depicts the resulting linear displacement rates obtained by the PS interferometry over the study area. The velocities, relative to a reference point on the fault (the black asterisk), are superimposed on the average amplitude SAR image. They are in the radar line-of-sight (LOS) reference, with red indicating -5 mm/yr (LOS) motion away from the satellite and blue indicating 5 mm/yr (LOS) motion toward the satellite. The gradual color change between the south and north side of the fault is caused by the right-lateral shear on the Ganos fault. The projection of PS data on vertical plane perpendicular to the average strike of the Ganos fault exhibits over a centimeter of fault-parallel motion across the entire region (Fig. 3). The gradient of deformation is highest near the trace of the fault but decays slowly with distance away from it. In the following we invert these PS data using elastic and viscoelastic interseismic models to gain insight into the mechanism of deformation at the fault.

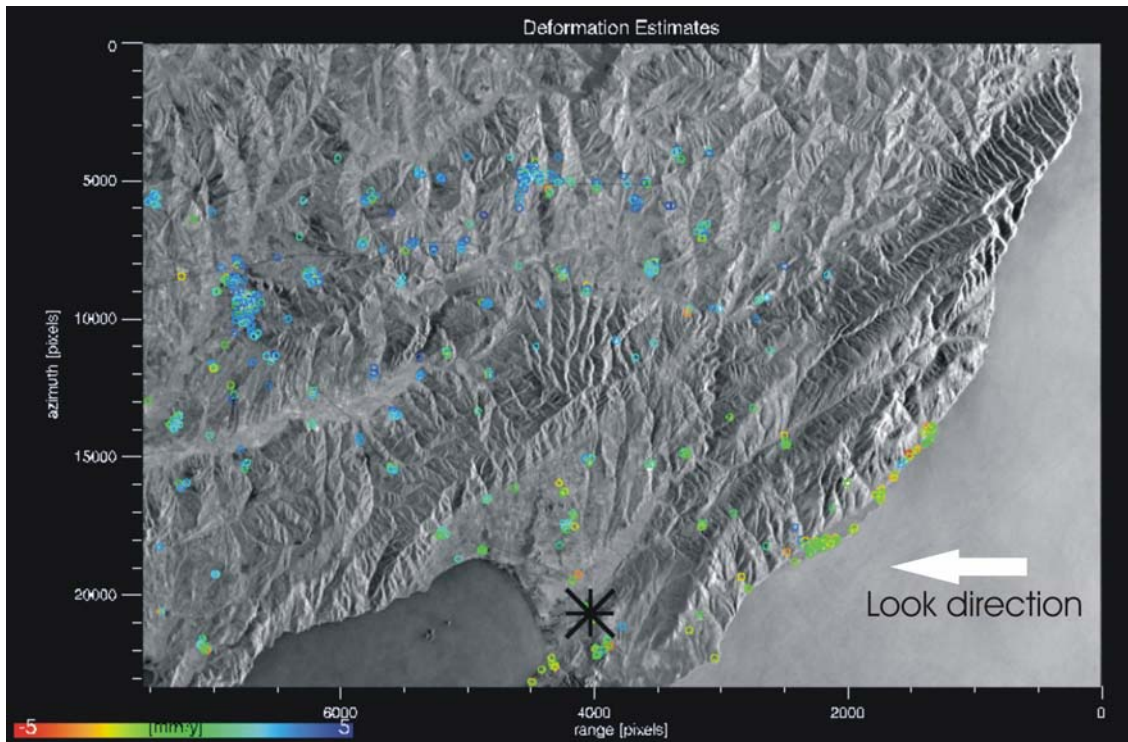


Fig. 2: Estimated line-of-sight (LOS) displacement rates at persistent scatterers across the Ganos fault between 1992 and 2000. The velocities are superimposed on the average amplitude SAR image. The black asterisk marks the reference point on the fault. Red corresponds to -5 mm/yr (LOS) motion away from the satellite and blue to 5 mm/yr (LOS) motion toward the satellite (Motagh et al., 2007).

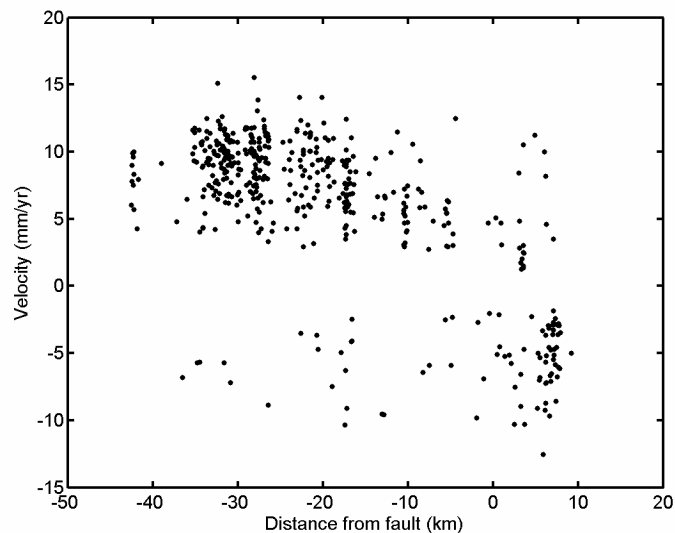


Fig. 3: Fault-parallel velocities onto profile perpendicular to the strike of the Ganos fault (Motagh et al., 2007).

Interseismic Model

To analyze the observed deformation at the Ganos fault, we examine two different models of the earthquake deformation cycle associated with strike-slip faults. The first, and most widely used, model is that of Savage and Burford (1973) in which the process of strain accumulation and release along transform faults is described by a buried screw dislocation in an elastic half-space. The second model, the so-called viscoelastic coupling model, incorporates the effect of viscoelastic flow at depth into the spatial and temporal patterns of

crustal deformation around transform faults. In this model crustal deformation occurs in response to transient stresses caused by periodic earthquakes rupturing the entire lithosphere in an Earth model consisting of an elastic upper crust (lithosphere) over a Maxwell viscoelastic half-space (Savage and Lisowski, 1998)

The viscoelastic coupling model is specified by five parameters: lithospheric thickness/locking depth H , relaxation time τ_R , recurrence time interval T , time since the last earthquake t , and far-field velocity v_0 . The elastic half-space model, on the other hand, depends only on two variables: locking depth H and slip rate v_0 . In order to estimate these parameters we perform a nonlinear inversion using a Levenberg-Marquadt optimization algorithm (Arnadottir and Segall, 1994). The time since the last great earthquake (1912) is known and considered fixed in the inversion ($t=93$). We also constrain the recurrence interval to $T=275$ years based on the average return period found by (Rockwell, 2001) using trenching and historical data. The two parameters H (elastic thickness) and v_0 (far-field velocity), are bound to lie within a range of 5-30 km and 14-30 mm/yr, respectively, on the basis of previous geological and geodetic studies at the fault. The a priori bound on the relaxation time τ_R is set to be broad, $1-10^4$ years, corresponding to viscosity values of 10^{18} to 10^{22} Pa-s.

The best fitting elastic half-space model is found for $H \sim 12$ km and $v_0 \sim 23$ mm/yr. Figs. 4a-b show the result of 1000 models from the bootstrap analysis. Both parameters in the elastic model are resolved well within a priori bounds set in the inversion. We find that at the 95% confidence interval slip rate of 20-27 mm/yr and locking depth of 9-17 km are consistent with geodetic observations. Fig. 4c illustrates the fit between the data and the forward models for the range of locking depths and slip rates determined above. The best fit model is represented by a dashed line.

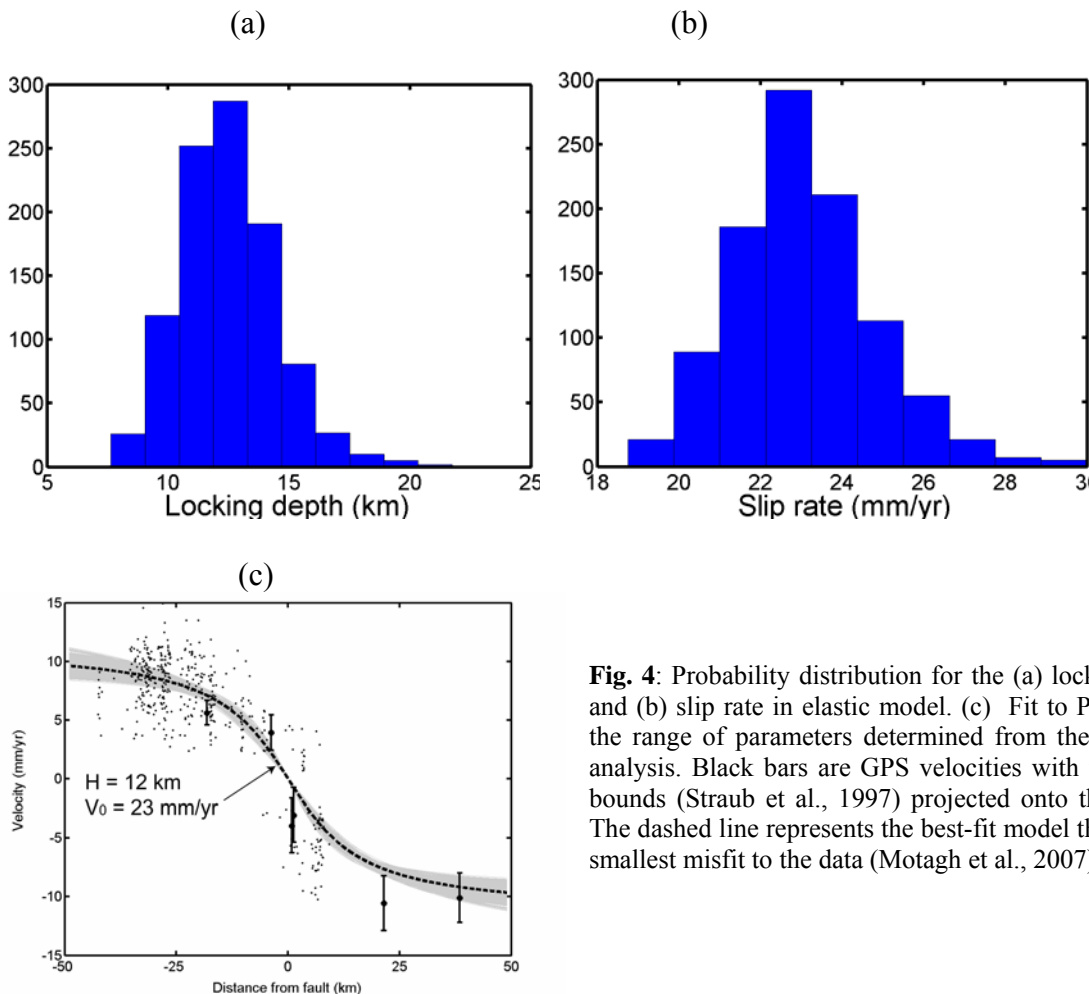


Fig. 4: Probability distribution for the (a) locking depth and (b) slip rate in elastic model. (c) Fit to PS data for the range of parameters determined from the bootstrap analysis. Black bars are GPS velocities with their error bounds (Straub et al., 1997) projected onto the profile. The dashed line represents the best-fit model that has the smallest misfit to the data (Motagh et al., 2007).

The best fitting viscoelastic half-space model is found for $H \sim 13$ km, $\tau_R \sim 142$ yr, with the slip rate of $v_0 \sim 21$ mm/yr. A bootstrap analysis from 1000 models (Fig. 5a-c) indicates that at the 95 % confidence interval elastic thickness of 8-17 km, far-field velocity of 18-24 mm/yr, and the asthenospheric relaxation time of 28-600 years are consistent with surface deformation data. Fig. 5d illustrates the fit between the data and the forward models for the range of model parameters determined above; the dashed line represents the best fit model that has the smallest misfit to the data.

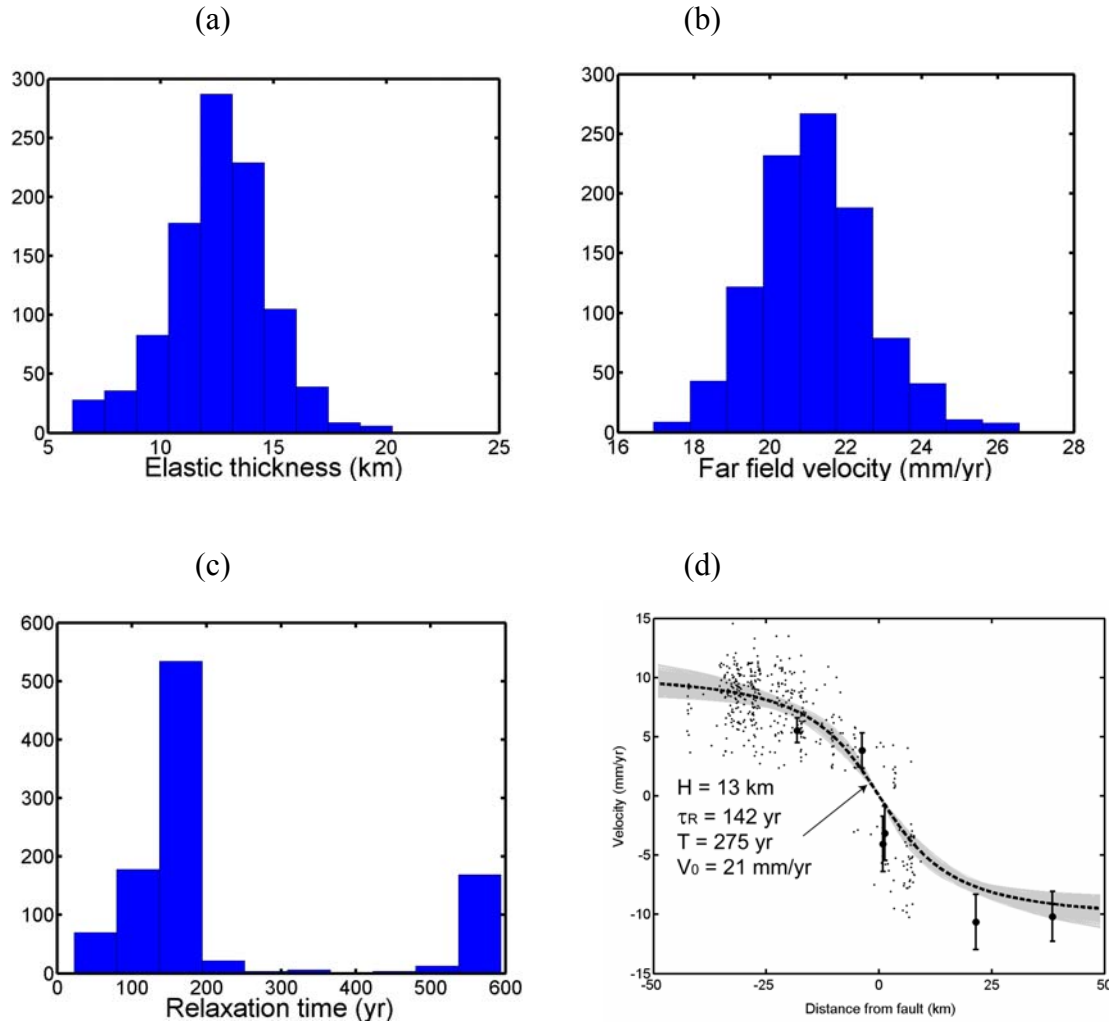


Fig. 5: Probability distribution for the (a) elastic thickness (locking depth), (b) slip rate and (c) relaxation time in viscoelastic model. (d) Fit to PS data for the range of parameters determined from the bootstrap analysis. Black bars are GPS velocities with their error bounds (Straub et al., 1997) projected onto the profile. The dashed line represents the best-fit model that has the smallest misfit to the data (Motagh et al., 2007).

Conclusions

By using the persistent scatterer technique, we have recovered the interseismic strain accumulation from 1992-2000 at the Gazikoy-Saros (Ganos) segment of the NAF. Inversion of deformation data using elastic and time-dependent viscoelastic coupling Earth model provides an estimate of parameters controlling the deformation at the fault. We have found that the fault locking depth is estimated in the range of ~ 8 -17 km regardless of the rheological model. The elastic half-space model implies an upper bound of 20-27 mm/yr for the slip rate on the Ganos fault while models incorporating viscoelastic rheology and seismic

cycle effects suggest a lower slip rate of 18-24 mm/yr, which agrees more closely with geological estimates. A bootstrap analysis of deformation data yields a lower bound of 28 years for the relaxation time, which corresponds to a viscosity of 1.3×10^{19} Pa-s, if we assume the average crust-upper mantle shear modulus of 30 GPa.

References

- Adam, N., B. M. Kampes, and M. Eineder (2004). The development of a scientific persistent scatterer system: Modifications for mixed ERS/ENVISAT time series. *ENVISAT/ERS Symposium*, Salzburg, 1-9 (cdrom).
- Ambraseys, N. N., and C. F. Finkel (1987). The Saros-Marmara earthquake of 9 August 1912. *Earth. Eng. Struct. Dyn.* **15**, 189-211.
- Arnadottir, T., and P. Segall (1994). The 1989 Loma Prieta earthquake imaged from inversion of geodetic data. *J. Geophys. Res.* **99**, 21835-21846.
- Kampes, B. M. (2006). Radar Interferometry : Persistent Scatterer Technique. *Springer*, ISBN-10: 140204576X, pp. 211.
- Motagh, M., J. Hoffmann, B. Kampes, M. Baes, and J. Zschau (2007). Strain accumulation across the Gazikoy–Saros segment of the North Anatolian Fault inferred from Persistent Scatterer Interferometry and GPS measurements. *Earth and Planetary Science Letters* **255**(3-4), 432-444.
- Rockwell, T., A. Barka, T. Dawson, S. Akyuz, and K. Thorup (2001). Paleoseismology of the Gazikoy-Saros segment of the North Anatolia fault, northwestern Turkey: Comparison of the historical and paleoseismic records, implications of regional seismic hazard, and models of earthquake recurrence. *J. Seismol.* **5**(3), 433-448.
- Savage, J. C., and R. O. Burford (1973). Geodetic determination of relative plate motion in central California. *J. Geophys. Res.* **78**, 832-845.
- Savage, J. C., and M. Lisowski (1998). Viscoelastic coupling model of the San Andreas fault along the big bend, southern California. *J. Geophys. Res.* **103**, 7281-7292.
- Straub, C., H.-G. Kahle, and C. Schindler (1997). GPS and geologic estimates of the tectonic activity in the Marmara Sea region, NW Anatolia. *J. Geophys. Res.* **102**, 27587 -27601.

7. Armutlu - A Key Region to Understand the Evolution of Seismicity at the Western End of the 1999 Izmit Earthquake Rupture

Bariş, Ş.¹, S. Sandberg², H. Grosse², S. Irmak¹, H. Woith², M. F. Özer¹, B. G. Lühr², D. Çaka¹, and J. Zschau²

¹Kocaeli University, Earth and Space Sciences Research Center, Kocaeli, Turkey

²Helmholtz Centre Potsdam GFZ German Research Centre for Geosciences, Section 2.1 "Earthquake Risk and Early Warning", Telegrafenberg, D-14473 Potsdam, Germany

Introduction

Ten major earthquakes with magnitudes above $M_s > 6.5$ migrated along the North-Anatolian fault zone (NAFZ) between 1939 and 1999. The western end of the 1999 Kocaeli earthquake rupture is located south of Istanbul next to the northern shoreline of the Armutlu Peninsula depicted by distinct clusters of micro-seismic activity. Thus, the local seismic network ARNET had been set-up by the end of 2005 in a co-operation between Kocaeli University and GFZ Potsdam to monitor the chronological evolution of seismicity in the framework of the CEDIM (Center for Disaster Management and Risk Reduction Technology) project "Megacity Istanbul". This project involves the analysis of the seismicity of the Greater Istanbul region, to obtain a better understanding of the tectonics associated with the branching of the North Anatolian Fault Zone (NAFZ), and to investigate the deformation of the Armutlu Peninsula. Additionally, possible interactions between seismic waves and pore-pressure variations in geothermal systems are studied at deep wells. These activities contribute to the implementation of an Anatolian plate boundary observatory (PBO) belonging to a series of GFZ-operated Earth System Observatories to systemically study coupled Earth processes.

Data quality and processing

Currently, 23 3-component-stations continuously record 100 Hz sampled seismic data (Fig.1). Eleven stations are GURALP broadband systems, provided by Kocaeli University and 12 are REFTEK systems with short-period L4-3D MARK seismometers provided by GFZ Potsdam. In September 2008, we replaced the short period station in Ciftlikköy (CFT) near the rupture end of the 1999 Kocaeli earthquake by a 1-Hz LENNARTZ borehole geophone installed at a depth of 100 m (Fig. 1), and an additional short period station has been installed in the centre of the Armutlu peninsula (Delmece Yaylasi). To determine the quality of the ARNET data, power spectral densities (PSD) were calculated using Welch's method and presented in periodograms (Welch, 1967). The frequency range analysed is between 0.1 Hz and 30 Hz. In summary, nearly all stations have noise levels more or less in the middle between the global high and low noise model by scale. Some of the results of the noise analysis are given in Figure 2.

For identifying earthquakes in the continuous data, picking and locating them, the zSacWin program by M. Yilmazer is used. For localisation, the program uses the code HYPO71PC of Lee and Lahr (1975). The events were located using two different velocity models, shown in Table 1. The first is the model used by Kandilli Observatory Earthquake Research Institute (KOERI), by default implemented in the location software, and the second one is the result of the tomography studies of Koulakov (2008), which includes the use of aftershocks following the İzmit 1999 earthquake, recorded and located by the German Task Force for Earthquakes (Milkereit et al., 1999).

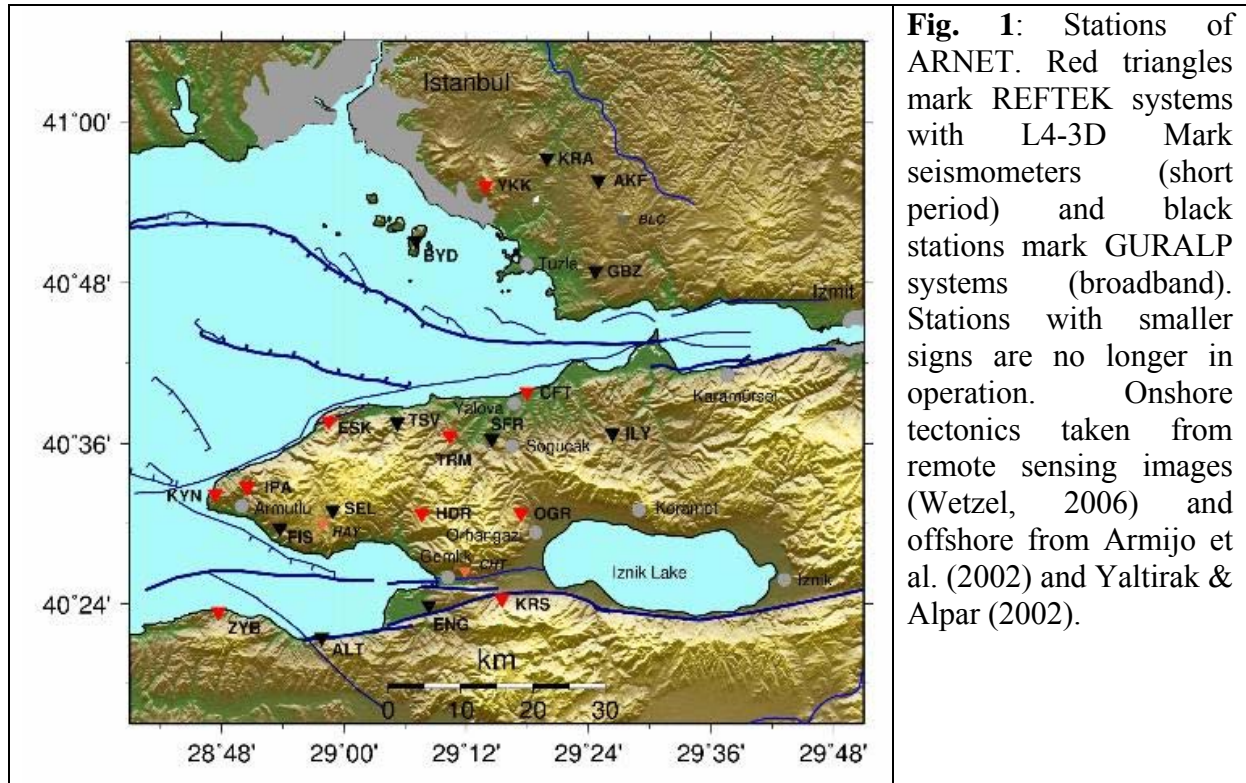


Fig. 1: Stations of ARNET. Red triangles mark REFTEK systems with L4-3D Mark seismometers (short period) and black stations mark GURALP systems (broadband). Stations with smaller signs are no longer in operation. Onshore tectonics taken from remote sensing images (Wetzel, 2006) and offshore from Armijo et al. (2002) and Yaltirak & Alpar (2002).

Table 1: 1D-velocity models used in this study. See text for more details.

Kandilli		Koulakov	
Depth [km]	Velocity [km/s]	Depth [km]	Velocity [km/s]
0.0	4.50	0.0	5.00
5.4	5.91	2.3	5.58
31.6	7.80	9.7	6.16
89.2	8.30	15.0	6.38
		20.0	6.50

The standard magnitude calculated by the program zSacWin is duration magnitude using the formula of Lee et al. (1972). Later, the local magnitude derived for northwestern Turkey by Baumbach et al. (2003) and Bindi et al. (2007) was implemented in the program.

Results

Within September 2005 until the end of February 2006 in total 485 seismic events were detected by the network. 115 of these events were located outside of the Armutlu net, mostly in the region around Bursa. From 370 events located inside the network, 237 were used for further investigation. For the rest, there were several reasons not to use them. We found that at least seven events were blasts in quarries near Gemlik and so they are excluded from the catalogue. As given by HYPO71PC, catalogue 1 (Fig. 3) has an average RMS value of 0.28 s for the location. The average horizontal error (ERH) is 2.8 km, while for the vertical error (ERZ), the average is 4.4 km. These errors do not reflect the real location errors, but, they are mostly an effect of the inadequacies of the 1D-velocity model in the inversion routine. The

duration magnitudes are in a range 0.4 and 2.8 with a magnitude of completeness of 1.3. Most of the events seem to have occurred in a depth range of 5 to 15 km. Only a few events are deeper than 20 km or were localised at depths shallower than 3 km, while between 3 and 5 km there seems to be a gap. A similar pattern had been observed for the distribution of the İzmit aftershocks in the study area according to Karabulut et al. (2002). From their study, it seems that these very shallow events only appear in an earthquake cluster at the northern coast of the Armutlu Peninsula.

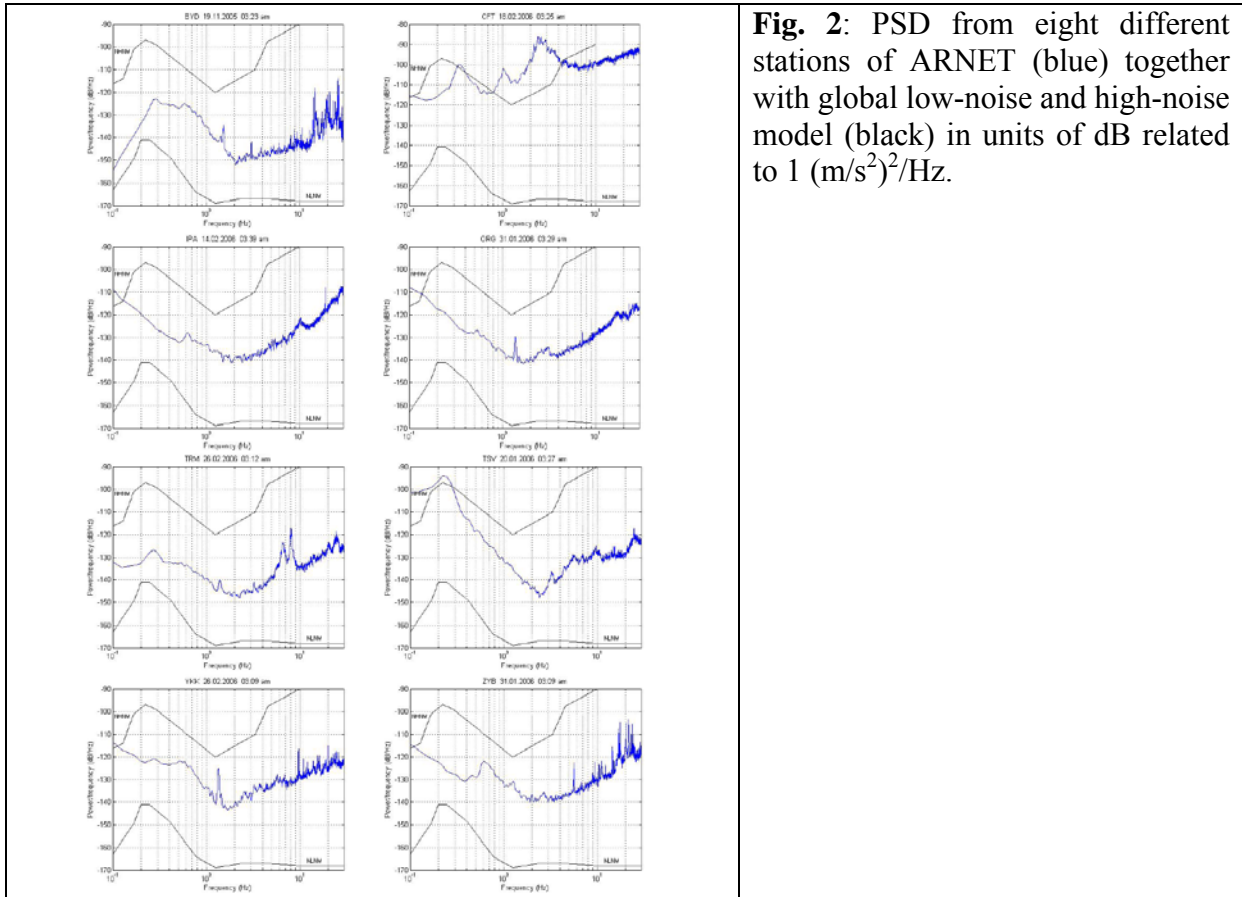


Fig. 2: PSD from eight different stations of ARNET (blue) together with global low-noise and high-noise model (black) in units of dB related to $1 \text{ (m/s}^2\text{)}^2\text{/Hz}$.

The events located with the 1D-velocity model given by Koulakov (2008) obtain an average RMS of 0.25 s, an average ERH of 2.7 km, and an ERZ of 3.5 km. The local magnitudes range from 0.5 to 3.5 with a magnitude of completeness of 1.0. The difference in the obtained magnitude range with respect to catalogue 1 is due to the fact that determine duration magnitude always has a problem of underestimating magnitudes. It strongly depends on the person who analyses the data and where the end of the duration is set. The spatial distribution and the depth sections of catalogue 2 are shown in Figure 3 and Figure 4. In catalogue 2, the depth distribution looks completely different compared to catalogue 1. The number of events at a depth of around 5 km decreased distinctly. Because 5 km is the initial depth in the location iteration process, this is interpreted that the KOERI model has problems to resolve the real depth of events.

However, the possible gap at depths of around 3 km can still be seen and in addition it now seems that there is a second depth with lower seismicity at around 6 to 7 km. The maximum depth of 20 km did not change. On the map, the spatial distribution also did not change much and shows the same main features already mentioned as catalogue 1. Now, the NE-SW strike direction of the dense cluster is even more distinct.

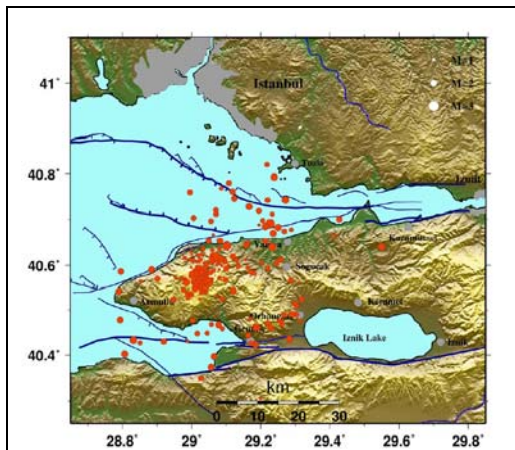


Fig. 3: Microseismicity between September 2005 and February 2006 of catalogue 1, located with the 1D-velocity model of KOERI, including duration magnitude information.

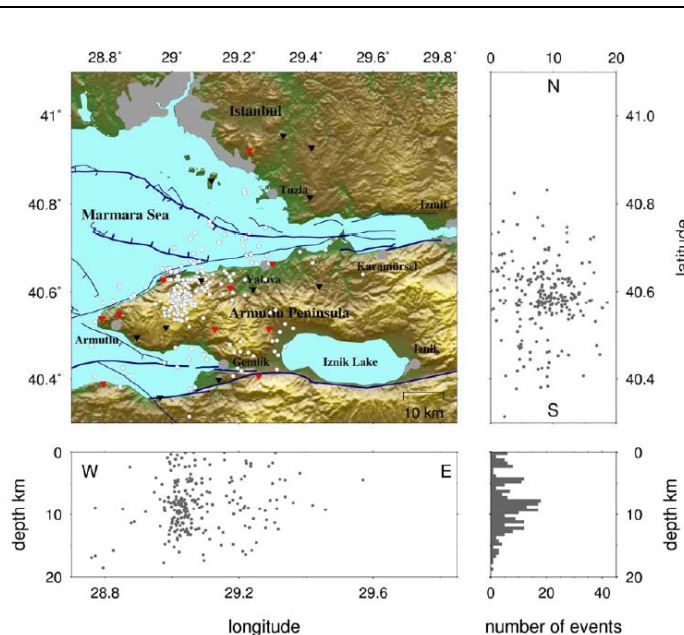


Fig. 4: Microseismicity between September 2005 and February 2006 and the resulting depth distribution of catalogue 2, located with the 1D-velocity model of Koulakov (2008). Triangles indicate the seismic stations as shown in Figure 1.

On October 24, 2006 a local magnitude 5.3 event occurred in the Gulf of Gemlik at 2:00 pm local time. Until 7:43 pm local time on the same day 34 aftershocks with local magnitudes between 1.2 and 3.9 were detected. The main shock shows two surprising phenomena. The location of the event in the Gulf of Gemlik is on an EW striking segment of the middle strand, i.e. the westward prolongation of the Iznik-Mekece segment of the NAFZ and thus, according to the main tectonic regime, it was expected that the rupture should strike EW. However, the aftershocks of the following six hours indicated propagation in a northern direction, hinting at a NNE-SSW striking rupture plain (Figure 5).

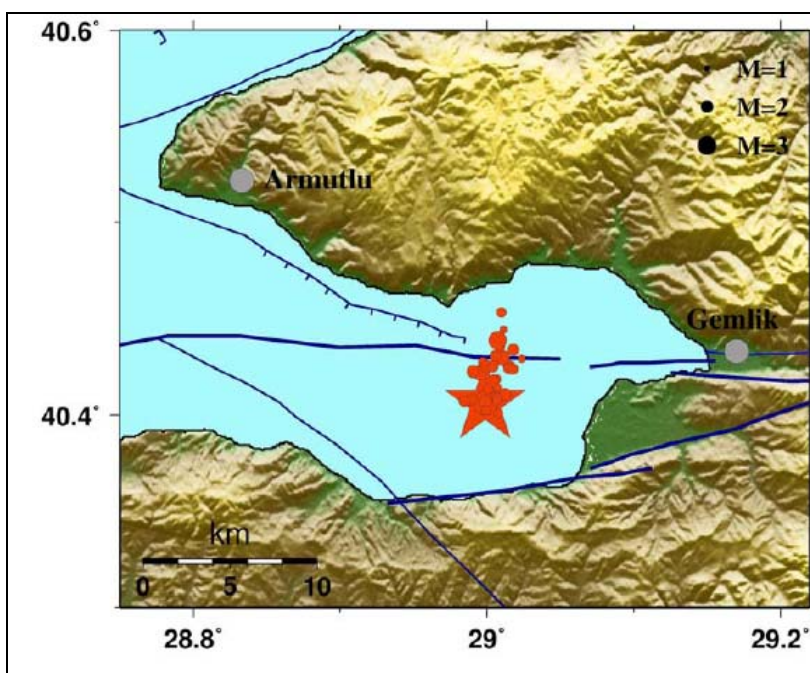


Fig. 5: Gemlik mainshock of October 24, 2006, and 34 aftershocks recorded within the first six hours, and located with Koulakov (2008) model including local magnitudes. The star marks the main shock with a local magnitude of 5.3.

The pressure monitored at the wellhead of a 500 m deep well within the geothermal field of Armutlu located about 20 km NW of the epicentre, responded dynamically to the earthquake: with the arrival of the P-wave the pressure dropped ca. 14 mbar, and oscillated thereafter for ca. 30 seconds. After the passage of the seismic waves, a static pressure increase of 2 mbar remained. The static pressure increase is attributed to an interaction between the seismic wave and the reservoir.

References

- Armijo, R., B. Meyer, S. Navarro, G. King, and A. Barka (2002). Asymmetric slip partitioning in the Sea of Marmara pull-apart: a clue to propagation processes of the North Anatolian Fault? *Terra Nova* **14**, 80-86.
- Baumbach, M., D. Bindi, H. Grosse, C. Milkereit, S. Parolai, R. Wang, S. Karakisa, S. Zünbül, and J. Zschau (2003). Calibration of an M_L Scale in Northwestern Turkey from 1999 Izmit Aftershocks. *Bull. Seism. Soc. Am.* **93**(5), 2289-2295.
- Bindi, D., S. Parolai, E. Görgün, H. Grosse, C. Milkereit, M. Bohnhoff, and E. Durukal (2007). M_L Scale in Northwestern Turkey from 1999 Izmit Aftershocks: Updates. *Bull. Seism. Soc. Am.* **97**(1B), 331-338.
- Karabulut, H., M. P. Bouin, M. Bouchon, M. Dietrich, C. Cornou, and M. Aktar (2002). The Seismicity in the Eastern Marmara Sea after 17 August 1999 Izmit Earthquake. *Bull. Seism. Soc. Am.* **92**, 387-393.
- Koulakov, I. (2008). Personal communication.
- Lee, W. H. K., R. Bennet, and K. Meagher (1972). A method of estimating magnitude of local earthquakes from signal duration. *U.S. Geol. Surv. Open-File Rep.*, pp. 28.
- Lee, W. H. K. and J. C. Lahr (1975). Hypo71 (revised): a computer program for determining hypocenters, magnitude and first motion pattern of local earthquakes. *U.S. Geol. Surv. Open-File Rep.*, 75-311.
- Milkereit, C., S. Zünbül, S. Karakisa, Y. Irvul, J. Zschau, M. Baumbach, H. Grosse, E. Günther, N. Umutlu, T. Kuru, E. Erkul, K. Klinge, M. Ibs von Seht, and A. Karahan (1999). Preliminary aftershock analysis of the $M_w=7.4$ Izmit and $M_w=7.1$ Düzce earthquake in western Turkey. In: *The 1999 Izmit and Düzce Earthquakes: preliminary results*, Barka, A., Kozaci, Ö., Akyüz, S., Altunel, E. (editors), Istanbul Technical University, 179-187.
- Welch, P. D. (1967). The Use of Fast Fourier Transform for the Estimation of Power Spectra: A Method Based on Time Averaging Over Short, Modified Periodograms. *IEEE Trans. Audio Electroacoustics* **AU-15**, 70-73.
- Wetzel, H.-U. (2006). Personal communication.
- Yaltrak, C., and B. Alpar (2002). Evolution of the middle strand of North Anatolian Fault and shallow seismic investigation of the southeastern Marmara Sea (Gemlik Bay). *Marine Geology* **190**, 307-327.

8. Attenuation of Macroseismic Intensity in the Marmara Sea Region, NW Turkey

M. B. Sørensen¹, D. Stromeyer¹, and G. Grünthal¹

¹Helmholtz Centre Potsdam GFZ German Research Centre for Geosciences, Section 5.3 “Engineering Seismology”, Telegrafenberg, D-14473 Potsdam, Germany

Introduction

When generating shake maps with the purpose of earthquake early warning, an essential parameter is the attenuation of seismic waves in the area of interest. Such information is also of crucial importance for seismic hazard assessment. Ground motion prediction equations (GMPE) are traditionally given in terms of recorded ground motion parameters, e.g. peak ground acceleration (PGA), based on strong motion data. When studying the damage potential of large earthquakes, such PGA-based relations have two drawbacks. First, the availability of recordings is limited and therefore one is often forced to apply attenuation relations based on recordings from different areas with similar tectonics. Second, there is no straightforward way to associate the recorded ground motions with damage which is a complex function of ground motion level, duration, local site conditions and building vulnerability.

As an alternative, to overcome these problems, ground motion attenuation is expressed in terms of macroseismic intensity. Intensities have the major advantage of much better and, what is important, of fast availability, as data are dependent on the availability of people and a built environment rather than instrumentation and therefore can be sampled closer and as far back in time as historical records allow. Furthermore, the macroseismic intensity is assigned based on the observed ground shaking/damage and thereby it can be directly related to the damage potential of future earthquakes. Another advantage is that intensity data are easy understandable by non-seismologists and easy convertible by risk management teams.

In the present study we derive a GMPE for macroseismic intensity for the Marmara Sea region, NW Turkey. In this region, especially the city of Istanbul is under a significant seismic hazard and potential seismic risk due to the likely rupture of a 100-150-km-long segment of the North Anatolian Fault just south of the city, within the lifetime of the present city environment. The capacity of the North Anatolian Fault for generating large earthquakes was latest manifested by the occurrence of the M=7.4 1999 Izmit earthquake. This event caused damage over an extended region around the rupturing fault plane and lead to the loss of more than 19000 lives.

GMPEs for macroseismic intensity have previously been derived by Erdik and Eren (1983) and Erdik et al. (1985), valid for the North Anatolian Fault in general. These relations give the MSK-64 intensity as a function of M_s and the natural logarithm of the rupture distance. More recently, Böse (2006) derived a relation for the Marmara Sea region based purely on simulated ground motions which are converted into intensity.

In this study we derive a GMPE using a model which takes into account the finite extent of the fault plane and represents site intensities as a function of fault distance, event depth and moment magnitude.

Method

In the following, the applied regression model is briefly outlined. For a more detailed description of the model and the associated uncertainties, the reader is referred to Sørensen et al. (in review). We seek a GMPE with a functional form based on the well-established attenuation model for point sources (Sponheuer, 1960):

$$I = I_0 - a \cdot \log \sqrt{\frac{R^2 + h^2}{h^2}} - b \cdot (\sqrt{R^2 + h^2} - h). \quad (1)$$

In this expression, I_0 is the epicentral intensity, R is epicentral distance and h is earthquake depth. The first term $a \cdot \log \sqrt{\frac{R^2 + h^2}{h^2}}$ describes the geometrical spreading (having its main effect at short distances) and the second term $b \cdot (\sqrt{R^2 + h^2} - h)$ describes the energy absorption (most significant at larger distances). The epicentral intensity is defined based on a regression model between I_0 , moment magnitude M_w and depth h (Stromeyer et al., 2004):

$$I_0 = c \cdot M_w + d \cdot \log(h) + e. \quad (2)$$

Combining (1) and (2) leads to the following model for the macroseismic intensity:

$$I = c \cdot M_w + d \cdot \log(h) + e - a \cdot \log \sqrt{\frac{R^2 + h^2}{h^2}} - b \cdot (\sqrt{R^2 + h^2} - h). \quad (3)$$

This expression is in many respects comparable with the common type of strong-motion attenuation relations (e.g. Joyner and Boore, 1993). For large earthquakes, the point source assumption fails and the finiteness of the fault must be accounted for. In this study, this is included by defining the distance R as the Joyner-Boore distance (i.e. shortest distance to the surface projection of the fault plane) instead of as the epicentral distance. In this respect, an attenuation relation is derived, which is symmetric around the rupturing fault plane.

Usually intensity datasets are characterized by great variety in the number of observations of the different intensity levels. In most cases the highest intensities are under-sampled as these are restricted to a relatively small area compared to the lower, more distributed intensities. To avoid bias in the data due to such effects, a weighting scheme has been applied where each intensity class (integer intensity level) has been assigned the same weight in the regression, regardless of the number of observations within the class.

Data

The macroseismic intensity dataset available for the Marmara Sea region consists of a number of isoseismal maps for selected large earthquakes. Most of these are collected by Eyidogan et al. (1991) in terms of Modified Mercalli Intensity (MMI), covering the time interval 1900-1988. In addition, an isoseismal map for the 1999 Izmit earthquake is available from Özmen (2000). We include data for earthquakes in the Marmara Sea region (26-31E, 39.5-41.5N), for which a minimum of four intensity levels are available as isoseismal contours, in total 7 events in the time period 1912-1999. An overview of the studied earthquakes and the available macroseismic data is given in Table 1.

In order to perform the regression for a GMPE, the isoseismal maps need to be digitized. Following digitization, it has been chosen to convert the isoseismal lines into IDP by covering the map area by a fine grid (2 km grid spacing). Each grid point was assigned the intensity value of the contour containing the point. Grid points outside the intensity contours of the isoseismal map are not included in the study. The obtained number of IDP is listed in Table 1.

Table 1: Macroseismic data included in this study.

Year	Date	M _w	I ₀	I _{min}	I _{max}	# IDP
1912	08 09	7.3	10-11	5	9	27015
1935	01 04	6.4	9	5	8	4375
1953	03 18	7.0	9-10	5	8	21720
1963	09 18	5.9	8	5	8	14985
1964	10 06	6.3	8-9	5	9	16308
1967	07 22	7.2	10	5	9	22302
1999	08 17	7.4	10-11	5	10	14490

M_w is moment magnitude, I₀ is epicentral intensity (variation is due to results of various authors being presented in most cases), I_{min} and I_{max} are minimum and maximum intensity contour levels in isoseismal maps. # IDP is number of intensity points available on a regular grid (see text).

In equation (3), Joyner-Boore distance (R), event depth (h) and moment magnitude (M_w) must be input for each event/IDP pair. It has therefore been necessary to collect basic source parameters for the studied earthquakes. For most of the events, the available information is limited, and different approaches have been followed depending on the available information. A summary of the source parameters is given in Table 2, for details about the assignment of parameters, the reader is referred to Sørensen et al. (in review).

Table 2: Source parameters of the earthquakes in the Marmara Sea region

Year	Date	Time	Lon	Lat	h	M _w	M _s	Strike	Dip
1912	08 09	01.28	27.10	40.67	10	7.3	7.3	-	-
1935	01 04	14.41	27.51	40.64	5	6.4	6.4	45	45
1953	03 18	19.06	27.40	40.00	10	7.0	7.0	60	90
1963	09 18	16.58	28.95	40.70	15	5.9	6.4	304	56
1964	10 06	14.31	27.90	40.05	14	6.3	6.8	100	40
1967	07 22	16.57	30.69	40.67	12	7.2	7.2	275	88
1999	08 17	00.01	29.97	40.76	17	7.4	7.4	-	-

The final dataset consists of 121195 IDP covering the intensity range 5-10, the magnitude range M_w=5.9-7.4 and a distance range of 0-335 km. These values represent also the limitations of the derived GMPE as it cannot be assumed that simple extrapolation outside these bounds will be successful.

Results

As can be seen in Table 2, the depth variation among the individual events is small, and as the event depths are furthermore associated with significant uncertainty, it was chosen to exclude the $d \cdot \log(h)$ - expression in the source term from the regression model to keep the problem as simple as possible. This in practice means that an average depth effect on the epicentral

intensity is included in the constant term e . The regression is then performed for the following relation:

$$I_S = x_1 \cdot M_w + x_2 + x_3 \cdot \log \sqrt{\frac{R^2 + h^2}{h^2}} + x_4 \cdot (\sqrt{R^2 + h^2} - h). \quad (4)$$

The following attenuation relation for macroseismic intensity in the Marmara Sea region was obtained with a relatively small mean regression error of $\sigma=0.672$:

$$I_S = 0.376 \cdot M_w + 5.913 - 2.656 \cdot \log \sqrt{\frac{R^2 + h^2}{h^2}} - 0.0020 \cdot (\sqrt{R^2 + h^2} - h) \quad (5)$$

Figure 1 shows an example of the performance of this relation in comparison with the observed input intensity data for an earthquake in 1967. For this as well as for all other events, the predicted intensities are within the range of the observed data. An important reason for the misfit between the observed and predicted intensity is the symmetric distribution of the predicted intensities around the fault plane. In reality intensities do not follow such isotropic distributions. It is, though, evident that the inclusion of the dimensions of the rupturing fault plane by using rupture distance instead of e.g. epicentral distance provides an improvement in the shape of the intensity curves which would else be circular.

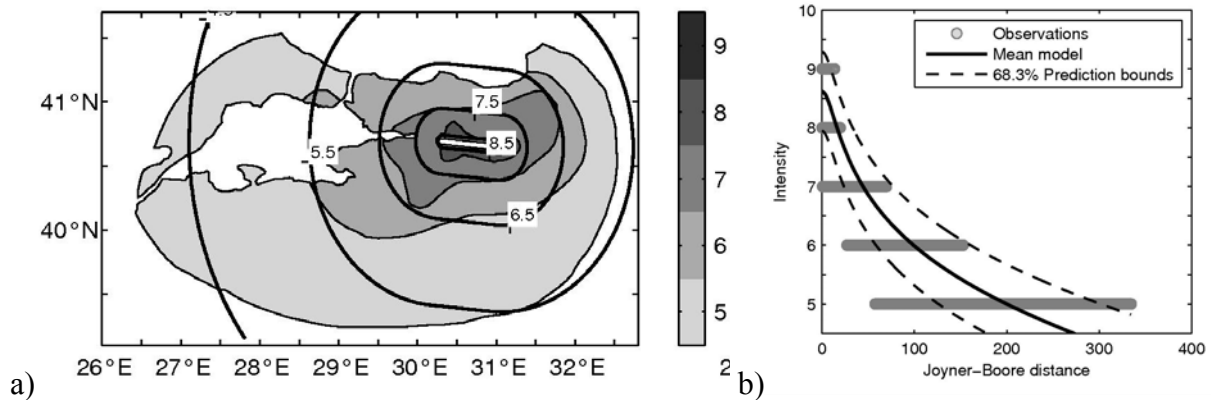


Fig. 1: Comparison of observed intensities for the 1967 earthquake with theoretical predictions from equation (5). a) intensity contours (black lines) in a map view compared to the observed isoseismal lines (grey scale). The intensity contours are drawn for the midpoint value between two integer intensities (e.g. for “half intensities”). The surface trace of the fault plane is shown as a white line. b) intensity vs. distance plot comparing the grided intensities based on the isoseismal map (circles) with the intensities predicted from equation (5) (solid line) together with the 68.3%-confidence bounds (dotted lines) corresponding to one standard deviation of normally distributed errors.

A comparison of our relation to the already existing intensity attenuation relations for the North Anatolian Fault shows that for most events, our relation performs better than the previously published relations, especially in the near-field (for details, see Sørensen et al., in review). Although the performance of the previous relations at some distance from the fault may be relatively good and will lead to realistic estimates of the ground motion, our relation provides an improved estimate of the macroseismic field due to a significant earthquake in the Marmara Sea region which can be justified physically and is valid for the entire distance range.

Acknowledgements

The presented work was carried out as part of the EC funded project SAFER (www.saferproject.net). The authors wish to thank Eser Durukal and Zehra Cagnan, Kandilli Observatory, Istanbul, for providing macroseismic information for Istanbul.

References

- Böse, M. (2006). Earthquake Early Warning for Istanbul using Artificial Neural Networks. PhD Thesis, University of Karlsruhe, pp. 181.
- Erdik, M., V. Doyoran, N. Akkas, and P. Gulkan (1985). A probabilistic assessment of the seismic hazard in Turkey. *Tectonophysics* **117**, 295-344.
- Erdik, M., and K. Eren (1983). Attenuation of Intensities for Earthquake Associated with the North Anatolian Fault. *Middle East Technical University Earthquake Engineering Research Center*, Ankara.
- Eyidogan, H., U. Güclü, Z. Utku, E. and Degirmenci (1991). Türkiye büyük depremleri makro-sismik rehberi (1900-1988). *Istanbul Teknik Üniversitesi, Maden Fakültesi, Jeofizik Mühendisliği Bölümü*, pp. 198.
- Joyner, W. B., and D. M. Boore (1993). Methods for regression analysis of strong-motion data, *Bull. Seism. Soc. Am.* **83**(2), 469-487.
- Özmen, B. (2000). Es-siddet Haritasi, in: *17 Augustos 1999 Izmit Körfezi depremi Raporu*, Editor Ramazan Demirtas, Ankara.
- Sponheuer, W. (1960). Methoden zur Herdtiefenbestimmung in der Makroseismik, *Freiberger Forschungsh.* **C88**, pp.120.
- Stromeyer, D., G. Grünthal, and R. Wahlström (2004). Chi-square regression for seismic strength parameter relations, and their incertainties, with applications to an Mw based earthquake catalogue for central, northern and northwestern Europe, *J. Seism.* **8**, 143-153.
- Sørensen, M.B., Stromeyer, D. and Grünthal, G., in review. Attenuation of Macroseismic Intensity – A New Relation for the Marmara Sea Region, NW Turkey, submitted to *Bull. Seism. Soc. Am.*

9. Site Characterization by Seismic Noise in Istanbul, Turkey

S. Parolai¹, M. Picozzi¹, A. Strollo^{1,2}, E. Durukal³, O. Özel⁴, S. Karabulut⁴, M. Erdik³ and J. Zschau¹

¹Helmholtz Centre Potsdam GFZ German Research Centre for Geosciences, Section 2.1 "Earthquake Risk and Early Warning", Telegrafenberg, D-14473 Potsdam, Germany

²Institute of Geosciences, Universität Potsdam, Karl-Liebknecht Strasse, 14476 Potsdam, Germany

³Boğaziçi Üniversitesi, Kandilli Rasathanesi ve Deprem Araştırma Enstitüsü, Department of Earthquake Engineering, 34684, Çengelköy, Istanbul, Turkey

⁴Istanbul University, Faculty of Engineering, Geophysical Engineering Department, Avcılar, Istanbul, Turkey.

Introduction and aim of the study

Istanbul is a megacity of 12 million inhabitants, who are exposed to a significant earthquake hazard. Moreover, the considerable rate of urbanization combined with uncontrolled land use makes such hazard even higher (Erdik et al., 2003). The main factor controlling the earthquake hazard for Istanbul is undoubtedly the proximity of the North Anatolian Fault, which in the Marmara Sea region forms a complex fault system (Erdik et al., 2003). From an analysis of the available earthquake records performed by Ambraseys and Finkel (1991), the city is estimated to be affected by a medium intensity (epicentral intensity of VII-VIII) earthquake with an average return period of 50 years. During the Izmit and Düzce 1999 earthquakes, this scenario was worsened by the recognition of site amplifications that were observed to locally modify the ground motion inside the metropolitan area. In particular, as shown by several studies (Tezcan et al., 2002; Ozel et al., 2004; Beyen and Erdik, 2004; Ansal et al., 2004), the Avcilar district in the western part of Istanbul suffered significant damage, largely due to the amplification of the earthquake ground motion. In fact, for this area, an intensity of VII (MSK) was assigned, while in the other districts of the metropolitan area an intensity of VI (MSK) was generally observed (Gruenthal, 1998; Ozmen, 2004). The anomalous amplification of the ground motion observed in the western part of the city is considered to be mainly related to the presence soft sediments overlaying a competent seismic bedrock. Therefore, recent studies (Ergin et al., 2004; Sørensen et al., 2006) have focused on estimating possible site effects in the metropolitan area of Istanbul, and in particular in its western part. Often, information is obtained through invasive techniques, such as drilling, down/cross-hole measurements, etc. However, due to their expensive nature, the widespread application of such techniques is only able to be performed after coming to a compromise with respect to cost, resulting in a limited exploration depth. In fact, microzonation works are frequently based on the use of the average shear-wave velocity in the uppermost 30m (V_{s30}), which is adopted by the National Earthquake Hazard Reduction Program (NEHRP) classification in the USA. However, several works (Wald and Mori, 2000; Stewart et al., 2003; Park and Hashash, 2004; Di Giacomo et al., 2005; Mucciarelli and Gallipoli, 2006) have showed that in a number of geological–geotechnical and morphological contexts, the V_{s30} classification is not always a suitable tool for site-effect estimation. Also for this reason, non-invasive and cost effective passive seismic techniques have recently become an attractive option for seismic site-effect studies. Especially in the last decade, environmental noise recordings performed by single station methods to estimate horizontal-to-vertical (H/V) spectral ratio curves (Fah et al., 2001; Arai and Tokimatsu, 2004) and by 2D micro-array techniques to estimate surface wave dispersion curves (Scherbaum and et al., 2003) have provided very promising results. Parolai et al. (2001) and Parolai et al. (2004) showed that the seismic noise H/V curves exhibit a good agreement with the H/V from earthquake recordings, especially with regard to the value of the fundamental resonance frequency of the sedimentary cover. Therefore, performing a large number of noise measurements over a region of interest allows a map of the fundamental frequencies to be obtained, which provides an overview of

the distribution of both the sedimentary cover thickness and, most importantly, of those areas where the amplification of the seismic motion in the frequency band of interest for buildings behaviour is expected.

Concerning 2D arrays, it has been shown (Tokimatsu et al., 1992; Ohori et al., 2002; Parolai et al., 2006;) that by using Rayleigh wave dispersion curves, the characterization of the local S-wave velocity profile can be obtained with a good accuracy, especially when a priori information about the total sedimentary cover thickness is available in advance. Further improvements are obtained by applying the joint inversion of phase velocity and H/V ratio curves (Scherbaum et al., 2003; Parolai et al., 2005; Arai and Tokimatsu, 2005), which allows the trade-off problem between the model parameters that hampers the separate inversion of these curves to be overcome. The application of this inversion scheme has also had success in estimating the S-wave velocity profile for sedimentary covers hundreds of meters thick (Parolai et al., 2005). Although for the engineering-geotechnical community, the lack of high resolution in the S-wave velocity profile can be considered a drawback, from the site-effect point of view, passive techniques, especially in the case of sedimentary cover thicker than 30–50 m, provide estimates of the local transfer function that are in very good agreement with both the empirical ones (Picozzi and Albarello, 2007; Parolai et al., 2007) and those obtained by 1D techniques (e.g., SASW and MASW) that allow the reconstruction of the shallower part of the S-wave velocity profile with a higher resolution (Richwalski et al., 2007).

In this work, as a preliminary activity for the microzonation characterization of Istanbul, 192 single station measurements (Fig. 1a) for the estimation of the H/V curves were carried out in the western part of the metropolitan area, in order to estimate the fundamental resonance frequency of the sedimentary cover. In particular, 42 of these noise measurements were performed at sites where accelerometers belonging to the permanent and temporary networks operated by the Kandilli Observatory and Earthquake Research Institute (KOERI) are located. Thus, for 29 sites of the considered accelerometric stations, the H/V curves from noise recording were compared with those calculated using weak motion recordings. This comparison of the results provided by the different methods was in fact directed towards performing a calibration of the passive seismic techniques in the area investigated, allowing a preliminary validation for the reconstructed sediment–bedrock interface geometry and the site effects estimates.

In addition, in order to provide additional useful information for site effects and microzonation studies, a series of eight 2D micro-array measurements utilizing short-period sensors and high dynamic digitizers were carried out in selected sites of the study area. The extended spatial autocorrelation technique (ESAC; Ohori et al., 2002; Aki, 1957; Okada, 2003), and frequency–wavenumber analysis (maximum likelihood method; Capon, 1969; Horike, 1985) were used for the estimation of the Rayleigh wave dispersion curves and wavefield analysis. For the first time, the resulting dispersion curves were used together with the H/V curve in a joint inversion scheme for the estimation of the S-wave velocity profiles in a megacity. Finally, theoretical site responses were calculated from the S-wave velocity profiles obtained from the micro-array data using the propagator matrix method for a 1D-layered medium (Wang, 1999).

Noise and earthquake H/V spectral ratio

From 24 June to 15 July 2007, an extensive survey of single station seismic noise recordings was carried out over the western metropolitan part of Istanbul. In total, 192 sites were investigated, 42 of which were performed at the accelerometric sites of the Istanbul Earthquake Rapid Response System (IERRS) operated by the Kandilli Observatory and Earthquake Research Institute of Bogazici University, and eight carried out using data collected at 2D array sites. Seismic noise measurements were carried out using seismic stations equipped with the EDL 24-bit digitizer connected to a Mark L-4C-3D 1Hz sensor

with GPS timing. All the sensors were calibrated, and, as showed by Parolai. et al. (2001), can be used to reliably analyze frequencies lower than 1 Hz.

Recordings of two local earthquake events with magnitude ML of 4.1 and 4.2 were available for 29 accelerometric station sites of the IERRS (Harmandar et al., 2006). The Fourier spectra of the events were computed using zero-baseline corrected and cosine tapered acceleration recordings of the three components. Therefore, 5 s time-windows starting 0.5 s before the S-onset (Birgören and Ozel, 2006) were selected. The spectral amplitudes from the two horizontal components were then combined by finding their root-mean-square average. Finally, the H/V spectral ratios of the earthquake data (EHV) were computed. Fig. 2 compares for some representative sites, the H/V spectral ratios estimated from seismic noise recordings (NHV) from seismic stations and following the procedure previously described, and those obtained using the two earthquake recordings. It is worth noting that, although the number of available earthquake records is limited, the two data sets show a general agreement in the estimation of the fundamental resonance frequencies, f_0 , including in some cases their amplitudes as well. Therefore, it is reasonable to have confidence in the reliability of the f_0 estimated by the NHV curves.

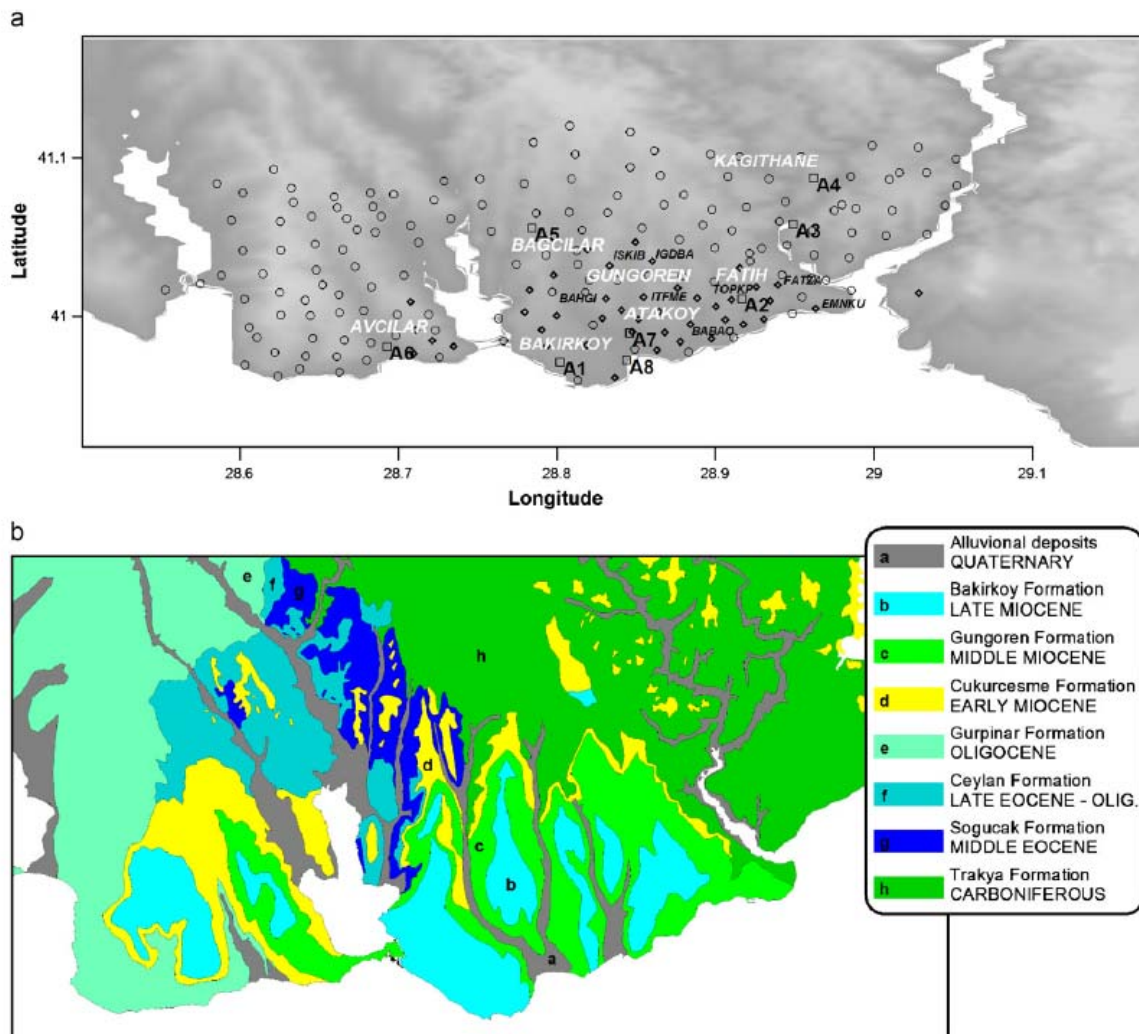


Fig. 1: Western part of Istanbul: (a) single station noise measurements at free field sites (dots), IERRS stations (rhombus, name of stations with earthquake recordings is indicated), and 2D array measurements (squares); (b) geological map.

The single station seismic noise measurement dataset was used with the aim of assessing the fundamental resonance frequency f_0 of soft sedimentary cover. Moreover, the lateral variability in f_0 also allows lateral variations in sedimentary thickness and its dynamic properties to be inferred. Only in one case was the H/V ratio curve severely affected by low frequency disturbance, most likely due to bad soil–sensor coupling and wind. Therefore, a map of f_0 using information from 191 measurement sites was obtained. It is also noted in the western part of the investigated area that for a large number of measurement sites, multiple peaks in the H/V curves were observed, in particular, those sites that typically show a first maximum in the frequency range between 0.15 and 0.3 Hz, and a second one at frequencies higher than 0.5 Hz. The presence of multiple peaks is interpreted as indicating the presence of multiple impedance contrasts at different depths. In this study, while drawing the map of resonance frequencies we considered the higher frequencies (i.e., with H/V maxima in the frequency range from 0.5 to 10 Hz) to be related to a shallower impedance contrast than those at very low frequencies. In fact, the shallower impedance contrasts probably determine the amplification in a frequency band closer to the fundamental resonance frequencies of buildings, and would be a better indicator of the local increase in damages. Considering the effect of instrumental self-noise in biasing the H/V shape, as showed by Strollo et al. (2007) and Strollo et al. (2008), the resulting fundamental resonance frequencies were considered reliable at least until 0.2 Hz, since in the favourable condition of a level of seismic noise higher than the NLNM, the instrumentation used allows the estimation of reliable H/V values down to nearly 0.15 Hz. Analysing the resulting map of resonance frequencies (Fig. 3a), it is straightforward to identify some general characteristics of the investigated area:

- the isoline of f_0 equal to 10 Hz indicates that the area with very thin sedimentary cover or outcropping bedrock is mainly on the eastern and northern part of the city;
- the central-southern area (e.g., Ataköy, Bakirköy, Güngören, etc.) is characterized by f_0 decreasing in a northeast–southwest direction from 10 Hz to about 0.3 Hz;
- the westernmost area shows more irregular f_0 features. In fact, in Avcilar, the f_0 are well above 0.5 Hz whereas most are about 1 Hz, while in the north, f_0 decrease until least 0.2 Hz, then increases again.

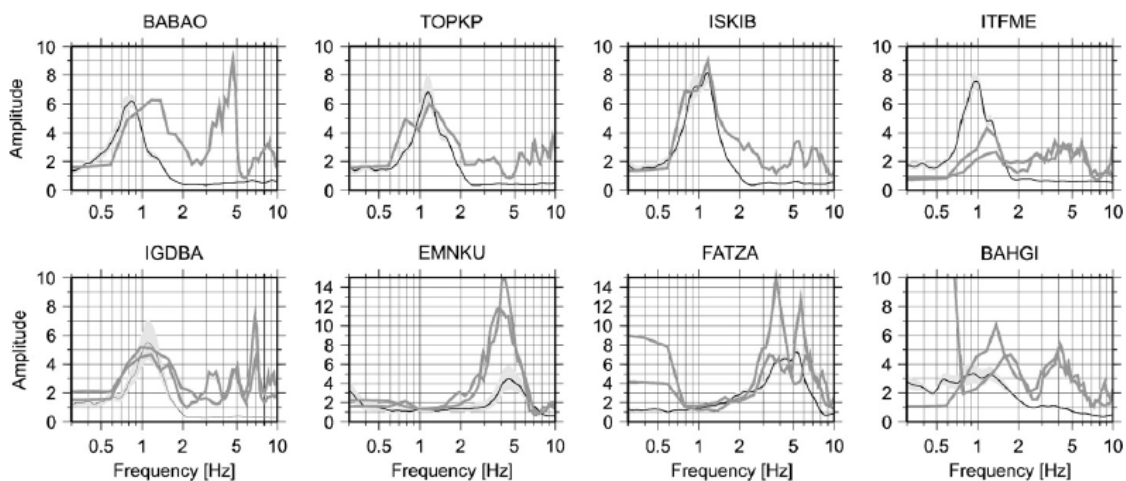


Fig. 2: Average H/V spectral ratios of noise (black line) 795% confidence interval (grey area) and H/V spectral ratios (dark grey lines) of one earthquake with M_4 recorded by IERRS stations BABAO, TOPKP and ISKIB, and two earthquakes with M_4 by IERRS stations ITFME, IGDBA, EMNKU, FATZA and BAHGI.

A comparison between the distribution of f_0 and the geological map (Figs. 3a and 1b) clearly highlights the agreement between the fundamental frequencies and geology. In particular, the f_0 limit of 10 Hz reproduces well the outcropping area of the Trakya and Dolayoba limestone formations. Other significant geostructural characteristics indicated by the f_0 map are as follows:

- for the central part of the investigated area, the very low f_0 (<0.5 Hz) in the Ataköy and Bakirköy districts (Fig. 3a) appears related to the presence of thicker segments of the Bakirköy formation;
- for the western part of the urban area (Avcilar district) f_0 values around 1Hz are observed, that could be related to the impedance contrast due to the contact between the soft Güngören and Cukurcesme formations overlying the stiff Bakirköy formation.

Fig. 3b shows the distribution of damage after the 17 August 1999 Kocaeli Earthquake (after Istanbul Governorate Disaster Management Centre). As observed in several previous studies (Cranswick et al., 2000; Kudo et al., 2002; Ozel et al., 2004; Ergin et al., 2004; Sørensen et al., 2006), the role of site effects in the damage distribution in the western part of Istanbul was considerable for this event. Although a discussion of the observed damage after the 17 August 1999 Kocaeli Earthquake is beyond the scope of this microzonation study, since information about the vulnerability of the structures in question is not available, we will consider a qualitative comparison between the f_0 map and the distribution of damage. In particular, the boundary between the “no damage” and “consistent damage” areas in the eastern and northern parts of the study area corresponds quite well to the isoline for the 10Hz f_0 map. Thus, at a first glance it is clear that the most damaged areas are located in the part of the city mainly covered by geologically softer sediments, where f_0 spans the frequencies of interest for buildings (i.e., from 0.5 to 10 Hz). Local differences may, of course, be due to vulnerability variations. Therefore, we believe that the f_0 map provides a valuable tool for identifying areas of a city that could experience heavier damage from future earthquakes due to the unfavourable geological conditions.

Array measurements

The S-wave velocity profiles were experimentally derived from seismic noise recordings carried out using arrays of sensors (Okada, 2003). Considering the high geological heterogeneity characterizing the investigated area, sensor arrays were installed at sites with different surficial geology (Fig. 1). The 2D array geometries were slightly variable due to practical restrictions. The inter-station distance chosen ranged between a minimum of 5 and 10 m, and a maximum between 100 and 150m, depending on the site. These ranges allow the analysis of a range of wavelengths that guarantee large depths to be investigated, but with still sufficient (i.e., from 5 to 10m) shallow resolution (Okada, 2003).

The arrays located in the Ataköy district (A7) and in the “Military area” (A8) consisted of 12 stations equipped with a 24-bit digitizer RefTek connected to a Mark L-4C-3D 1Hz sensor with GPS timing. The stations recorded for more than 1 h at 100Hz sampling rate. For A7, due to instrumental malfunctions, data from two stations could not be used. All other arrays consisted of 13 stations equipped with the EDL 24-bit digitizer and the same sensors of the previous array.

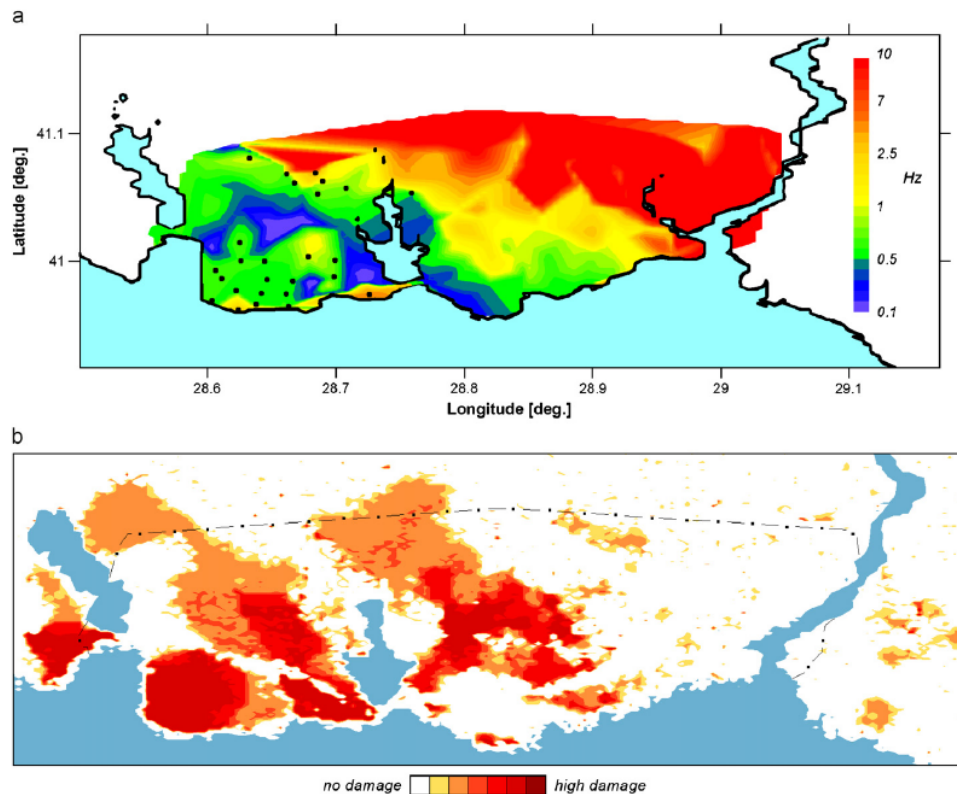


Fig. 3: (a) Map of the resonance frequency of the soil cover in the study area estimated by seismic noise recordings. Measurements where multiple peaks are observed (black dots) are also indicated; (b) Distribution of damage in Istanbul 17 August 1999 Kocaeli Earthquake (redrawn after Istanbul Governorate Disaster Management Centre). The dotted broken line bounds the investigated area.

Ambient seismic noise was recorded at 200Hz sampling rate and the stations were operated continuously for about 2 h. Before the analysis, all recordings were corrected for the instrumental response, considering the calibration parameters of each sensor. The H/V curves were computed for all stations of each array, following the procedure described previously. For estimating dispersion curves of Rayleigh waves, a total of 120 non-overlapping signal windows of vertical component recording, each window being 30 s long, were considered. In this study, the Extended Spatial Auto Correlation (ESAC; Ohori et al., 2002; Aki, 1957; Okada, 2003) and the frequency–wavenumber (FK), specifically the maximum likelihood method (MLM; Capon, 1969; Horike, 1985), methods were adopted. For the sites where both high-quality Rayleigh wave dispersion and H/V ratio curves were derived, a joint inversion scheme (Parolai et al., 2005) was used to estimate the local S-wave velocity profile. In particular, the joint inversions of dispersion and H/V curves were performed following the scheme proposed by Picozzi and Albarello (2007). This scheme uses a combination of genetic algorithms and generalized least-squares methods to obtain the global minimum of the non-linear solution fitness. The results of the inversion analysis for some array measurements are shown in Figs. 4. For most of the arrays (i.e., A1, A2, A5, A6, A7 and A8), it was possible to perform a joint inversion analysis using dispersion and H/V curves of equivalent quality. Only for arrays A3 and A4 were the inversions performed using the dispersion curve alone. The estimated S-wave velocity profiles provide a valuable overview of the different velocity structures in the western part of Istanbul (Figs. 4). The large variability and complexity of the velocity structure, characterized by different impedance contrasts, has been previously confirmed by different authors (Ozel et al., 2004; Sørensen et al., 2006), and could be responsible for the significant variability in ground motion that lead to the irregular distribution of damage after the 17 August 1999 Kocaeli Earthquake (Fig. 3b). More details can be found in Picozzi et al. (2008).

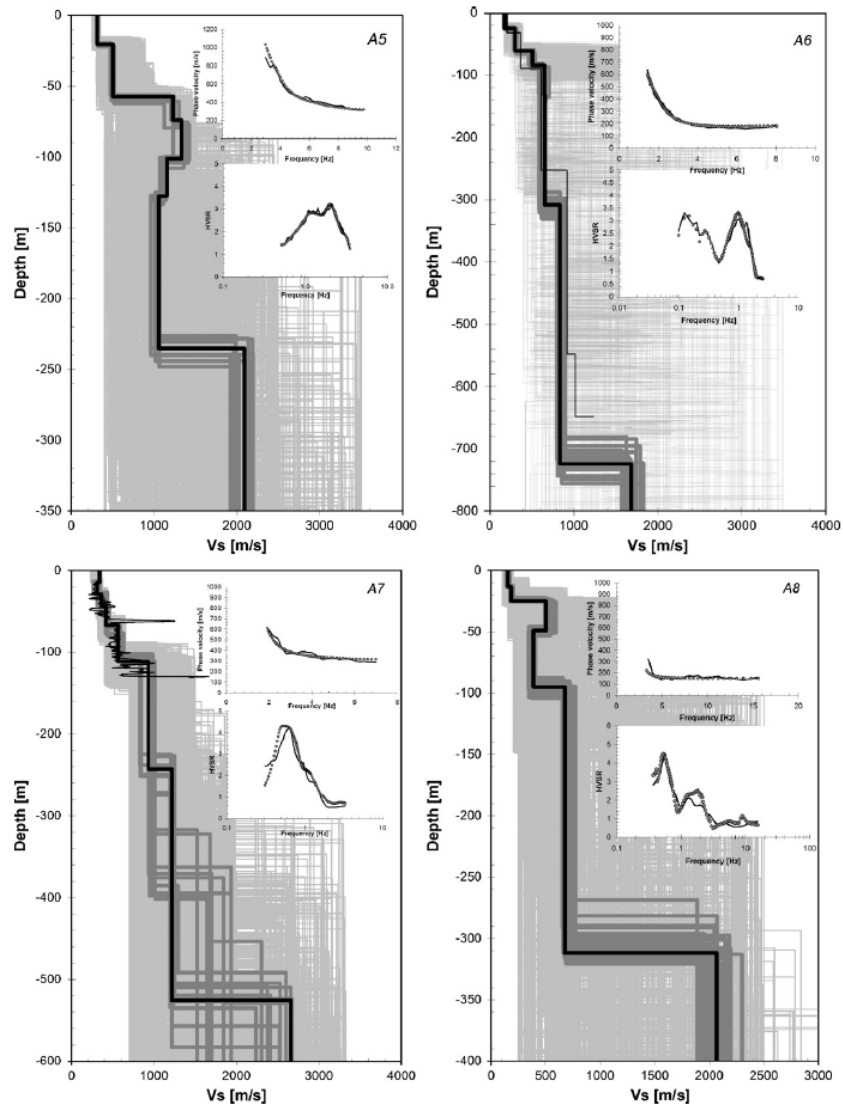


Fig. 4: Inversion results and fit to the dispersion and H/V ratio curves (insets) for the arrays A5, A6, A7 and A8. All four figures show tested models (thin grey lines), the minimum cost model (black line), and models lying inside the minimum cost +10% range (thick dark grey lines). Top inset: observed phase velocities (black line) and the phase velocities for the minimum cost model (grey dots). Bottom inset: average observed H/V ratio (black line) and the H/V ratio for the minimum cost model (grey dots). For array A6, the S-wave velocity profile from Kudo et al. (2002) (thin black line) is also reported. For array A7, the S-wave velocity profile (thin black line) determined from Suspension PS Logging testing performed at Borehole SK-3 at the Ataköy Vertical Array Site (see report in this volume) is also reported.

Theoretical site response

The final step in the 2D array recording analysis consists of estimating the theoretical site-response function, starting from the retrieved S-wave velocity profiles. The procedure followed is discussed in Parolai et al. (2007), and is based on computing synthetic seismograms using the improved Thompson–Haskell propagator matrix method (Wang, 1999). FFT spectra of recordings were calculated and the theoretical horizontal-to-vertical spectral ratios (THV) computed. Although this method provides a simplified wavefield with respect to reality (i.e., it does not take into account wave diffraction and scattering), it allows site-response functions to be obtained that are able to capture the main features of the experimental ones (Parolai et al., 2007). Fig. 5 shows the comparison between the THV ratio curves for the model of the array A2 located in the Fatih district, and the empirical EHV

amplification function evaluated at the nearby (≈ 1 km) IERRS station TOPKP (Fig. 1a). As shown by Harmandar et al. (2006), the spatial variation of ground motion over this distance is very small, and the results can be reasonably compared. We note how the THV response is able to capture all of the main characteristics of the empirical EHV. In particular, differently from the H/V from seismic noise that only fits well the fundamental resonance peak (f_0) at about 1 Hz, the THV reproduces both f_0 and also the overall shape of the EHV in the frequency range from 2 to 10 Hz.

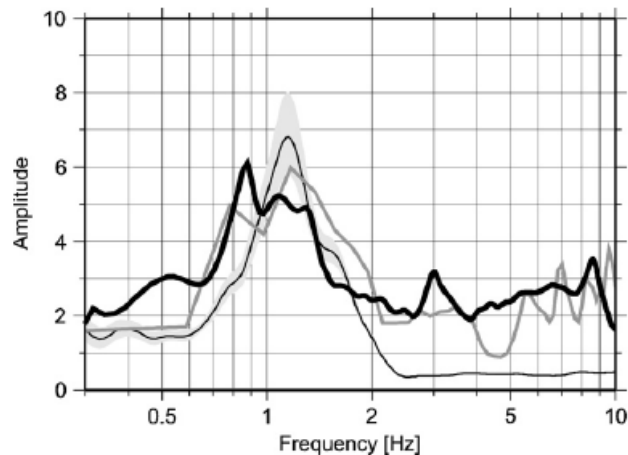


Fig. 5: IERRS station TOPKP. Average H/V spectral ratios from seismic noise (thin black line) 795% confidence interval (grey area), H/V spectral ratios of an earthquake (dark grey line) with M_4 recorded by IERRS stations (Table 1), H/V ratios (thick black line) at the surface station from synthetic seismograms considering the model obtained by the array A2.

Conclusions

The western part of the megacity Istanbul has been studied by means of an extensive survey of environmental seismic noise measurements. Comparison of H/V curves from single station seismic noise measurements with those obtained by earthquake recordings indicates that the former are a good proxy for the fundamental resonance frequency. Therefore, a high number of single station seismic noise measurements has been carried out in western Istanbul allowing the mapping of fundamental resonance frequency. The fundamental frequency map is in remarkable agreement with the geological map, both in identifying the boundaries of the Paleozoic bedrock outcrops in the northern and eastern parts of the investigated area (characterized by H/V curves without amplification or fundamental resonance frequencies over 10 Hz), and the identification of areas with soft sedimentary covers in the southwestern part. Other studies (Tezcan et al., 2002; Kudo et al., 2002; Ergin et al., 2004; Sørensen et al., 2006; Birgören and Ozel, 2006; Bakir et al., 2007) focused their activities only at sites characterized by the presence of soft sediments. They concluded that such situations are responsible for the anomalous ground motion amplification during earthquakes. Our results confirm this conclusion, having, in addition, a broader area coverage. In fact, the fundamental frequency map presented in this study provides a general overview of those area in the whole western Istanbul characterized by fundamental resonance frequencies that lie in the same range of those observed for the typical residential buildings in these regions (i.e., from 0.5 to 10 Hz). Seismic noise measurements using 2D arrays were carried out in areas with different surficial geology. The joint inversion of Rayleigh wave dispersion and H/V curves, using a combination of different methods to manage the severe non-linearity of the problem, allowed the retrieval of the S-wave velocity structure for some hundreds of meters. The estimated S-wave velocity profiles confirm the existence of different mechanical structures in the western part of the metropolitan area, which are in most of the cases (A1, A2,

A3, A5, A6, A7 and A8) characterized by strong impedance contrasts. The complex nature of such S-wave velocity structures determine theoretical site responses characterized, for most of the sites, by amplification factors well above than 2 in the frequency band from 0.2 to 10 Hz. Comparing the theoretical site response from 2D arrays with the empirical ones from an earthquake recorded at the nearby seismic station TOPKP indicates that, 2D array seismic noise methods allow for the estimation of the most relevant and reliable information about the local S-wave structure for site response. Therefore, further 2D array seismic noise measurements and analysis will be subject of future investigations.

References

- Aki, K (1957). Space and time spectra of stationary stochastic waves, with special reference to microtremors. *Bull. Earth. Res. Inst.* **35**, 415–456.
- Ambraseys, N. N., and C. F. Finkel (1991). Long-term seismicity of Istanbul and of the Marmara Sea region. *Terra Nova* **3**, 527–539.
- Ansal, A., J. Laue, J. Buchheister, M. Erdik, S. M. Springman, J. Studer, and D. Koksak (2004). Site characterization and site amplification for a seismic microzonation study in Turkey. *Proceedings of the 11th International Conference on Soil Dynamics and Earthquake Engineering (11th ICSDEE) and the 3rd International Conference on Earthquake Geotechnical Engineering (3rd ICEGE)*, Berkeley, CA, 7–9 January 2004. 53–60.
- Arai, H., and K. Tokimatsu (2004). S-wave velocity profiling by inversion of microtremor H/V spectrum. *Bull. Seism. Soc. Am.* **94**(1), 53–63.
- Arai, H., and K. Tokimatsu (2005). S-wave velocity profiling by joint inversion of microtremor dispersion curve and horizontal-to-vertical (H/V) spectrum. *Bull. Seism. Soc. Am.* **95**(5), 1766–1778.
- Bakir, P. G., G. Roeck, G. Degrande, and E. Reynders (2007). Seismic demands and analysis of site effects in the Marmara region during the 1999 Kocaeli Earthquake. *Nat. Hazards* **42**(1), 169–191.
- Beyen, K., and M. Erdik (2004). Two-dimensional nonlinear site response analysis of Adapazari plain and predictions inferred from aftershocks of the Kocaeli Earthquake of 17 August 1999. *Soil Dyn. Earth. Eng.* **24**, 261–79.
- Birgören, G., and O. Ozel (2006). Determination of site effects and ground motion lengthening in Istanbul area derived from small earthquake recordings. *Proceedings of the 8th US National Conference on Earthquake Engineering*, San Francisco, CA, USA, 18–22 April 2006, paper no. 1908.
- Capon, J. (1969). High-resolution frequency–wavenumber spectrum analysis. *Proc. IEEE* **57**(8), August 1969, 1408–1418.
- Cranswick, E., O. Ozel, M. Meremonte, M. Erdi, E. Safak, C. Mueller, D. Overturf, and A. Frankel (2000). Earthquake damage, site response, and building response in Avcilar, West of Istanbul, Turkey. *International Journal for Housing Science and Its Applications*, ISSN 0146-6518, special issue: Kocaeli Earthquake 1999, Oktay Ural (editor-in-chief), **24**(1), 85–96.
- Di Giacomo, D., M. R. Gallipoli, M. Mucciarelli, S. Parolai, and S. M. Richwalski (2005). Analysis and modeling of HVSR in the presence of a velocity inversion: the case of Venosa, Italy. *Bull. Seism. Soc. Am.* **95**, 2364–2372.
- Erdik, M., N. Aydinoglu, Y. Fahjan, K. Sesetyan, M. Demircioglu, B. Siyahi, E. Durukal, C. Ozbey, Y. Biro, H. Akman, and O. Yuzugulu. (2003). Earthquake risk assessment for Istanbul metropolitan area. *Earth. Eng. Vib.* **2**(1), 1-25.
- Ergin, M., S. Özalaybey, M. Aktar, and M. N. Yalc-in (2004). Site amplification at Avcilar, Istanbul. *Tectonophysics* **391**, 335–346.
- Fäh, D., F. Kind, and D. Giardini (2001). A theoretical investigation of average H/V ratios. *Geophys. J. Int.* **145**, 535–549.
- Gruenthal, G. (1998). European macroseismic scale 1998 (EMS-98). *Cahiers du Centre Européen de Géodynamique et de Séismologie 15*, Luxembourg, 1-99.
- Harmandar, E., E. Durukal, M. Erdik, and O. Ozel (2006). Spatial variation of ground motion in Istanbul. *European Geophysical Union, Vienna, 2006*, Poster presentation ID 1633, potential for very large earthquake disasters in the European Mediterranean region.
- Horike, M (1985). Inversion of phase velocity of long period microtremors to the S-wave velocity structure down to the basement in urbanized areas. *J. Phys. Earth* **33**, 59–96.
- Kudo, K., T. Kanno, H. Okada, O. Ozel, M. Erdik, T. Sasatani, S. Higashi, M. Takahashi, and K. Yoshida (2002). Site-specific issues for strong ground motions during the Kocaeli, Turkey, earthquake of 17 August 1999, as inferred from array observations of microtremors and aftershocks. *Bull. Seism. Soc. Am.* **92**(1), 448–465.

- Mucciarelli, M., and M. R. Gallipoli (2006). Comparison between Vs30 and other estimates of site amplification in Italy. *First European conference on earthquake engineering and seismology (a joint event of the 13th ECEE and 30th General Assembly of the ESC)*, Geneva, Switzerland, 3–8 September 2006, paper no. 270.
- Ohori, M., A. Nobata, and K. Wakamatsu (2002). A comparison of ESAC and FK methods of estimating phase velocity using arbitrarily shaped microtremor analysis *Bull. Seism. Soc. Am.* **92**, 2323–2332.
- Okada, H. (2003). The Microtremor Survey Method. *Geophysical Monograph Series 12*. Washington, American Geophysical Union, 2003.
- Ozel, O., T. Sasatani, K. Kudo, H. Okada, T. Kanno, S. Tsuno, M. Yoshikawa, S. Noguchi, M. Miyahara, and H. Goto (2004). Estimation of S-wave velocity structures in Avcilar–Istanbul from array microtremor measurements. *J. of Faculty of Science, Hokkaido University Series VII Geophysics*, Vol. 1, No 1.
- Ozmen, B (2004). Iseismic Map of Izmit Earthquake. *Izmit Körfezi Depreminin Hasar Durumu (Rakamsal Verilerle), damage in the Izmit Bay Earthquake (with quantitative data)*, Türkiye Deprem Vakfı, İstanbul, 2004.
- Park, D., and Y. M. A. Hashash. Probabilistic seismic hazard analysis with non linear site effects in the Mississippi embayment. *Proceedings of the 13th World Conference on Earthquake Engineering*, Vancouver, CD-Rom edition 2004, paper no. 1549.
- Parolai, S., P. Bormann, and C. Milkereit (2001). Assessment of the natural frequency of the sedimentary cover in the Cologne area (Germany) using noise measurements. *J. Earth. Eng.* **5**(4), 541–564.
- Parolai, S., D. Bindi, M. Baumbach, H. Grosser, C. Milkereit, S. Karakisa, and S. Zünbül. (2004) Comparison of different site estimation techniques using the Izmit 1999 earthquake aftershocks. *Bull. Seism. Soc. Am.* **94**(3), 1096–1108.
- Parolai, S., S. M. Richwalski, C. Milkereit, and D. Fäh (2006). S-wave velocity profiles for earthquake engineering purposes for the Cologne area (Germany). *Bull. Earth. Eng.* **4**, 65–94.
- Parolai, S., M. Picozzi, S. M. Richwalski, and C. Milkereit (2005). Joint inversion of phase velocity dispersion and H/V ratio curves from seismic noise recordings using a genetic algorithm, considering higher modes. *Geophys. Res. Lett.* **32**, L01303, doi:10.1029/2004GL021115.
- Parolai, S., M. Mucciarelli, M. R. Gallipoli S. M. Richwalski, and A. Strollo (2007). Comparison of empirical and numerical site responses at the Tito test site (Southern Italy). *Bull. Seism. Soc. Am.* **97**(5), 1413–1431.
- Picozzi, M., and D. Albarello (2007). Combining genetic and linearized algorithms for a two-step joint inversion of Rayleigh wave dispersion and H/V spectral ratio curves. *Geophys. J. Int.* **169**, 189–200.
- Picozzi, M., A. Strollo, S. Parolai, E. Durukal, O. Özel, S. Karabulut, J. Zschau, and M. Erdik (2008). Site characterization by seismic noise in Istanbul, Turkey. *Soil. Dyn. Earth. Eng.*, doi:10.1016/j.soildyn.2008.05.007
- Richwalski, S. M., M. Picozzi, S. Parolai, C. Milkereit, F. Baliva, D. Albarello, K. Row-Chowdhury, H. van der Meer, and J. Zschau (2007). Rayleigh wave dispersion curves from seismological and engineering geotechnical methods: a comparison at the Bornheim test site (Germany). *J. Geophys. Eng.* **4**, 349–361.
- Scherbaum, F., K. G. Hinzen, and M. Ohrnberger (2003). Determination of shallow shear wave velocity profiles in Cologne, Germany area using ambient vibrations. *Geophys. J. Int.* **152**, 597–612.
- Sørensen, M., I. Oprsal, S. Bonnefoy-Claudet, K. Atakan, P. M. Mai, N. Pulido, and C. Yalciner. (2006). Local site effects in Ataköy, Istanbul, Turkey, due to a future large earthquake in the Marmara Sea. *Geophys. J. Int.* **167**(3), 1413–1424.
- Stewart, J. P., A. H. Liu, and Y. Choi (2003). Amplification factors for spectral acceleration in tectonically active regions. *Bull. Seism. Soc. Am.* **93**, 332–352.
- Strollo, A., S. Parolai, K.-H. Jäckell, S. Marzorati, and D. Bindi (2007). The effect of seismic instrumentation using short-period electromagnetic sensors on seismic noise analysis in the frequency band 0.1–1 Hz. *Bull. Seism. Soc. Am.* **98**(2), 671–681.
- Strollo, A., D. Bindi, S. Parolai, and K.-H. Jäckell (2008). On the suitability of 1 s geophone for ambient noise measurements in the 0.1–20 Hz frequency range: experimental outcomes. *Bull. Earth. Eng.* **6**, 141–147, DOI 10.1007/s10518-008-9061-x.
- Tezcan, S. S., E. Kaya, L. E. Bal, and Z. Özdemir (2002). Seismic amplification at Avcilar, Istanbul. *Eng. Struct.* **24**, 661–667.
- Tokimatsu, K., S. Tamura, and H. Kojima (1992). Effects of multiple modes on Rayleigh wave dispersion characteristics. *J. Geotech. Eng.* **118**, 1529–1543.
- Wald, L. A., and J. Mori (2000). Evaluation of methods for estimating linear site-response amplifications in the Los Angeles Region. *Bull. Seism. Soc. Am.* **90**, S32–S42.
- Wang, R (1999). A simple orthonormalization method for stable and efficient computation of Green's functions. *Bull. Seism. Soc. Am.* **89**(3), 733–741.

10. The Ataköy Vertical Array, Turkey: Preliminary Results

S. Parolai¹, A. Ansal³, A. Kurtulus³, A. Strollo^{1,2} and J. Zschau¹

¹Helmholtz Centre Potsdam GFZ German Research Centre for Geosciences, Section 2.1 "Earthquake Risk and Early Warning", Telegrafenberg, D-14473 Potsdam, Germany

²Institute of Geosciences, Universität Potsdam, Karl-Liebknecht Strasse, 14476 Potsdam, Germany

³Boğaziçi Üniversitesi, Kandilli Rasathanesi ve Deprem Araştırma Enstitüsü, Department of Earthquake Engineering, 34684, Çengelköy, Istanbul, Turkey

Introduction and aim of the study

It has been long recognized that the ground shaking during earthquakes can be significantly modified by the mechanical properties of surficial geological formations, typically referred to as local soil conditions. Therefore, realistic ground-motion predictions of future earthquakes can be only achieved by combining realistic source, wave-propagation, and site-response models. The increasing number of observations in the last few decades has contributed toward the understanding of strong motion site effects by the engineering and seismological communities leading to advancements in the state of knowledge and modeling of sediment response in situ (Field et al., 1997). Nonetheless, further resolution and more effective representation of the physics in the near surface requires a good estimate of the input motion and of wave propagation in shallow layers, and by far the best source of information is provided by downhole arrays.

Downhole measurements are a valuable complement to in situ and laboratory geotechnical investigation techniques. In fact, they provide critical constraints both on interpretation methods for surface observations as well as information on the real material behaviour and overall site response over a wide range of loading conditions (Assimaki et al., 2006). The amount and quality of information from downhole arrays in seismically active areas is the key to both improve the understanding of in situ soil behaviour and to assess the modeling and parametric uncertainty of employed methodologies for strong-motion site-response analysis, and for shallow geology investigations.

With this aim, a vertical array of accelerometers was installed in Ataköy (western Istanbul) where, during the 1999 Kocaeli earthquake the peak ground acceleration was measured to be 0.17 g, much higher than the values recorded (0.05-0.09 g) east of the Golden Horn by the KOERI rapid response system (Dalgic, 2004).. It is worth noting that east of the Golden Horn the Paleozoic rocks of the Trakya formation are outcropping while in Ataköy Oligocene and Miocene sediments overlie the Paleozoic bedrock, hinting to the influence of site effects on ground motion.

Array description

In December 2005, a drilling program consisting of four boreholes of 25m, 50 m, 70 m and 140 m deep was realized (ZETAŞ[®], 2006) (Figure1). PVC pipes were installed in the borehole and the space between the PVC pipes and boreholes was grouted with cement grout. Within the 150 m deep borehole, based on the encountered subsoil conditions, representative and/or undisturbed soil samples were obtained and Standard Penetration Test (SPT) carried out at regular intervals of 1.5 m. Refusal was defined when the blowcount was greater than 100 blows per 50 mm.

The array was instrumented with 3 Shallow Boreholes accelerometers (SBEPI) at 25, 50 and 70 m depth and a Down borehole accelerometer (ES-DH) at 140 m depth, connected to a 12 channels K2 at the surface. Furthermore a K2 with internal episenor was installed at the surface. Data can be accessed via internet by the Kandilli Observatory and the GFZ.



Fig. 1: Drilling operation at the Ataköy site.

A total of 60 SPT samples and (3) undisturbed samples (from depths 35. m, 49 m, and 52 m) were chosen for laboratory tests, including sieve analysis, aiming at estimating natural moisture content and Atterberg's limits.

Figure 2 summarizes the stratigraphy at the site and the results of the SPT tests.

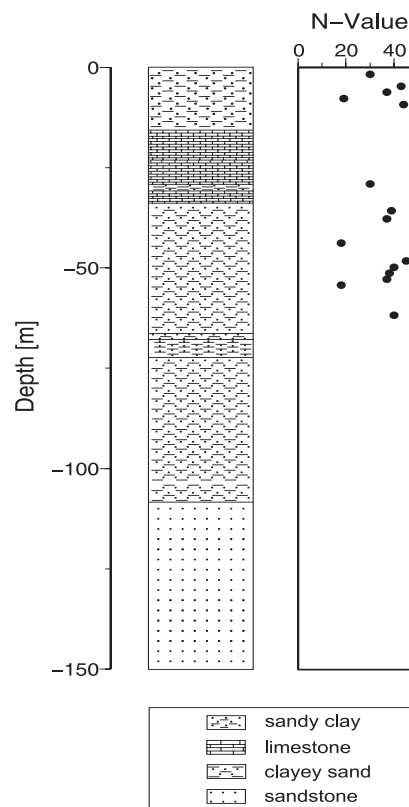


Fig. 2: Left) Ataköy vertical array stratigraphic column. Right) SPT values versus depth.

Suspension PS velocity loggings

Suspension PS velocity logging is a method for determining shear and compressional wave velocity (V_s and V_p) profiles of soils and rocks. Measurements are made in a single, cased/uncased, fluid filled borehole (Nigbor and Imai, 1994). The measurements procedure is as follow. A probe, that has a solenoid source at his end and 2 geophones mounted at a distance of 1 m, is lowered to the bottom of the borehole and then raised at specific depth intervals to take measurements. At each depth the source is activated in one direction and the

output from the two horizontal geophones, which include the S-wave, is recorded. The source is then activated in the reverse direction, producing a reverse polarity wave. Finally, the source is activated in the first direction again and the output from the vertical component (mainly dominated by P-waves) is recorded. The probe is then raised to the next investigated depth. Typically measurements are carried out at 0.5-1 m intervals. The analysis consists in picking the first break or the first peak for estimating the arrival time and then, knowing the distance between the geophones, calculating the velocity in the corresponding depth interval. In Ataköy a PS Logging system manufactured by OYO Corporation, Japan was used. It consists of a probe (Model 3302A), cable, winch (Type 350) and logger (control/recording) (Model 3660A). The probe is approximately 8 meters in length. The source used produce energy mainly in the frequency band 500-5000 Hz. The test was carried out in November 2006.

The results of the PS logging test are shown in Figure 3. The results show that there is a general trend of V_s to increase with depth. The average S-wave velocity in the uppermost 35 m is about 220 m/s, while it increases to about 530 m/s in the interval 35 m-100m depth. Below the depth of 100 m the velocity values are more scattered.

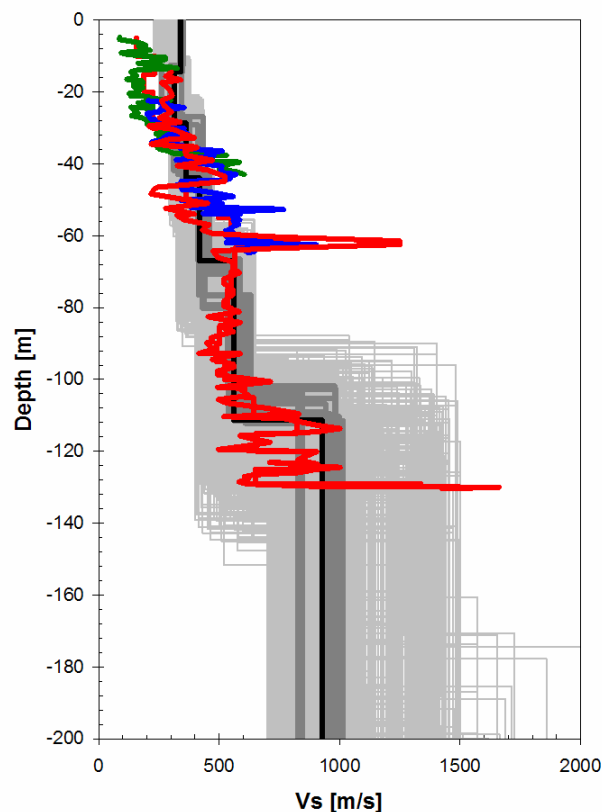


Fig. 3: Joint inversion results for Ataköy using the Picozzi and Albarello (2007) inversion scheme: all tested models (light grey), the minimum misfit model (black), models lying inside the minimum misfit +10% range (dark grey). Green, blue and red lines depict the PS logging results for the tests carried out in the 50,70, and 140 m deep boreholes, respectively.

Micro array measurements

The recent improvements in the quality of seismic instrumentation, as well as in computing power have enabled seismologists to re-direct their attention towards analyzing seismic noise recorded by arrays (e.g. Horike, 1985; Hough et al., 1992; Ohori et al., 2002; Okada, 2003; Scherbaum et al., 2003; Parolai et al., 2005), a method originally proposed by Aki (1957). The objective of such studies is the determination of (local) shear-wave velocity profiles

down to depths prohibitive both for the costs they would imply and the technical demands they would require for standard geophysical methods in urban areas.

Therefore, in order to estimate the S-wave velocity structure at the vertical array site (Ataköy), micro-array measurements of seismic noise were performed. The dispersion curves obtained by applying the Extended Spatial Correlation (ESAC) method were inverted for the S-wave velocity structure. The obtained results can be compared with those derived by PS logging and by deconvolution of the earthquake related wavefield in the borehole.

An array of 12 stations was installed in the area selected for the vertical array installation in Ataköy on 20 September 2005. The stations worked contemporarily for more than 1 hour recording noise at 100 samples/sec, which is adequate for the inter-station distance considered (~10 m to ~230 m). Every station was equipped with a 24 bit digitizer connected to a Mark L-4C-3D 1Hz sensor and with GPS timing. For the analysis, the data recorded by each station of the array were divided in 60 s- windows. A total of 44 non-overlapping windows were considered. Only the vertical component was analyzed to obtain the Rayleigh wave dispersion curve. Recordings were corrected for the instrumental response considering the calibration parameters of each sensor. Due to malfunctioning, data from two stations could not be used. Figure 1 shows the array geometry.

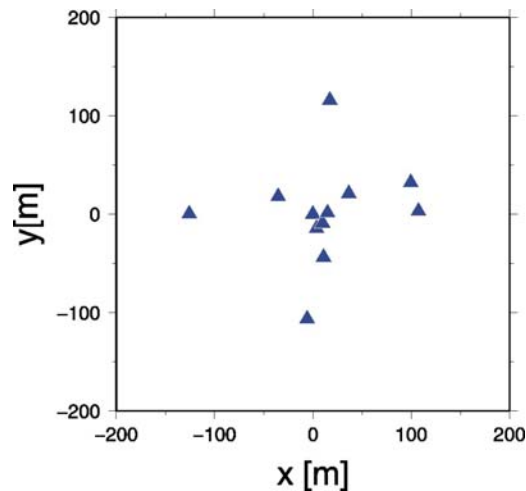


Fig. 4: Station distribution of the array in Ataköy.

The calculation of the dispersion curve (Figure 5) was carried out following Ohori et al. (2002), Okada (2003) and Parolai et al. (2006).

Horizontal-to-vertical (H/V) spectral ratios (Nakamura, 1989) from the 44 windows of noise recordings at each station were calculated as well. Their Fourier spectra were computed and smoothed using a Konno and Ohmachi (1998) window with the coefficient b fixed to 40. For every station a mean H/V curve was calculated using a logarithmic average of the individual H/V curves. Figure 5, upper right, shows the mean H/V curve at the central station of the array.

The inversion was performed following Parolai et al. (2005) and using the modified Genetic Algorithm (GA) proposed by Yamanaka and Ishida (1996). The P-wave velocity was fixed to 700 m/s in the first layer, and it was then chosen to increase from 1400 m/s in the second layer to 1800 m/s in seventh one. The half-space P-wave velocity was fixed to 2250 m/s. Furthermore, the inversion was also performed following the scheme proposed by Picozzi and Albarello (2007), attempting also for inverting for the Poisson's ratio. The two inversions produced very similar S-wave velocity profiles, while the P-wave structure was somewhat different. This highlights the weak dependency of the phase velocity and H/V curve inversion on the V_p structure.

In both cases, the dispersion curve constrains the model only down to 130-180 m. The deeper part is constrained by the H/V data alone. All models lying inside the minimum cost +10%

show little variability down to 230 m depth. Below 230 m, the larger variability indicates that the trade-off between velocity and thickness of the layers is not fully solved by the H/V inversion.

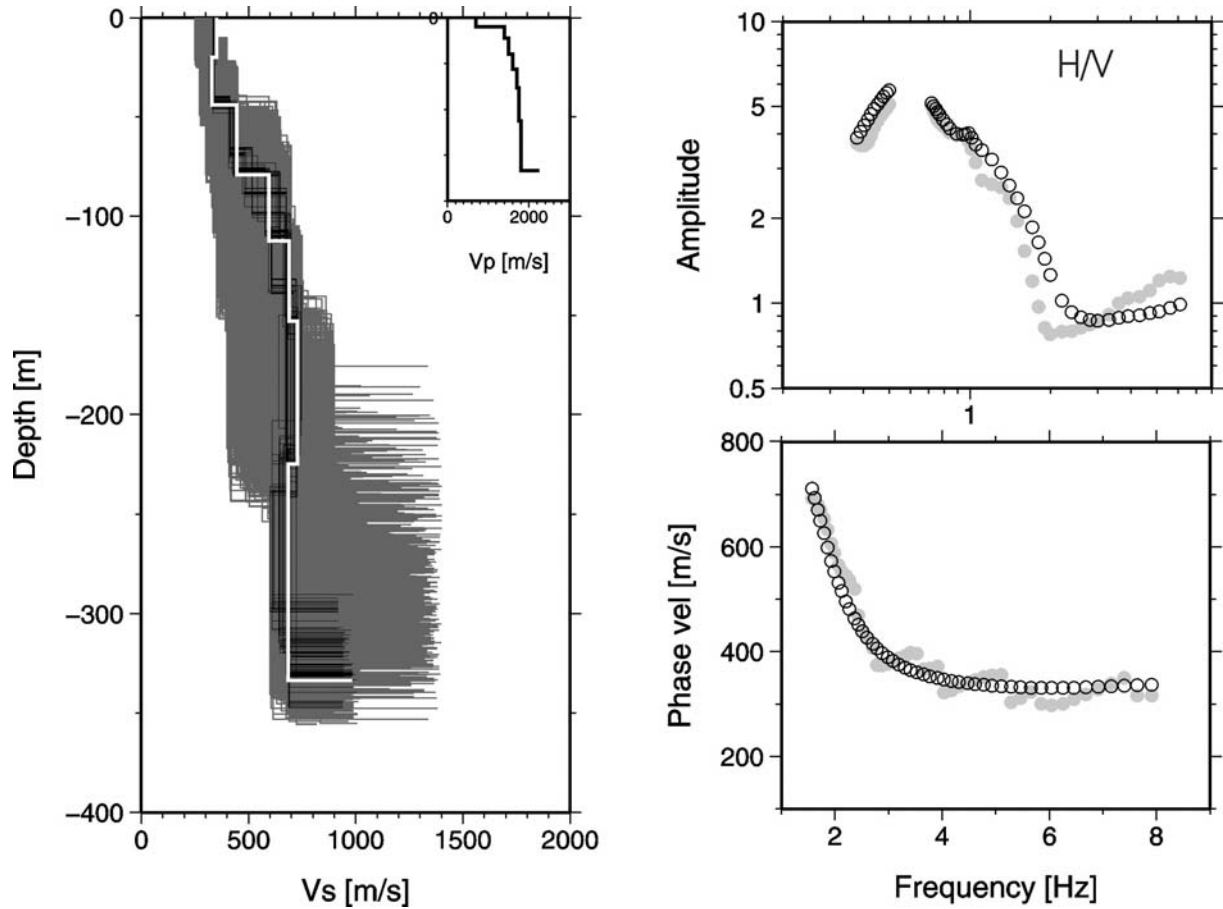


Fig. 5: Left: Joint inversion results for Ataköy using the Parolai et al. (2005) inversion scheme: all tested models (dark grey), the minimum misfit model (white), models lying inside the minimum misfit +10% range (black). The inset shows the P-wave velocity model using equation (1) in the joint inversion procedure. Right top: observed (grey circles) and calculated (white circles) H/V spectral ratio. Right bottom: observed (grey circles) and calculated (white circles) apparent phase velocities.

Deconvolution of the wavefield

Starting from December 2006, eight seismic events with magnitude between 2.8 and 4.6 have been recorded by the Ataköy vertical array. The application of the standard spectral ratio between the Fourier transform of the signals recorded at the surface and within the boreholes with that recorded at the array bottom accelerometer (140 m) showed a peak at nearly 1 Hz. The independency of frequency of this peak on the station depth suggests that it might be due to a spectral hole at that frequency in the Fourier transform of bottom station recording due to destructive interference of up-going and down going waves. In fact, the period of 1 second correspond to four times the travel time of S-waves as estimated by the microarray and the Ps-logging measurements. In order to assess if the downhole recordings are affected by down-going waves, we deconvolved the wavefield recorded in the boreholes with that recorded at the surface similarly to Metha et al. (2007). Figure 6, shows the recordings of one event and the corresponding deconvolved records. From this figure, it is clear the presence of an up-going and a down going wave propagating with a velocity that agrees well with that estimated for S-waves by micro-array measurements.

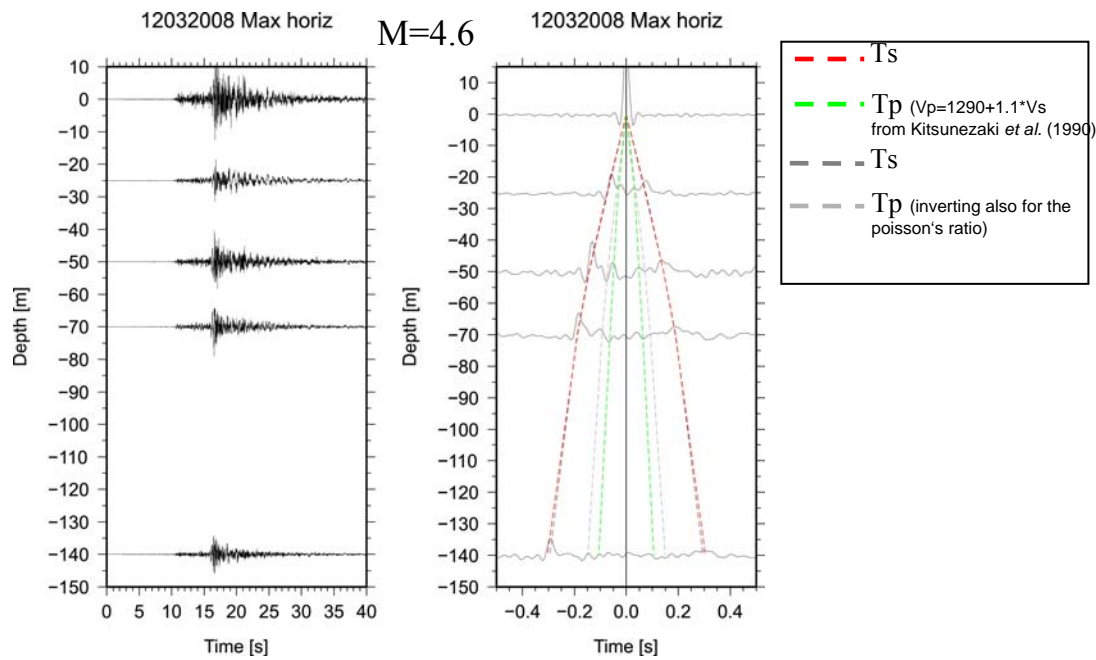


Fig. 6: Left: Horizontal component ground motions recorded at different depths. Right: The upgoing and downgoing waves. The S-wave travel time computed from the velocity model derived by using the Parolai et al. (2005) inversion scheme (dashed red line) and the S-wave travel time computed from the velocity model derived by using the Picozzi and Albarello (2007) inversion scheme (dashed dark grey line) are indicated. The P-wave travel time computed from the velocity model derived by using the Parolai et al. (2005) inversion scheme (dashed green line) and the P-wave travel time computed from the velocity model derived by using the Picozzi and Albarello (2007) inversion scheme (dashed light grey line) are also shown.

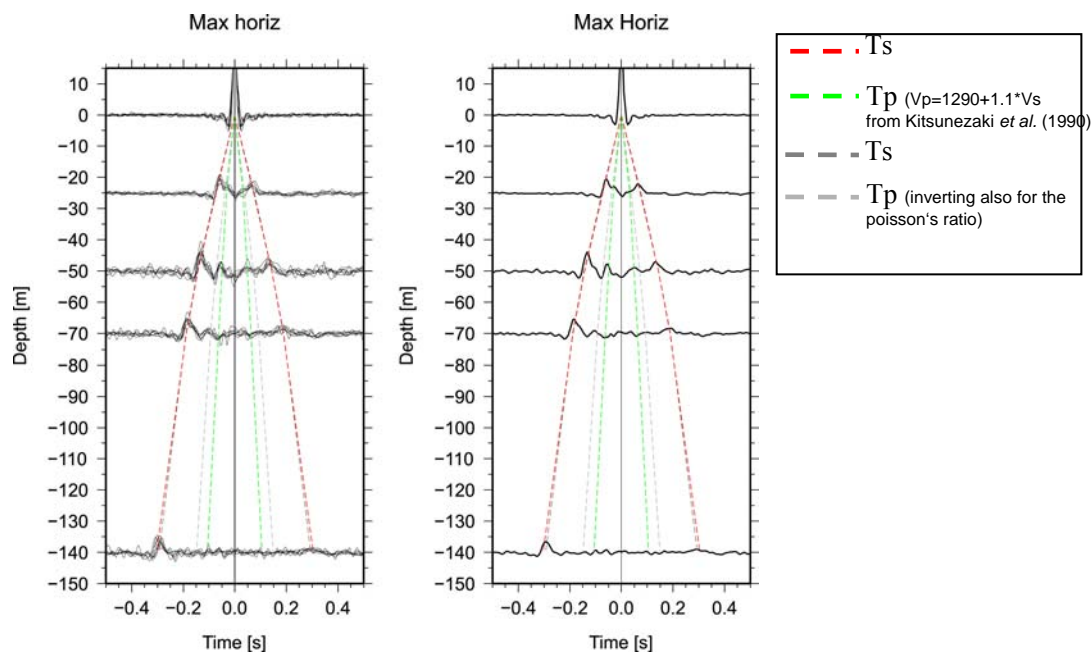


Fig. 7: Left: Horizontal component ground motions recorded at different depths. Right: The upgoing and downgoing waves. The S-wave travel time computed from the velocity model derived by using the Parolai et al. (2005) inversion scheme (dashed red line) and the S-wave travel time computed from the velocity model derived by using the Picozzi and Albarello (2007) inversion scheme (dashed dark grey line) are indicated. The P-wave travel time computed from the velocity model derived by using the Parolai et al. (2005) inversion scheme (dashed green line) and the P-wave travel time computed from the velocity model derived by using the Picozzi and Albarello (2007) inversion scheme (dashed light grey line) are also shown.

Figure 7, shows the up-going and down-going waves obtained deconvolving the waveforms of the horizontal components for all the events and their stacking. Similarly, Figure 8 shows the up-going and down-going waves obtained deconvolving the waveforms of the vertical components for all the events and their stacking. In this case, the waves are propagating with a velocity consistent with the P-wave velocity model obtained by following the Parolai et al. (2005) inversion scheme. This result indicates that P-wave velocities are already quite high close to the surface, with values typical for saturated media.

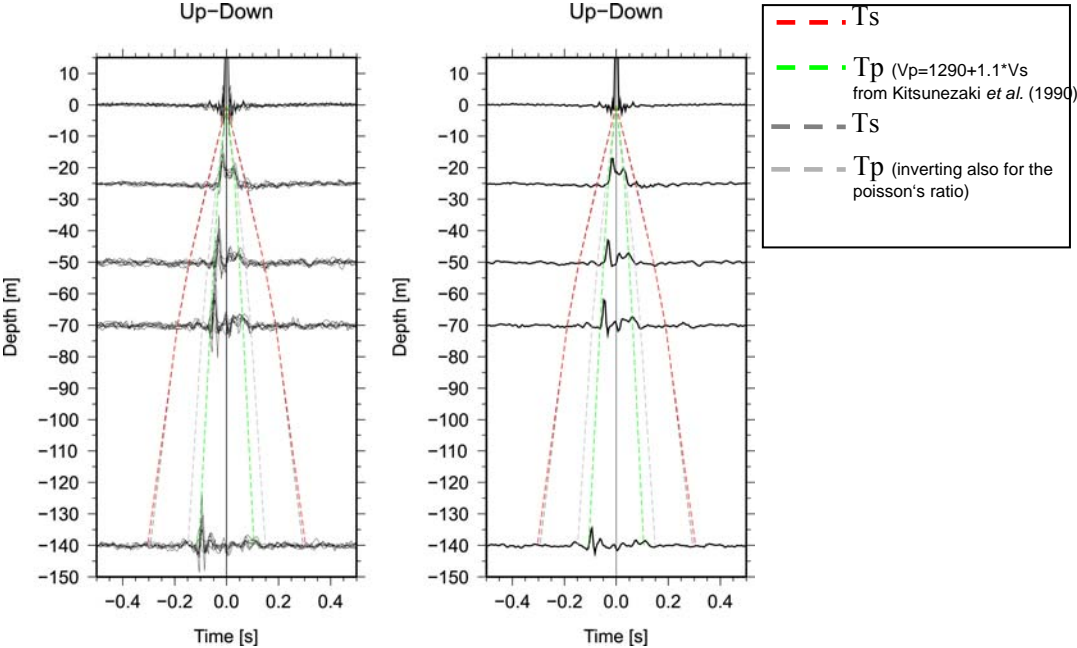


Fig. 8: Left: Vertical component ground motions recorded at different depths. Right: The upgoing and downgoing waves. The S-wave travel time computed from the velocity model derived by using the Parolai et al. (2005) inversion scheme (dashed red line) and the S-wave travel time computed from the velocity model derived by using the Picozzi and Albarello (2007) inversion scheme (dashed dark grey line) are indicated. The P-wave travel time computed from the velocity model derived by using the Parolai et al. (2005) inversion scheme (dashed green line) and the P-wave travel time computed from the velocity model derived by using the Picozzi and Albarello (2007) inversion scheme (dashed light grey line) are also shown.

Conclusions

Several geophysical/geotechnical investigations have been carried out at the Ataköy vertical array site. In particular it was found out that the S-wave velocity model derived by the analysis of noise collected by a microarray is in good agreement (in terms of average velocities) with the PS logging results. The reliability of the S-wave velocity profile obtained by micro-array analysis was then confirmed by the comparison with the propagation of up-going and down-going waves computed by deconvolution of the recorded wavefield at different depths. This indicates that micro-arrays are a useful tool in site effects investigation for urban area.

The derived velocity model can be used to estimate a preliminary site response by numerical simulation for comparison with empirical data.

The vertical array data set will be exploited for in-situ measurements of damping, for estimation of soil non-linearity and for estimating the input ground motion necessary for engineering calculations.

References

Aki, K. (1957). Space and time spectra of stationary stochastic waves, with special reference to microtremors.

- Bull. Earthq. Res. Inst.* **35**, 415-456.
- Assimaki, D., W. Li, J. H. Steidl, and K. Tsuda (2008), Site amplification and attenuation via downhole array seismogram inversion: a comparative study of the 2003 Miyagi-Oki aftershock sequence. *Bull. Seism. Soc. Am.* **98**, 301-330.
- Dalgic, S. (2004). Factors affecting the greater damage in the Avclar area of Istanbul during the 17 August 1999 Izmit earthquake. *Bull. Eng. Geol. Env.* **63**, 221-232.
- Field, E. H., P. A. Johnson, I. A. Beresnev, and Y. Zeng (1997). Nonlinear ground-motion amplification by sediments during the 1994 Northridge earthquake. *Nature* **390**, 599-602.
- Herrmann, R. B., C. J. Ammon, J. Julia, and T. Mokhtar (1999) Joint inversion of receiver functions and surface-wave dispersion for crustal structure. *Proc. 21st Seismic Research Symposium Technologies for monitoring the comprehensive Nuclear test Ban treaty*, September 21-24, 1999, Las Vegas, Nevada, USA, published by Los Alamos National Laboratory, LA-UR-99 4700.
- Horike, M. (1985). Inversion of phase velocity of long period microtremors to the S-wave velocity structure down to the basement in urbanized areas. *J. Phys. Earth* **33**, 59-96.
- Hough, S. E., L. Seeber, A. Rovelli, L. Malagnini, A. De Cesare, G. Selvaggi, and A. Lerner-Lam (1992). Ambient noise and weak motion excitation of sediment resonances: results from the Tiber Valley, Italy. *Bull. Seism. Soc. Am.* **82**, 1186-1205.
- Kitsunezaki, C., N. Goto, Y. Kobayashi, T. Ikawa, M. Horike, T. Saito, T. Kurota, K. Yamane, and K. Okuzumi (1990). Estimation of P- and S- wave velocities in deep soil deposits for evaluating ground vibrations in earthquake. *J. JSNDS* **9**, 1-17 (in Japanese with English abstract).
- Konno, K., and T. Ohmachi (1998). Ground-Motion Characteristic Estimated from Spectral Ratio between Horizontal and Vertical Components of Microtremor. *Bull. Seism. Soc. Am.* **88**, 228-241.
- Mehta, K., R. Snieder, and V. Grazier (2007). Downhole receiver function: a case study. *Bull. Seism. Soc. Am.* **97**, 1396-1403.
- Nakamura, Y. (1989). A method for dynamic characteristics estimations of subsurface using microtremors on the ground surface. *Q. Rept. RTRI Japan* **30**, 25-33.
- Nigor, R. L., and T. Imai (1994). The suspension P-S velocity logging method. *Proc. XIII International Conference on Soil Mechanics and Foundation Engineering*, 5-10, January 1994, New Delhi, India.
- Ohori, M., A. Nobata, and K. Wakamatsu (2002). A comparison of ESAC and FK methods of estimating phase velocity using arbitrarily shaped microtremor analysis. *Bull. Seism. Soc. Am.* **92**, 2323-2332.
- Okada, H. (2003). The microtremor survey method. *Geophysical monograph series* **12**, American Geophysical Union, Washington.
- Parolai, S., M. Picozzi, S. M. Richwalski, and C. Milkereit (2005). Joint inversion of phase velocity dispersion and H/V ratio curves from seismic noise recordings using a genetic algorithm, considering higher modes. *Geoph. Res. Lett.* **32**, L01303, doi: 10.1029/2004GL021115.
- Parolai S, S.M. Richwalski, C. Milkereit, and D. Faeh (2006). S-wave velocity profiles for earthquake engineering purposes for the Cologne area (Germany). *Bull Earth. Eng.* **4**, 65-94.
- Picozzi M, and D. Albarello (2007). Combining genetic and linearized algorithms for a two-step joint inversion of Rayleigh wave dispersion and H/V spectral ratio curves. *Geophys J. Int.* **169**, 189-200.
- Scherbaum, F., K.-G. Hinzen, and M. Ohrnberger (2003). Determination of shallow shear wave velocity profiles in Cologne, Germany area using ambient vibrations. *Geophys. J. Int.* **152**, 597-612.
- Yamanaka, H., and H. Ishida (1996). Application of Generic algorithms to an inversion of surface-wave dispersion data. *Bull. Seism. Soc. Am.* **86**, 436-444.
- ZETAŞ® (2006). Factual report on drilling for strong ground motion network, 03/04/2006. ZETAŞ® Zemin Teknolojisi A.Ş.

11. Karlsruhe-Istanbul Mobile Network - The KIMNET Experiment

J. Ritter¹, and the KIMNET Research Group (H. Alcik², E. Durukal², M. Erdik², J. Groos¹, N. Kafadar², P. Knopf¹, A. Mert², O. Özel², R. Plokarz¹, W. Scherer¹, and F. Wenzel¹)

¹Geophysical Institute, Universität Karlsruhe (TH), Herzstr. 16, 76187, Karlsruhe, Germany

²Boğaziçi Üniversitesi, Kandilli Rasathanesi ve Deprem Araştırma Enstitüsü, Department of Earthquake Engineering, 34684, Çengelköy, Istanbul, Turkey

The Karlsruhe-Istanbul Mobile Network (KIMNET) is an initiative to enhance urban seismology with the aim to mitigate future earthquake impact in metropolitan regions. KIMNET is planned by the Geophysical Institute of the Universität Karlsruhe (TH) (GPI-KA) and the Kandilli Observatory and Earthquake Research Institute of the Bosphorus University (KOERI). As exemplary target we want to monitor the ground motion across the Istanbul municipality area for about two years. This experiment will acquire basic data for several research targets. These targets include improvement of near-real time data transfer of continuous broadband seismic waveforms, near-real time processing of the seismic data and seismic engineering applications including monitoring.

As a first step several methods for near-real time data transfer were explored with the aim to acquire the full waveforms within less than one minute world-wide at reasonable costs. The seismological measurements are done with the mobile stations of the KARlsruhe BroadBand Array (KABBA). KABBA consists of 35 units with 24-bit recorders, broadband seismometers, GPS time synchronisation and data processing facilities (<http://www-gpi.physik.uni-karlsruhe.de/pub/kabba/>). For KIMNET a sampling rate of 100 samples per second is planned for three channels (24-bit resolution) at about 30-32 stations. These measurements will sum up to 4 Bytes X 100 samples/s X 3 X 30 ~36 kByte/s or ~129 MByte/hour. Several options for data transmission were examined with the customary conditions during typical field measurements: no direct internet access, no DSL access, unstable electric power supply etc. Data transmission via satellite was excluded due to high costs, large antennas and high power consumption. Our preferred solution is data transmission over the cell phone network which is nowadays available in all major cities including the provision of high data transfer rates. Cell phone networks provide services such as GSM (up to 2-4 kBit/s upload), EDGE (~200 kBit/s) and UMTS (~1.4 MBit/s), further high speed services (e.g. HSDPA) are currently tested and/or under development. Once the data stream is inside the cell phone network, then the final transmission from the local provider to the GPI-KA is via the internet. At GPI-KA the data will be achieved in a disk array and provided via WebDC (http://geofon.gfz-potsdam.de/geofon/new/web_dc.html).

The available KABBA data loggers are EARTHDATA PR-24 loggers. Four units were upgraded for testing the near-real time data transfer in summer 2008. The data stream for the online data transfer is taken directly from the digitiser; additionally the data are stored on hard disks as backup copy. First tests using EDGE and UMTS for data transmission in and around Karlsruhe were promising. Four sites with completely different conditions were tested during two months: Karlsruhe city (excellent UMTS signal), Karlsruhe periphery (poor EDGE signal), a research facility outside Karlsruhe (EDGE) and a small village in the countryside (EDGE). The overall data return rate was more than 90%. As the only major problem we identified the signal quality or signal strength of the cell phone network at the station sites. The signal strength can also vary in time due to operation by the provider. Low signal strength causes time delays for single data packages which in turn delay the whole data

transfer. During the KIMNET experiment other ways of data transfer will be tested as part of the effort to enhance urban seismology.

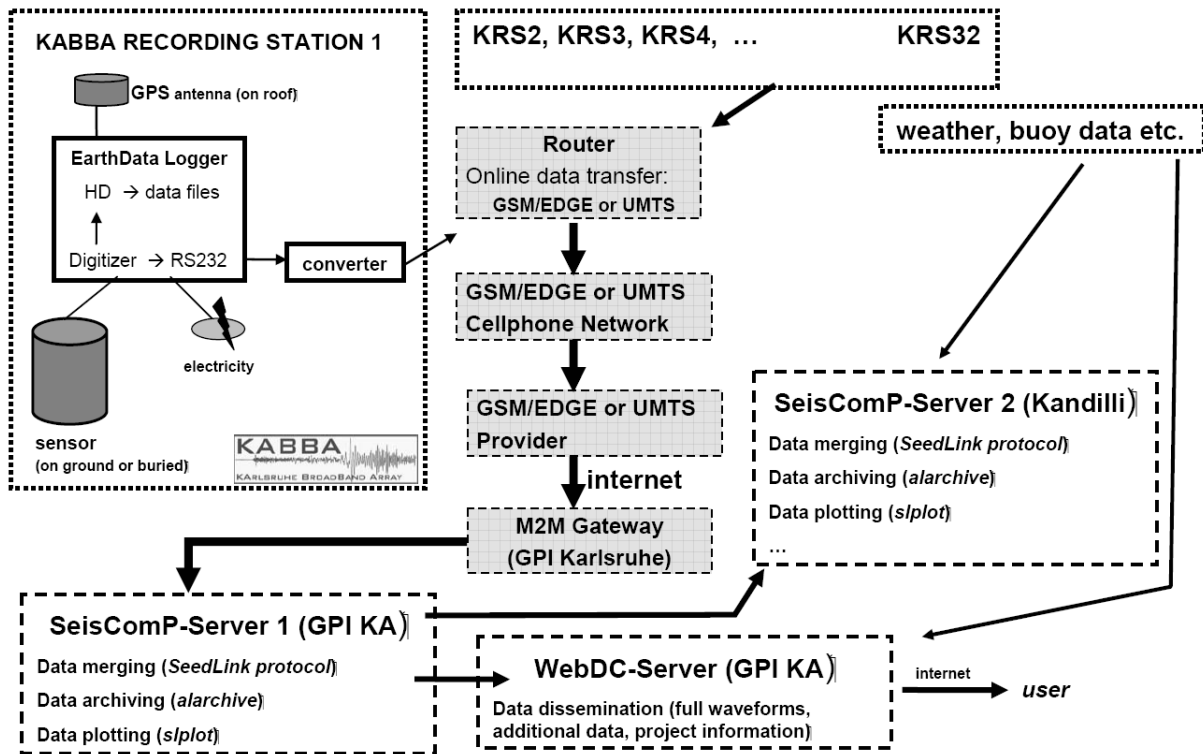


Fig. 1: Planned design of the KIMNET experiment (status Sept. 2008; subject to further changes). The seismological broadband recording stations KRS1-KRS32 will transmit the data via the cell phone network and internet to Karlsruhe. Other environmental data (weather, traffic etc.) will be added. Data dissemination is done via the WebDC tool.

12. Test Installation of the Self-Organising Seismic Early Warning Information Network in the Ataköy District, Istanbul, Turkey.

C. Milkereit¹, M. Picozzi¹, I. Veit¹, K.-H. Jäckel¹, K. Fleming¹, J. Zschau¹, F. Kühnlenz², B. Lichtblau², J. Nachtigall², J.-P. Redlich², J. Fischer², C. Zulfikar³, and M. Erdik³

¹Helmholtz Centre Potsdam GFZ German Research Centre for Geosciences, Section 2.1 "Earthquake Risk and Early Warning", Telegrafenberg, D-14473, Potsdam, Germany

²Humboldt Universität zu Berlin, Department of Computer Science, Rudower Chaussee 25, 12489 Berlin, Germany

³Boğaziçi Üniversitesi, Kandilli Rasathanesi ve Deprem Araştırma Enstitüsü, Department of Earthquake Engineering, 34684, Çengelköy, Istanbul, Turkey

Abstract

As part of its commitment to the EDIM and SAFER projects, GFZ is engaged in the development of the Self-Organising Seismic Early Warning Information Network (SOSEWIN). SOSEWIN is a new concept in earthquake early warning systems, employing advances in sensor, communications and computing technologies to develop low-cost sensing units that will form dense seismic networks linked by ad-hoc wireless communications. These networks will eventually possess a self-organising character, allowing them to adapt to changing circumstances. Currently, a prototype of the sensing unit has been developed by GFZ, with experimental clusters established in Potsdam and Berlin, and a test network in the Ataköy district of Istanbul. The next steps will involve incorporating the seismological processing and alarm protocols into the units.

Introduction

Rapid urbanisation, the interconnection of economies and growing dependence on technology makes modern society increasingly vulnerable to natural disasters. This is particularly true when considering so-called mega cities (defined by the United Nations as metropolitan areas with populations exceeding 10 million), the majority of which are in the developing world. A number of mega cities face serious threats from earthquakes, for example Mexico City, Jakarta, Tokyo, Cairo and Istanbul, the latter being the target city of the EDIM (Earthquake Disaster Information, Marmara Sea) project, as well as one of the test sites for the SAFER (Seismic eArly warning For EuRope) project.

Several cities already have some form of earthquake early warning system (EWS) either in operation or under development. Traditionally, an EWS consists of relatively small numbers of high quality sensors linked to centralised processing facilities. For example, Istanbul hosts the Istanbul Earthquake Rapid Response and Early Warning System (IERREWS, Erdik et al., 2003), made up of 100 strong-motion stations in dial-up mode extending across the more densely populated parts of the city for rapid response purposes, and 10 on-line stations located close to the Marmara Sea segments of the North Anatolian Fault for early warning, with the central processing facility at the Kandilli Observatory and Earthquake Research Institute (KOERI).

In contrast to such a system, the EWS being developed as part of the GFZ German Research Centre for Geosciences (GFZ) contribution to the EDIM and SAFER projects, in collaboration with the Department of Informatics, Humboldt Universität zu Berlin (HUB) and KOERI, termed the Self-Organising Seismic Early Warning Information Network (SOSEWIN), is characterised by the following features:

- Each seismological sensing unit or Sensing Node (SN) is made up of low-cost "off-the-shelf" components. Each unit at present costs several hundred Euros, in contrast to

1,000's to 10,000's for standard seismological stations, allowing denser networks numbering 100's to 1000's over areas served currently by the order of 10's of standard stations;

- The SNs will undertake their own seismological data processing, preliminary analysis and archiving, and will contribute to the different levels of alarming;
- The aim eventually will be for the SOSEWIN to be a decentralised, self-organising ad-hoc wireless mesh network (WMN), whose self-organising capability will allow it to adapt continuously to changing circumstances, e.g. the addition or removal of nodes, interference in communications due to local (and possibly time-varying) phenomena, loss of sections of the network, individual nodes malfunctioning etc..
- Communications will be based on wireless local area network (WLAN) protocols.

The development of the SOSEWIN focuses on two points. The first is the design of the SNs themselves, which is mainly the responsibility of GFZ, while the second is its self-organising character and which is largely being undertaken by HUB. As we are using low-cost components, the sensitivity expected from the SNs will be much lower than that from standard instruments. However, since this is an EEWs, we are only concerned with larger, potentially damaging events, as well as concentrating on urban areas, which are in any case seismically noisier environments.

The fundamental organisational unit of the SOSEWIN is the cluster, which is a group of SNs that are headed by a Leading Node (LN), to whom each SN within its cluster communicates (Figure 1). Which SN belongs to which cluster, and which node serves as the LN, will be defined by a clustering algorithm where the main constraint is to maintain the optimal communications capability, meaning each SN is able to communicate with its LN in the fastest way (e.g. minimizing the number of steps, or K-hops, from node to node) with the least interference and data loss, and likewise for the LN to communicate with its neighbouring LN. One constraint that has been decided upon is that a SN within a cluster is at the most 2 K-hops from its LN.

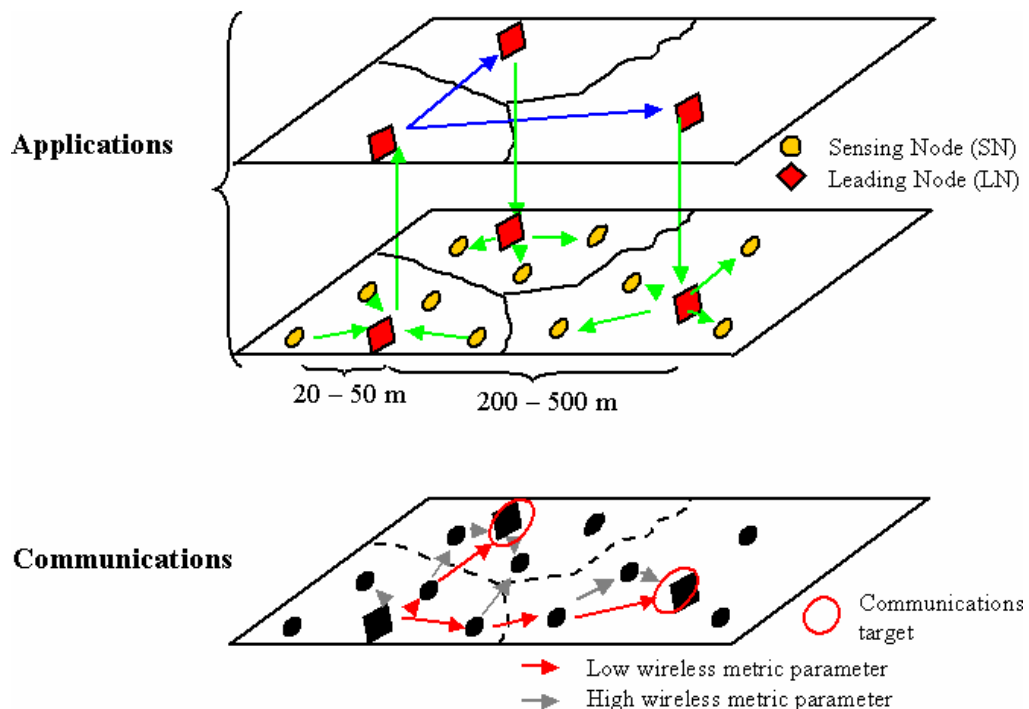


Fig.1: Layout of the Self Organising Seismic Early Warning Information Network based on groups of Sensing Nodes (yellow) which form clusters with a Leading Node. The Leading Nodes (red) decide on the detection validity and classification of seismic events.

The general arrangement of the SOSEWIN is characterized by a two-level architecture consisting of a lower *communications layer* and an upper *applications layer*. Both layers may in turn, as the number of nodes increases, be structured into additional sub layers, for example a "Leader of Leading Nodes" layer may need to be defined. The communications layer, where the clustering organisation will operate, offers peer-to-peer communications between the nodes. The distances involved, as currently planned and realised in Istanbul, are of the order of 50 to 300 m between neighbouring SNs, potentially leading to separations of 200 to 1500 m between neighbouring LNs (given the 2 K-hop constraint). While geometrical/seismological constraints (shape and areal extension of each cluster, number of SNs within a cluster, etc.) will also be used as organisational criteria, they are secondary to optimising the communications. The lower sub layer of the applications layer regulates the activities of the SNs within their clusters, based on criteria specified for the cluster as a whole (e.g. the number of SNs that lead to a group alarm) and the individual SNs (e.g. event trigger thresholds). The higher sub layer is the critical layer in terms of distributing alarms among LNs and issuing them to end users, which again requires the use of the most efficient communications routing protocols.

Sensing Unit

The main components of the SN are described by Figure 2 and consist the sensors, the digitizer board, and the WRAP (wireless router applications platform) computer board. As mentioned, all components are bought off-the-shelf, with the exception of the digitizer board's Analogue-Digital Converter (ADC) which has been developed within GFZ. The sensors incorporated into the SN include 3 accelerometers arranged to provide three component (X, Y and Z) data, and an additional sensor to measure an environmental parameter, such as noise, temperature, water pressure etc.. The accelerometers are based on MEMS (Micro Electro Mechanical Systems), originally designed to serve as controllers for air bag safety units, but have also been successfully deployed in seismic networks (e.g. Holland, 2003), as well as for field acquisition by the exploration sector (Hons et al., 2008). The units used in the SNs have a measurement range of +/- 1.7 g, with a bandwidth of 25 Hz and noise of 0.5 mg, adequate for our EEW purposes.

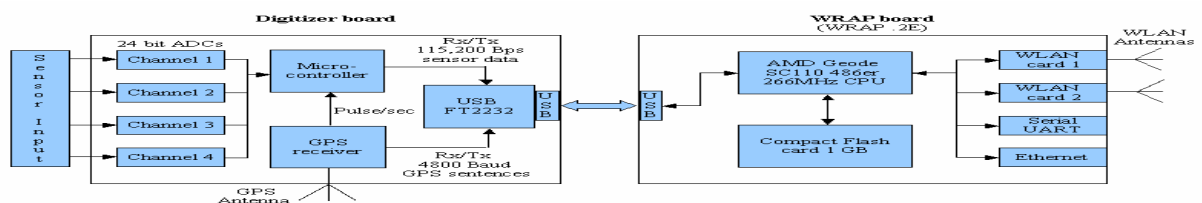


Fig. 2: Schematic overview of the architecture of the prototype Sensing Node.

The prototype digitizer board consists of four ADC that sample the 3-component accelerometers and environmental sensor, a GPS unit that provides time and geographical coordinates, and a USB interface. The ADC has a resolution of 24 bits (effectively 19 bits), with sampling variable between 50 to 400 samples per second (sps), although for the time being 100 sps is being used. The USB chip combines the readings from the ADC units and the GPS device and sends them in two streams (one for the sensor data, one for the GPS) to the WRAP board. While ideally all SNs should have GPS, some may not be able to use it, for example a SN installed in a basement. This brings up the sometimes incompatible requirement for good coupling between the sensor and the ground for accurate ground motion measurements, and access to clear communications. Hence, there will be procedures where a SN without GPS timing will be able to synchronise itself with one that does.

The WRAP board is an embedded PC produced by PC Engines and is in effect a 486er embedded PC with a 266 MHz CPU, the operating system being Linux OPENWRT. It has one access point for a CompactFlash card which acts as the hard disk (currently 1 GB in size, but easily increased), and two positions for WLAN (2.5 or 5GHz) Mini PCI cards. In addition, it has a power supply plug, a serial port and 100 MBit/s Ethernet, while power may also be supplied using PoE (Power over Ethernet).

Seismological processing and alert protocols

The seismological processing and alert protocols have yet to be incorporated into the SNs currently deployed, but this will occur in the near future. Nonetheless, simulations to test different methodologies are being carried out, using both real and synthetic data. Since one of the limiting criteria of the SOSEWIN's development is the use of lower-cost components, there is a need to employ relatively simple, rapid and robust methods suitable for real-time processing.

The first step involves filtering the accelerometer data from the ADC using a 4th order band-pass (0.075 to 25 Hz) Butterworth filter (e.g. Wu and Kanamori, 2005) to be followed by its integration to velocity and displacement using the recursive formulation of Kanamori et al. (1999). The event detection (P-wave trigger) algorithm is the STA/LTA method, which relies on finding the ratio between the average recorded absolute ground motion over a short time period (STA) and that for a longer time period (LTA), resulting in the STA/LTA or signal-to-noise ratio (SNR), making use of the recursive formulation of NORSAR (Schweitzer et al., 2002; Trnkoczy, 2002). A SN is thus triggered when the SNR exceeds some threshold value, which must be defined for each station due to local conditions. For the P-wave detection, we use the vertical component, as this has been found from other tests to give the most reliable results. Once the P-wave arrivals are detected, the LTA value is frozen and remains so until the event is considered over. This will be when the energy, expressed as the integral of the squared velocity (Kanamori et al., 1999) and determined for a defined time interval (e.g. 1 second), has decreased to 5% of the peak value.

The general scheme of the alerting and alarm process consists of four levels.

1. Idle, where "all is well", i.e. sufficiently severe ground shaking has not been detected.
2. SN alert, where a sensor (or the LN) has detected strong enough ground shaking.
3. Group alert, where within a given cluster, $\geq 50\%$ of the SNs have triggered.
4. System alert, where ≥ 3 LNs have verified that an event has occurred, with a network-wide alert now issued.

These stages may be described in greater detail by the so-called state machines of the SNs and LNs (Figure 3), which summarise the various stages each unit will pass through during an earthquake. The SN state machine (Figure 3a) describes the seismological activities of the SOSEWIN, while the state machine of the LN (Figure 3b) outlines the decision making/alert issuing actions.

The various states of the SN (Figure 3a) may be summarised as follows:

- State SN0 is the default or *monitoring state*, with no severe ground shaking being detected and continuous processing of the accelerometric data undertaken.
- State SN1 is the *event detection state* (arrow A). It communicates this to its LN (arrow B). Event characterisation (CAV, Arias, predominant period, energy, S-wave detection) now begins. If after a certain time (the *expiring alert time*, dependent upon SN spacing) $< 50\%$ of the SN in this cluster trigger, the LN informs the SN to return to state SN0 (arrows C and D).
- State SN2 is the *seismic event characterisation state*. It reaches this state after SN1 (arrow E) or directly from its default state if directed to do so by its LN (arrow F). Although event characterisation started in SN1, the situation is such that in SN1,

"something **may** have happened", while here, "something **has** happened".

- State SN3 is the *disaster management state*, and is a sub-state of LN0. It reaches this state after the event is considered over (arrow G). Activities such as the creation of peak ground motion files appropriate for the ShakeMap tool (Wald et al., 2006) are now undertaken.

For the LN (Figure 3b), what needs first to be emphasised is that it is still a SN, and, therefore, includes itself in all seismological activities. Its state machine therefore consists of the following:

- LN0 is the default or monitoring state where the LN monitors the health of the SNs within its cluster, the only communications being with its SNs and the neighbouring LNs.
- State LN1 (arrow A) is the *pre-alert state* or *sensor alarm state*, when a SN communicates to the LN that it (or the LN itself) has been triggered. From this point on the cluster cannot be reorganised. Again, if after the expiring alert time fewer than 50% of the SN within a cluster are triggered, the LN informs the triggered SNs that they are to return to their SN0 state and the LN itself returns to LN0 (arrow B), with the previous trigger noted as a false alarm.
- State LN2 (arrow C) is the *group alarm state* (i.e. $\geq 50\%$ of the SN within a cluster have triggered within the expiring alert time). The LN informs its neighbouring LNs (arrow D) that an event has possibly been detected. These LN are then in state LN1, and inform their SN. However, if after a certain time no other LN indicate that an event has occurred, all LNs return to LN0 (arrow E) and the event noted as a false alarm.
- State LN3 (arrow F) is the *alert state* or *system alarm* i.e. 2 or more of the nearest LNs indicate that an event has been detected, that is they have also reached state LN2 (arrow G). At this point, an alert is issued throughout the network.
- State LN4 (arrow H) is the *disaster management state* when the event is finished and an "all clear" issued. The network is checked, and, if necessary, reorganisation undertaken.

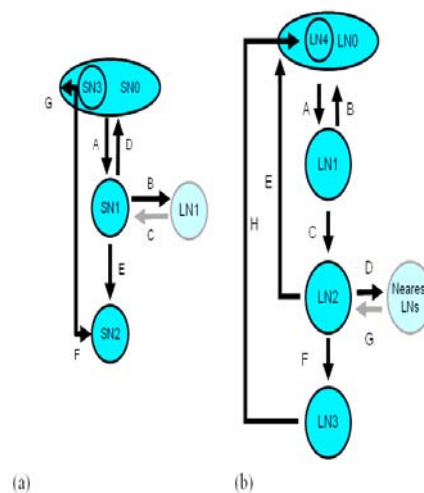


Fig. 3: The state machines of the (a) Sensing Node and (b) Leading Node (see the text for an explanation of the various states).

The Ataköy network.

The test network in the Ataköy district of Istanbul (Figure 4) consists of 20 SNs, two of which serve as DSL Gateways (provided by Turkish Telecom). The stations have been established on the roofs of residential blocks, as example of which is shown in Figure 5, as well as the SN's recording of a smaller seismic event that occurred some 140 km from Istanbul. The ground motion is monitored continuously and all data are transferred in near real-time (several seconds delay) via the Gateways to a server at GFZ operating the SeisComp. SeisComp (Seismological Communication Processor) is a new concept for a networked seismographic data collection and analysis system, originally developed for the GEOFON network of the GFZ and further extended within German-Indonesian Tsunami Early Warning (GITEWS) system. It allows the online data acquisition, data recording, monitoring and controlling, real-time communication, as well as third party user access and automatic real-time data processing (quality control, event detection and location). In this way, data are received from the Ataköy network with a 1 or 2 second delay and are immediately further distributed to the project partners through the internet. While most of the SNs are powered by the mains power supply provided by the apartment block, some (4) are only powered by solar panels, although all SNs are equipped with a buffer battery in the event of power interruption or poor weather.

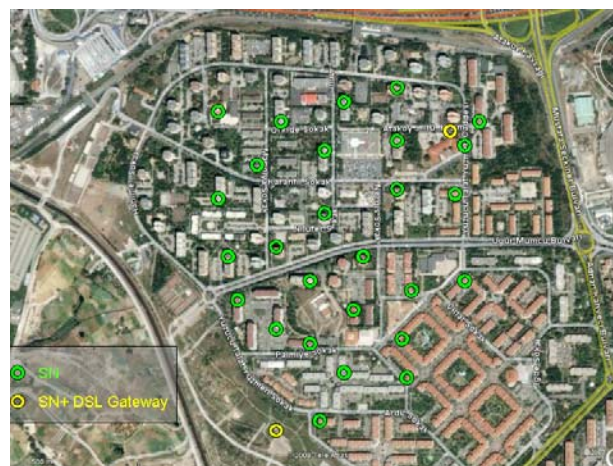


Fig. 4: The test SOSEWIN in the Ataköy district of Istanbul. One of the reasons for choosing this district is the presence of one of the high-quality stations of the IERREWS. This will allow a comparison between the results obtained using this network and the strong motion station.

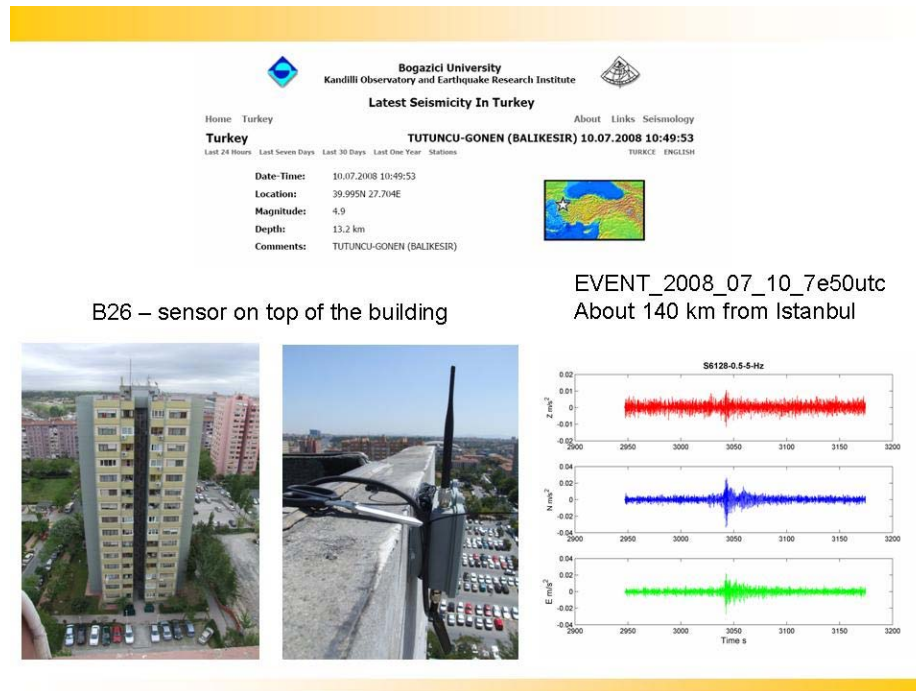


Fig. 5: Example of a SN deployed as part of the test network in the Ataköy district, Istanbul. Also shown are the recordings of a small event that occurred around 140 km from Istanbul.

Next stages

As mentioned, the seismological processing and alerting protocols will soon be incorporated into the SNs currently deployed. At this point, the actual self-organising character has not been fully developed, hence a "half-way" measure will be followed where a given SN will be allotted the role of LNs.

The next generation of SN is already being considered. Of particular interest are more recent MEMS that offer greater sensitivity, the extension of the digitizing board to 8 channels instead of the current 6, and the incorporation of larger, better quality CompactFlash cards.

References

- Erdik, M., Y. Fahjan, O. Ozel, O. Alcik, A. Mert, and M. Gul (2003). Istanbul earthquake rapid response and the early warning system. *Bull. Earth. Eng.* **1**, 157-163.
- Holland, A. (2003). Earthquake data recorded by the MEMS accelerometer. *Seism. Res. Lett.* **74**(1), 20-26.
- Hons, M., R. Stewart, D. Lawton, and M. Bertram (2008). Field data comparisons of MEMS accelerometers and analog geophones. *The Leading Edge*, July 2008, 896-902.
- Kanamori, H., P. Maechling, and E. Hauksson (1999). Continuous monitoring of ground-motion parameters. *Bull. Seism. Soc. Am.* **89**(1), 331-316.
- Schweitzer, J., J. Fyen, and S. Mykkeltveit (2002). Seismic Arrays. *IASPEI New Manual of Seismological Practice*, ed. P. Bormann, GeoForschungsZentrum Potsdam, Vol. 1, Chapter 9.
- Trnkoczy, A. (2002). Understanding and parameter setting of STL/LTA trigger algorithm, *IASPEI New Manual of Seismological Practice*, ed. P. Bormann, GeoForschungsZentrum Potsdam, Vol. 2, IS 8.1.
- Wald, D. J., B. C. Worden, V. Quitoriano, and K. L. Pankow (2006). ShakeMap Manual; Technical Manual, Users Guide, And Software Guide; <http://pubs.usgs.gov/tm/2005/12A01/pdf/508TM12-A1.pdf>
- Wu, Y.-M., and H. Kanamori (2005). Experiment on an onsite early warning method for the Taiwan early warning system. *Bull. Seism. Soc. Am.* **95**(1), 347--353.

13. Realities of and Expectations from the Compulsory Earthquake Insurance

Arzu Taylan¹

¹City and Regional Planning Department, Middle East Technical University, Ankara, Turkey.

1. Introduction

In Turkey, The legal-institutional regulations and interventions concerning natural disaster management have been limited with the ‘post-hoc’ interventions and policies for a long period. The nature of such interventions are described in the Disaster Law (No. 7269). The ‘fatalist’ attitude that only focused on post-disaster activities, however, prevented to take necessary measures that can decrease and compensate the loss of lives and physical damages both of which are the result of vulnerable building stock and urban environment (Balamir 1999; 2001). The losses caused by earthquakes, on the other hand, increased the economic burdens of the country, and slowed down its development. The way to retreat from ‘fatalist’ society and to transform into a ‘resilient’ society, however, depends on the solution of two fundamental problems: ‘*to provoke the direction of investments into risk mitigation*’ and ‘*to compensate the earthquake losses*’. The Compulsory Earthquake Insurance (CEI) as a public-private institution is, in fact, involved with both of these aims due to its use of insurance techniques. However, there is developed any strategy or policy to facilitate the opportunities of CEI in the mitigation of risks in the housing stock, although it will ameliorate the efficiency of CEI, in turn. A strategy, which will decrease the losses and provide financial compensation, requires the legal and institutional regulation of the process. This strategy also requires understanding the role, opportunities and limits of actors, and their decision making in this process. This paper intends to evaluate the current system of CEI in terms of the threats to CEI and the failures rising from its working process. Through the institutional evaluation of CEI, the paper attempts to find out the possible solutions with a range of policy alternatives. Further, the policy options are to be evaluated in terms of an empirical study, which intends to find out the opinions of insured Homeowners about CEI. The empirical study has been carried out for the doctoral dissertation of the writer under the Supervision of Prof. Dr. Murat Balamir¹ and Co-Supervision of Prof. Dr. Ute Werner^{2,3}.

2. Legal and Institutional System of CEI

CEI has been in effect after the 1999 Kocaeli and Düzce Earthquakes and it is a noteworthy step to compensate the financial losses of earthquakes and to decrease the financial burden of homeowners and State. With the implementation of CEI, State aimed to free itself from its responsibility for earthquake loss compensation. Instead, this responsibility is suggested to be transferred to the CEI system, which operates across the country and to the ‘Homeowners’ (Hs) that are liable to purchase this insurance. With its legal source (Decree No. 587), institutional structure as public-private partnership (DASK) and insurance pool (TCIP), where the premiums are accumulated, CEI was envisaged as a ‘state-backed national insurance system’. As a natural disaster insurance that uses insurance techniques, CEI provides opportunities to share, finance and transfer the risks, before earthquakes strike. The insurance premiums that are paid by Hs are accumulated in TCIP. These premiums, in turn,

¹ City and Regional Planning Department, Middle East Technical University, Ankara, Turkey.

² Center for Disaster Management and Risk Reduction Technology (CEDIM), Karlsruhe, Potsdam, Germany.

³ University of Karlsruhe, Institute for Finance, Banking and Insurance, Chair for Insurance Science (LVW), Karlsruhe, Germany

are given back to Hs as compensation of the losses, if their houses are damaged after an earthquake.

Since CEI contributes to the development of the society by decreasing the burden of the State during reconstruction of houses, it can be defined as an ‘investment tool’ that prevents any loss in the rental and use value of the national housing stock due to earthquakes. The accumulation of insurance premiums that are collected across the country are transferred to TCIP and the financial losses of insureds are compensated from this pool. This system makes CEI also a ‘social solidarity’ mechanism. Nevertheless, CEI carries the ‘individual responsibilities’ into ‘social/collective responsibilities’ since it partitions the possibility of capital loss risk among the Hs who are liable to purchase it. CEI, then, pays the indemnification to the persons who faces a loss. Besides, CEI optimizes ‘social justice’ through redistributing the accumulated capital among the insured Hs after earthquakes. However, the working system of CEI is precarious whether it realizes these economic and social benefits due to the threats to its system and the response of CEI to those threats.

3. The Threats of and the Failures of CEI

The threats in natural disaster insurance mainly arise from the difficulties confronted by insurance industry due to increasing economic losses of natural disasters that can cause bankruptcy and insolvency (Beck 1996: 31). The underlying reasons of catastrophic loss risk are involved with basic factors such as the characteristics of natural disaster risk and the capacity and techniques of insurers: First, being low probability-high consequence events, natural disaster risk is difficult to calculate by insurance techniques (Kunreuther 1998). Second, since natural disasters are geographically focused events, one single event can cause high correlation of claims in a single area at the same time (Ganz 1998). Third, occurring infrequent and being produced in urbanization process, they are highly uncertain and ambiguous to estimate. Fourth, information problems such as adverse selection and moral hazard increases the uncertainty of risks (Li 1998), especially in developing countries (Andersen 2005:27). Fifth, the unwillingness for risk mitigation by both insurers (Kunreuther & Slovic 1978) and homeowners (Kunreuther 1998) increases the catastrophic loss risk (Li 1998).

On the other hand, insurers apply some techniques to prevent their catastrophic loss risk such as selection of good risks, not offering coverage in high risk areas and setting high premiums (Kunreuther 1998; Linerooth-Bayer et al. 2003). In turn, when the demand for insurance decreases, people with good risks and high income can afford to insurance premiums. In this situation, insurance can constitute an equitable system and justice in itself. However, this system of insurance may create social inequalities in society due to excluding high risk and low income people (Ericson et al. 2003). Nevertheless, the States continue to offer aid after disasters (Kunreuther 2000). Due to the threats outlined above and due to applying some insurance techniques, when responding these threats, CEI can be inefficient and can cause social inequalities; thereby, endanger social solidarity. To prevent such a failure of CEI, it can be expected to have a high penetration ratio, affordable premiums, a certain form - as voluntary and compulsory with supporting policies- that provide high penetration, to reach everybody in society, and in its efforts in risk assessments and risk mitigation. For this reason, the following section attempts to evaluate CEI’s working system through these factors.

3.1. Low Penetration Ratio: Uncertain Form, Inaffordability?

To reach all legal houses, in fact, CEI is envisaged as ‘compulsory’ and ‘affordable’ with low premiums. However, the current implementation of CEI can not reach all legal housing stock that is evident with the low penetration ratio as nearly 18%.

a. Uncertain Form: Compulsory or Voluntary?

Compulsory: CEI is not compulsory in reality. The only obligation can be accepted as the cease of State from paying the damage losses. However, State-aid for reconstruction continued after the foundation of CEI. Although another obligation can be the requirement of CEI policy during house selling and buying process, these transactions in the housing stock occur rarely. Nevertheless, there is any other control and/or punishment and sanction for un-insured Hs.

Voluntary: Under these conditions, CEI can be said as working as voluntarily, which can also be an alternative method for its working. However, there is any incentive to encourage people to purchase CEI voluntarily and insurance penetration ratio is still low.

b. Determination of Premiums –Affordability?

Risk-Ratio: Current premium determination is made according to risk levels of houses. However, if the lowest income Hs live in high risk areas, they have to pay highest price premiums, although they cannot afford these prices.

Flat-Rate: If all Hs will pay same price for premiums, justice in the payment can be provided. But, in this case, there will be any encouragement or obligation to make high risk homeowners reduce risks.

3.2. Fragmentation of Society: Exclusion?

Legal Housing Stock: Since CEI works with risk-rated premiums in voluntary conditions, it is possible that the lowest income Hs will not purchase CEI policy. Therefore, another high risk level is excluded from insurance protection. If CEI will work as compulsory with punishments, the lowest income Hs will suffer since they can not afford to pay. Whether compulsory or voluntary, CEI does not offer any policy about premium payment and risk reduction for those the low income but high risk Hs.

Illegal Housing Stock: To prevent catastrophic losses and insolvency of its system, CEI attempts to select the risks to insure by excluding high degree risks, i.e. illegal housing stock. Therefore, the most vulnerables – low income levels- are excluded from its system without any opportunity and choice to get the right for financial protection. For this reason, CEI can be criticized for fragmenting the society, creating a new type of injustice and strengthening the existing social differences and inequalities without giving any choice and opportunity.

3.3. Ambiguity and Incalculability of Risks

Despite the selection of risks or excluding the high risks and most vulnerables, the risks in the covered housing stock of CEI are still uncertain due to lack of controls during urbanization process. Whether CEI will be implemented as compulsory or voluntarily, the risks are to be known and to be brought into a certain level. Otherwise, the information asymmetry problems (moral hazard and adverse selection) emerge. Therefore, the insurance pool of CEI is precarious whether it includes the insured houses at an acceptable risk level.

Inaccurate Risk Estimations: CEI does not have capacity to have a sufficient surveillance system to evaluate the risk levels in the housing stock. Although there is implemented risk ratio premiums, it is precarious that these risk estimations are made accurately. The only used materials are earthquake hazard map at the country scale -which ignore the urban scale and urban risks- and building construction type -which does not give any idea about the risk of building-. Besides, CEI has any cooperation with local administrations who can provide accurate information about risks.

Lack of Deductibles: There is any incentive to encourage Hs for informing their risks. At least, there can be envisaged premium deductible mechanisms for less risk houses.

Lack of Risk Mitigation: There is offered any financial or technical incentive by CEI to encourage Hs for mitigating risks.

4. Homeowners' Evaluations of CEI

As being at the centre of governance, insurance institution is also dealt with the 'Hs' who are the main responsables for risk mitigation and insurance purchase. The empirical study has been carried out among the Insured Homeowners (I-Hs) that live in a highly risk zone of Istanbul: Zeytinburnu. According to survey results, 72% of I-Hs noted that insurance system is a form of social solidarity, which provides sharing the earthquake losses by all society (N=125; Mean=3.90)⁴, when. 81% of I-Hhs (N=141) denoted that CEI should work through its Law and complete its legislation process to realize its aims (42% of them disagreed and 13% of them was uncertain). Nevertheless, 48% of I-Hs thought that state should forgone from assisting for housing to un-insured houses (N= 120, Mean=3.38). 62% of I-Hs agreed that housing assistance should be given only to the insured homeowners (N=117, Mean=3.60). 50% of I-Hs thinks that un-insured Hs should be delivered less housing assistance (N=111, Mean=3.16).

4.1. Penetration Ratio

85% of I-Hs thought that everyone must purchase insurance (N=142, Mean=4.32). 73% of I-Hhs agreed that insurance should be thought as a tax for earthquake (N=131, Mean=3.88). Similarly, 87% of I-Hhs denoted that it is not fair that some people purchase insurance (N=132, Mean=4.23). 69 % of I-Hhs designated that they are confused about the reluctance of people for participating to the CEI's system (N=125, Mean=3.87). For %79 of I-Hs 'security feeling provided by insurance' (N=138, Mean=3.42), for 79% of I-Hs 'damage probability of their house' (N=132, Mean=3.33); and for 88% of I-Hs 'being worry about their family' (N=128, Mean=3.30) were the most influential factors in their CEI policy purchase decision.

a. Uncertain Form: Compulsory or Voluntary

Compulsory or Voluntary: 64% of I-Hs (N=118) explored that they bought CEI since they thought that it was compulsory. 51% of insured homeowners (I-Hs) thought that it is necessary to make CEI compulsory to prepare the society against earthquake (N=123, Mean 3.43). 85% of I-Hs noted that nobody will buy insurance if the earthquake insurance is not made compulsory; everybody will expect State aid after an earthquake (N=123, Mean: 4.24). Similarly, 75% of I-Hs explained the reason of why people do not purchase CEI is the expectation State- aid (N=123, Mean=3.91). For 72% of I-Hs the cease of the State from paying for losses (N=3.30, Mean=3.30) and for 64% I-Hs their observation about homeowners as the main responsible for damage losses (N=103, Mean=2.84) were found influential in their CEI purchase decision. 86% of I-Hs thought that people should be encouraged and persuaded to buy insurance voluntarily(N=121, Mean: 4.17). However, only 46% of I-Hs agreed with the statement of 'earthquake insurance should be bought completely voluntarily and it should be a matter of personal choice. No one should be forced to protect him/herself' (N=122, Mean: 3.14).

Effective Punishments: 59% of I-Hs (N=111) explained that the punishment of CEI has no influence on their decisions to purchase CEI. 63% of I-Hs denoted that CEI is not forced by the State so that it does not matter whether it is compulsory or not (N=120, Mean= 3.57), when 81% of I-Hs agreed that the legislation of CEI should be enacted with effective punishments (N=125, Mean=4.07). Similarly, to oblige earthquake insurance, 64% of I-Hs thought that un-insured Hs should be imposed with effective punishments (N=124, Mean= 3.73). However, 62% of I-Hs disagreed with the statement that there should be imprisoning for un-insureds (N=123, Mean=2.38). Similarly, 37% of I-Hs disagreed also with monetary punishment for un-insureds, although 35% of them agreed and 28% is uncertain (Mean=3.06).

⁴ 5 point likert scale

Effective Incentives: Despite, 55 % of I-Hs (N=110) explored that they bought CEI policy since they thought it is necessary for the house buying-selling procedure. Rather than payments in the form of insurance premiums, 65% of I-Hs denoted that premiums of CEI can be reflected to other obligatory payments such as electricity, water, telephone (N=127, Mean=3.71), when 58 % of I-Hs thought that premiums of CEI can be reflected to the property-house tax (N=123, Mean=3.57). On the other hand, 83% of I-Hs agreed that buildings can be certified for their purchase of CEI each year in the case of all homeowners in the buildings are insured (N=128, Mean=4.13). Likely, 91% of I-Hs thought that there should be provided discounts from CEI premiums for the buildings that renew their insurance policy each year (N=129, Mean=4.40). Besides, 89% of I-Hs agreed that housing taxes can be discounted for the buildings that renew their insurance policy each year (N=127, Mean=4.31).

b. Premium Determination and Inclusion through Affordability

76% of I-Hs did not think that only those with high risk should be forced to buy earthquake insurance (N= 121, Mean=2.21), when 88% of I-Hs agreed that everyone including people with low risk should purchase earthquake insurance (N=136, Mean=4.31). 60% of I-Hs agreed with CEI premiums should differ according to risk levels (N=124, Mean=3.73), while 53% of I-Hs thought that CEI premiums should be equal for everyone (N=125, Mean=3.42). With respect to income inequalities, 70% of I-Hs did not agree that earthquake insurance should only be compulsory for the high and moderate income homeowners (N=118, Mean= 2.38). On the other hand, although 55% of I-Hs did not think that Hh's in illegal and unlicensed houses have low income (N=123, Mean=2.76), 60% of I-Hs evaluated risk-rated premiums as not favor for low income Hs (N=121, Mean=3.55). Similarly, 54% of I-Hs found it unfair if low income Hh's under high risk pay all premium (N=125, Mean=3.49). For this reason, 59% of I-Hs thought that there should be set low premiums for low income Hh's (N=130, Mean=3.58). In the same way, 77% of I-Hs thinks that State should provide insurance support to low income Hh's (N=130, Mean=4.01).

4.2. Inclusion of Illegal Housing Stock

58% of I-Hs thought that the buildings without license should also be included to CEI (N=130, Mean=3.64). In addition, 59% of I-Hs denoted that the premiums of illegal and unlicensed buildings can/should be higher to be included in CEI (N=124, Mean=3.64). Similarly, 43% of I-Hs said that there should be given less housing assistance for homeowners of illegal houses (N=111, Mean=3.07). Nevertheless, 43% of I-Hs thought that illegal houses should not deliver any housing assistance (N=107, Mean=3.33). In the same way, 31% of I-Hs disagreed and 31% of them agreed that everyone including owners of illegal houses should be given housing assistance (N= 115, Mean=2.61).

4.3. Reducing the Risks and their Uncertainty

91% of I-Hs thought that CEI should offer discounts in insurance premiums for the retrofitted buildings (N=128, Mean=4.35). Similarly, 91 % of I-Hs thought CEI should certify robust-retrofitted buildings to encourage risk mitigation (N=119, Mean=4.43). In addition, 96% of I-Hs expected technical assistance for retrofitting from municipality to the buildings that renew their insurance policies each year (N=129, Mean=119). In the same way, 87% of I-Hs expected priority to get credits from banks or State for retrofitting the buildings, which renew their insurance policies each year (N=127, Mean=4.35).

5. Conclusion

The major threats such as catastrophic loss and insolvency arises from high levels of risks and their incalculability by CEI in housing stock. The ambiguity of risks is also strengthened through moral hazard and adverse selection. On the other hand, CEI attempts to solve its problems and threats as if it works only as a financial system under market forces by ignoring its social tasks. Instead of attempting to solve its problems with social sensitivity, CEI accepts the fallibility of its system against the uncertain risks in the housing stock. Therefore, CEI reduces the uncertainty of its system by transferring a substantial amount of the accumulated premiums, i.e. nations' wealth, into the global reinsurance markets. However, this attempt to work efficiently by governing the risks itself causes to criticize CEI by endangering social solidarity. On the other hand, CEI has other opportunities to deal with these risks without destroying its social dimensions. According to the evaluations of I-Hs, CEI should work as a social solidarity mechanism. In fact, the catastrophe loss risk can be decreased, when the insurance penetration ratio can be increased. In the same way, CEI is expected by I-Hs to reach everybody including Hs from all income levels and all risk levels by making it really compulsory. Although Hs do not preferred punishments, what they denoted and expected was the increase of incentives to make everybody insured. To make nobody suffer, Hs explored that CEI can take premiums through other compulsory payments such as electricity and water or real-estate taxes. However, what the Hs strongly expected was incentives such as discounted premiums or discounted real-estate taxes.

In addition, to make low income Hs insured, CEI is expected to create a solidarity mechanism that offers low premiums or State support. In fact, CEI is at the core of governance of natural disaster risks with its 'public-private' partnership and its opportunities arise from insurance techniques. Fulfilling its social duties and working efficiently only depends on its governance with other institutions as 'urban planning' and 'local administrations' in the framework of 'natural disaster risk management' (Balamir 2004). Although insurance cannot directly be involved in development and change of built environment, the use of insurance techniques provides CEI to be a financial incentive during risk mitigation. In this way, CEI can include all housing stock in terms of: 1- converting the uncertain risks into calculable risks; 2- offering coinsurance and deductibles mechanism based on risk levels. On behalf of the uncertainty of risks, Hs are willingness to inform their risks to CEI if there are offered premium deductibles, certifications and also technical and financial assistance for risk mitigation in their buildings. Through its cooperation with other institutions, therefore, CEI can be used to provide risk mitigation opportunities in both legal and illegal housing stock. Indeed, I-Hs did not prefer illegal houses to be included to CEI under the same conditions with themselves or legal houses. They preferred them to be treated at least one level below the legal houses. However, people with high risk level or illegal houses can gain the opportunity to have financial protection in earthquakes. Therefore, social justice, solidarity and responsibility can be increased in society.

References

- Andersen, T. J. (2005). Applications of Risk Financing Techniques to Manage Economic Exposures to Natural Hazards. Sustainable Development Department, Technical Papers Series, Inter-American Development Bank, Washington, D.C.
- Balamir, M. (2004). The Current Developments and the Expectations in the Earthquake Issues (Deprem Konusunda Güncel Gelişmeler ve Beklentiler). *Planning Journal* **27**, 15-23.
- Balamir, M. (2001) . Disaster Policies and Social Organisation. Unpublished paper presented at the *Disasters and Social Crisis sessions of the European Sociological Association Conference*, Helsinki 27 August-3 September, Finland.
- Balamir, M. (1999). Reproducing the Fatalist Society: An Evaluation of the Disasters and Development Laws and Regulations in Turkey. In E. Komut (ed.) *Urban Settlements and Natural Disasters*, International Union of Architects and Chamber of Architects of Turkey, 96-107.

- Beck, U. (1996). Risk Society and the Provident State. In S. Lash, B. Szerszynski, B. Wynne, B. (Eds.), *Risk, Environment and Modernity: Towards a New Ecology*. London; Thousand Oaks, California: Sage Publications.
- Ericson, R. V.; A. Doyle, and D. Barry (2003). *Insurance as Governance*. Toronto; Buffalo: University of Toronto Press.
- Ganz, S. (1998). Public Policy Options and Earthquake Insurance. Paper represented in Western Earthquake Insurance Summit presented by Western States Seismic Policy Council, www.wsspc.org.
- Kunreuther, H. (2000). Insurance As Cornerstone For Public-Private Sector Partnerships. *Natural Hazards Review*, **1**(2).
- Kunreuther, H. (1998). Insurance as an Integrating Policy Tool for Disaster Management: The Role of Public-Private Partnerships, paper represented in Western Earthquake Insurance Summit presented by Western States Seismic Policy Council, www.wsspc.org.
- Kunreuther, H. and P. Slovic (1978). Economics, Psychology and Protective Behavior. *Psychology and Economics*, **68**(2).
- Li, W. (1998). Hazard Insurance and Mitigation Measures For Natural Hazards, paper represented in Western Earthquake Insurance Summit presented by Western States Seismic Policy Council, www.wsspc.org.
- Linerooth-Bayer, J., M. J. M. Field, R. Verheyen and K. Compton (2003). Insurance-Related Actions and Risk Assessment in the Context of the Background paper for UNFCCC workshops.

14. Effects of the Marmara Earthquake of 1999 on Micro and Small Businesses

C. Menny¹, and U. Werner¹

¹Institute for Finance, Banking and Insurance, Universität Karlsruhe (TH), Kronenstr. 34, 76133, Karlsruhe, Germany

Approaches for loss estimation

Different reports about the same natural disaster often show an astounding difference in the estimations of overall losses. For the Northridge earthquake, for example, the estimation of total losses reaches from 25 billion US\$ up to 49.3 billion US\$ (Petak, 2001, p. 5). These differences give a hint that the mechanisms, which cause losses and recovery after a disaster, are not yet very well understood. The hardest problem in loss estimation is the assessment of indirect losses. These are losses arising from other reasons than direct physical damages, like infrastructure failure or failure of suppliers. Research in this field can be divided in two main categories: models and empirical studies. Methods for modeling are linear programming, Input-Output (IO) models (Boisvert, 1992; Gordon et al., 1996; Cho, 2001) and computable general equilibrium models (CGE) (Rose and Guha, 2004). Empirical research is done with surveys (Kroll et al., 1990; Tierney et al., 2000; Alesch et al., 2001; Webb et al., 2003) and with econometric models (Rossi et al., 1978; Ellson et al., 1984; Terrell and Bilbo 2007).

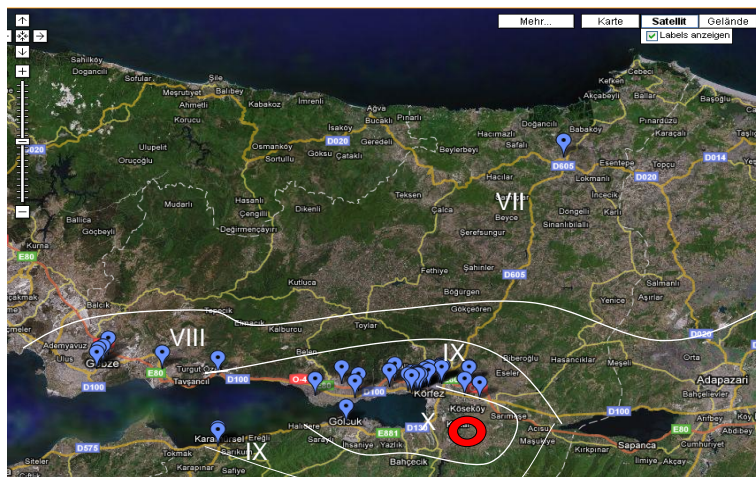
The main problem with **modeling** seems to be that the model methodologies were originally not intended to simulate the effects of massive shocks. IO-models are very rigid to price changes and to processes of input substitution. Moreover, the models have an inherent equilibrium constraint, which forces the clearance of the market, regardless of the severity of the disaster impacts, which is rather unrealistic (Rose and Guha, 2004, p. 124). Some of the disadvantages mentioned can be overcome by CGE models. They are nonlinear and can respond to price changes while incorporating the substitution of inputs and supply side constraints. The main problem of CGE models is, however, that they are mostly intended for long-run equilibrium analysis. When applied to short-run analysis, the flexibility of the models will therefore overestimate the adaptation potential of the economic system and as an effect the results will underestimate the real losses from a disaster (Okuyama, 2007, p. 117). A problem with all the modeling approaches mentioned is that the failure of output and demand is simulated without taking into account the multitude of possible reasons for a failure. Some modeling approaches try to master this shortcoming by modeling the failure and recovery of certain aspects that might have a strong effect on the economy, like certain infrastructures. Models exist for the failure of the transportation system (Gordon et al., 2004; Boarnet, 1998; Cho, 2001), the failure of electricity (Rose et al., 1997), and the failure of water supply (Rose and Liao, 2005). Nevertheless, a real disaster will normally not only cause multiple infrastructure failures, but a range of other effects influencing and hampering economic processes.

Another problem is the validation of the models. Only one case could be found, where **empirical data** on the effect of electricity failure was compared to the results of a model (Rose and Lim, 2005, p. 10). To analyze disasters with econometric models has its shortcomings as well. Econometric models and statistics do not distinguish between direct and indirect losses, thus concealing the various effects and their repercussions on each other. As a result, the total economic consequences of a disaster as expressed by economic indicators often seem to lie within the historically observed economic variability of the region, at least for industrialized countries (Okuyama, 2007, p. 118). We, therefore, fully agree with Okuyama who stated: "While these extensions of the conventional economic

models shed some light on the temporal feature of disaster impacts, the modeling scheme is still considered somewhat ad hoc, since no definitive theories have been established for their application to the idiosyncrasy of conventional models” (Okuyama, 2007, p. 119). To develop such a theory and to understand the factors which cause business failures, disruptions, losses, as well as the recovery process, an in-depth analysis of affected businesses is necessary. This has to be done by empirical research. Only a limited number of surveys on businesses after disasters were conducted in the past. Examples include research done in California after the Loma Prieta earthquake in 1989 (Kroll et al., 1990; Webb et al., 2003) and the Northridge earthquake in 1994 (Alesch et al., 2001), after floods in Iowa in 1993, and after Hurricane Andrew in Florida in 1992 (Tierney et al., 2000). All the surveyed events have occurred in the US. The events caused fatalities and massive losses of several billion US Dollars. Nevertheless they were not critical for the economy. Their rather small overall economic impact can be measured, e.g., by the losses to GDP ratio. For the Northridge earthquake this was 0,6%⁵. Results for the Marmara earthquake are expected to be quite different, amounting to more than 5 % of the losses to GDP-ratio⁶, and with effects different from the US. Since the effects of a devastating event on micro and small businesses have not been studied yet, a survey was conducted in the Marmara region in December 2007. One of the guiding hypotheses was that micro businesses have different reaction patterns than small and medium-sized businesses. The findings of the survey can thereby shed a light on questions not dealt with so far.

Survey of micro and small businesses in the Marmara region

For analyzing the effects of a disastrous earthquake on micro and small businesses and their reaction patterns, 203 business-owners were interviewed. A basic condition for being included in the survey was that the business owner was running a business in August 1999, at the time of the Marmara earthquake. Another criterion was the size of the business as measured by the number of employees at the time of the event. 166 of the businesses had up



(Miksát, J; Wenzel, F; Sokolov, V. 2005, p. 867, Google earth)

to 9 employees, 37 of them had more than 9 employees in 1999. Furthermore the surveyed businesses roughly reflected the sectoral dispersion in the Turkish economy (Ozar 2006, p. 31). To achieve a regional representation of the 1999 earthquake, more than 50% of the interviews were conducted in the center of Kocaeli, in Izmit.

The blue marks on the map indicate the sites of the interviews given. The red circle

is located near the epicenter of the earthquake. The white roman numbers within the boundaries of the seven Kocaeli regions show the intensity of the earthquake on the modified Mercalli scale.

In the interviews several questions were asked about:

- business characteristics,

⁵ 49.3 billion US Dollars of losses / 7,775.5 billion US Dollars GDP in 1994

⁶ 13 billion US Dollar of losses / 245 billion US Dollar GDP in 1999

- damages,
- business disruptions, losses and repair costs,
- reasons for business disruptions and recovery,
- methods and sources of refinancing,
- observations about other businesses in the respective city district.

First results: Direct and indirect losses, causes and consequences

Losses reported

68% of the interviewed business owners reported damages on their business from the earthquake:

42% suffered light damages, 17% suffered moderate and 10% suffered heavy damages.

41% of all interviewed businesses were **out of business** for some time. Most of them (82%) could reopen within 1 month and 18% were out of business for up to 1 year.

66% of all businesses suffered **disruptions** of their operations. Most of them (76%) recovered within 3 months, 24% of them had disruptions for up to one year. The resulting losses from

Median of losses from building damage, interior damage and business disruptions (in US Dollar)			
	Median losses from building damages	Median losses from interior damages	Median losses from business failure and disruptions
Losses per enterprise	600	2.250	3.000
Losses per person (+owner)	500	500	1.500

business failures and disruptions clearly exceeded the losses from physical damages.

Causes identified

An analysis of variance (ANOVA) of the **overall losses** was conducted with 3 factors:

1. Damages to the business building and interior (representing direct damages).
2. The region where the business

building was located (representing the hazard).

3. The number of disturbances, which affected the business (representing exposure).

The disturbances considered comprised: The failure of infrastructure, the failure of suppliers, the inability of employees to come to work, financial problems, the loss of important data, and a lack of demand.

The model can explain 44% of the variance of overall business losses (corrected $R^2=44.3$).

Another ANOVA was conducted for losses occurring only from **business disruptions**. Here the explaining variables were:

1. The damage to the business building,
2. a lack of demand,
3. the regional location of the business and
4. the business sector.

Hotels and restaurants had the lowest disruption losses, together with businesses in the construction sector. This model can explain 42% of the variance of disruption losses (corrected $R^2 =42.1$).

Factors influencing recovery

To explain the variance of the **failure-and-disruption-time** of the analyzed businesses another ANOVA-model was developed. Here the most important explanatory factors were the

1. damages to business buildings and interior,
2. the region where the business was located and
3. the catchment area of the businesses.

Businesses with customers not only from the close neighborhoods, but from other regions of

Turkey, had a significantly shorter disruption time. These variables explain 33% of the variance of the dependent variable, failure-and-disruption-time (corrected $R^2=33,1$).

The recovery time for the businesses was much shorter than the time it took for the demand to reach the pre-disaster levels in the different city districts. Obviously, the lack of customer's demand was a problem for many entrepreneurs (51%). Some business owners reported that it took up to two years until the business activity was back to normal in their district. The financial crisis in 2001 exacerbated the situation for many entrepreneurs. Surprisingly, 59% of them claimed that the financial crisis was the worst crisis for their business since its foundation. Only 24% said so about the earthquake.

It was estimated by the business owners that about 20% of the businesses in their neighborhood never reopened after the incident and that 17% of businesses had to close within the two years following the event. These numbers are far lower than the numbers given in several brochures and books about business continuity planning. There it is often claimed that 40% of businesses never reopen and, furthermore, that 25% are being closed within the two years following a disaster (Doughty, 2000, p. XI; D'Amico, 2004, p. 176; US_Congress 28.02.2007, p. 2). Thus, more research is needed to determine the crucial factors influencing recovery: is it the size of a business that matters or other characteristics of the local economic context?

References

- Alesch, D. J., J. N. Holly, E. Mittler, and R. Nagy (2001). Organizations at risk: What happens when small businesses and not-for-profits encounter natural disasters. Public Entity Risk Institute.
- Boarnet, M. G. (1998). Business losses, transportation damage, and the Northridge earthquake. *Journal of Transportation and Statistics* **1**(2), 49–63.
- Boisvert, R. (1992). Indirect losses from a catastrophic earthquake and local, regional and national interest. *National Research Council (Publ.). The Economic Consequences of a Catastrophic Earthquake*. Nat. Academy Press Publications, 207–265.
- Cho, S. (2001). Integrating transportation network and regional economic models to estimate the costs of a large urban earthquake. *Journal of Regional Science* **41**(1), 39–65.
- D'Amico, V. (2004). Ten steps for surviving a disaster!. *Handbook of Business Strategy 2004* **5**(1), 173–178.
- Doughty, K. (Publ.) (2000). Business Continuity Planning - Protecting your Organization's Life: Auerbach Publications.
- Ellson, R. W., J. W. Milliman, and R. Blaine-Roberts (1984). Measuring the Regional Economic Effects of Earthquakes and Earthquake Predictions. *Journal of Regional Science* **24**(4), 559–579.
- Gordon, P., J. E. Moore, H. W. Richardson, M. Shinozuka, and D. An (2004). Earthquake disaster mitigation for urban transportation systems. An integrated methodology that builds on the Kobe and Northridge experiences. *Modeling spatial and economic impacts of disasters*, Okuyama, Y., Chang, S. E. (Eds.), 205–232.
- Gordon, P., H. W. Richardson, B. Davis, C. Steins, and A. Vasishth (1996). The Business Interruption Effects of the Northridge Earthquake. *Lusk Center Research Institute*, University of Southern California, Los Angeles, CA. Los Angeles.
- Kroll, C., J. Landis, Q. Shen, and S. Stryker (1990). The Economic Impacts of the Loma Prieta Earthquake. A Focus on Small Business. *Berkeley Planning Journal* **5**(5), 39–58.
- Miksat, J, F. Wenzel, and V. Sokolov (2005). Low Free-Field Accelerations of the 1999 Kocaeli Earthquake?. *Pure Applied Geophysics* **162**, 857-874
- Okuyama, Y. (2007). Economic modeling for disaster impact analysis. Past, present, and future. *Economic Systems Research* **19**(2), S. 115–124.
- Ozar, S. (2006). Micro And Small Enterprises. In *Turkey: Uneasy Development. ERF Research Report*, Research Report Series No.: 0420. Bogazici University. Istanbul.
- Petak, W. J. (2001). The Northridge earthquake, USA and its economic and social impacts. *EuroConference on Global Change and Catastrophe Risk Management, Earthquake Risks in Europe*, IIASA, Laxenburg Austria, July 6-9, 2000.
- Rose, A., and S. Liao (2005). Modeling Regional Economic Resilience to Disasters: A Computable General Equilibrium Analysis of Water Service Disruptions. *Journal of Regional Science* **45**(1), 75–112.

- Rose, A., and D. Lim (2005). Business interruption losses from natural hazards. Conceptual and methodological issues in the case of the Northridge earthquake. *Environmental Hazards* 4, 1–14.
- Rose, A., and G. S. Guha (2004). Computable general equilibrium modeling of electric utility lifeline losses from earthquakes. *Modeling spatial and economic impacts of disasters*, Okuyama, Y., Chang, S.E. (Eds.), 119–141.
- Rose, A., J. Benavides, S. Chang, P. Szczesniak, and D. Lim (1997). The regional economic impact of an earthquake. Direct and indirect effects of electricity lifeline disruptions. *Journal of Regional Science* 37(3), 437–458.
- Rossi, P.H., J. D. Wright, S. R. Wright, and E. Weber-Burdin (1978). Are There Long-Term Effects of American Natural Disasters? Estimations of Effects of Floods, Hurricanes and Tornados Occuring 1960 to 1970 on US Counties and Census Tracts in 1970. *Mass Emergencies* 3, 117–132.
- Terrell, D., and R. Bilbo (2007). A Report on the Impact of Hurricanes Katrina and Rita on Louisiana Businesses. *Louisiana Recovery Authority, Louisiana Economic Development, and the Louisiana Department of Labor*.
- Tierney, K., J. Dalhammer, and G. Webb (2000). Businesses and Disasters. Empirical Patterns And Unanswered Questions. *Natural Hazards Review* 1(2), 83–90.
- US_Congress (28.2.2007). Gulf Coast Back to Business Act of 2007. H.R. 1243 IH. 1st Session. (110th CONGRESS). Online "<http://www.govtrack.us/data/us/bills.text/110/h/h1243.pdf>".
- Webb, G., K. Tierney, and J. Dalhammer (2003). Predicting long-term business recovery from disasters: A comparison of the Loma Prieta Earthquake and Hurricane Andrew. Preliminary Paper #328. *Disaster Research Center - University of Delaware*.

15. Economic Assessment of Indirect Earthquake Losses on the Macro and Micro Scale

D. Borst^{1,2}, R. Mechler^{3,2}, and U. Werner^{1,2}

¹Center for Disaster Management and Risk Reduction Technology (CEDIM), Karlsruhe, Potsdam, Germany

²Institute for Finance, Banking and Insurance, Chair for Insurance Science (LVW), University of Karlsruhe, Karlsruhe, Germany

³International Institute for Applied Systems Analysis (IIASA), Laxenburg, Austria

Introduction

Disasters cause losses to vulnerable communities and societies. In order to reduce these losses, an effective disaster risk management is needed, of which risk analysis is the first step (cf. Thieken et al., forthcoming). Disaster risk comprises adverse effects spanning economic, social and environmental impacts which are linked to each other in manifold ways. Therefore, informing decision makers at best integrates facts and figures from all the three fields (cf. EMA Emergency Management Australia, 2002, p. 3). In terms of the economy, disasters cause direct losses, i.e. physical destruction to built-environment and networks, which then lead to interruptions of economic activities of production and consumption. Losses from business interruptions are often called the indirect effects of a disaster (cf. Okuyama, 2007, p. 115).

Several studies on loss estimation have been undertaken within the last two decades in different parts of the world. Still, the conceptualization of losses is complicated, and indirect losses are not as readily apparent as property damage (cf. Rose, 2004, p.31). Therefore, it is not surprising that for Istanbul no comprehensive application of one of the existing methodologies on indirect losses has been carried out, despite the remarkable general research efforts against the background of the high probability of a severe earthquake to be expected in close distance of this mega-city.

Filling this gap for Istanbul, the present paper describes two approaches suitable to cope with indirect losses: On the micro scale, a production theory-based framework has been developed for modelling business disruptions due to losses of input factors. The following section describes the model developed for the textile sector as a key sector of the city economy. Section 3 deals with a macro-economic view on loss assessment, before the last section provides some concluding remarks.

Micro-Economic Framework of Indirect Loss Estimation

According to the traditional theory of production in business administration, the flow of production output of a business measured as the quantity of output Q is produced by combining various input factors such as labour, materials and machines (cf., e.g., Gutenberg, 1951). Normally, inputs are commonly available and can be employed according to market conditions in a profit-maximizing manner. In contrast, after a disaster, production factors are supposed to be damaged and markets disrupted. The so called Leontief production function with the following equation meets the modelling requirements for this kind of situation:

$$Q = \text{Min} ((a_1/A), \dots, (a_n/Z)) \quad (1)$$

This means that the least available input factor a_i determines the overall output of production, whereas any additional usage of other factors would be wasted without generating any further output.

The availability of a certain input factor depends on the disaster impacts on stock and flow variables which are shown in a System Dynamics depiction for the general case of labour in the following figure 1:

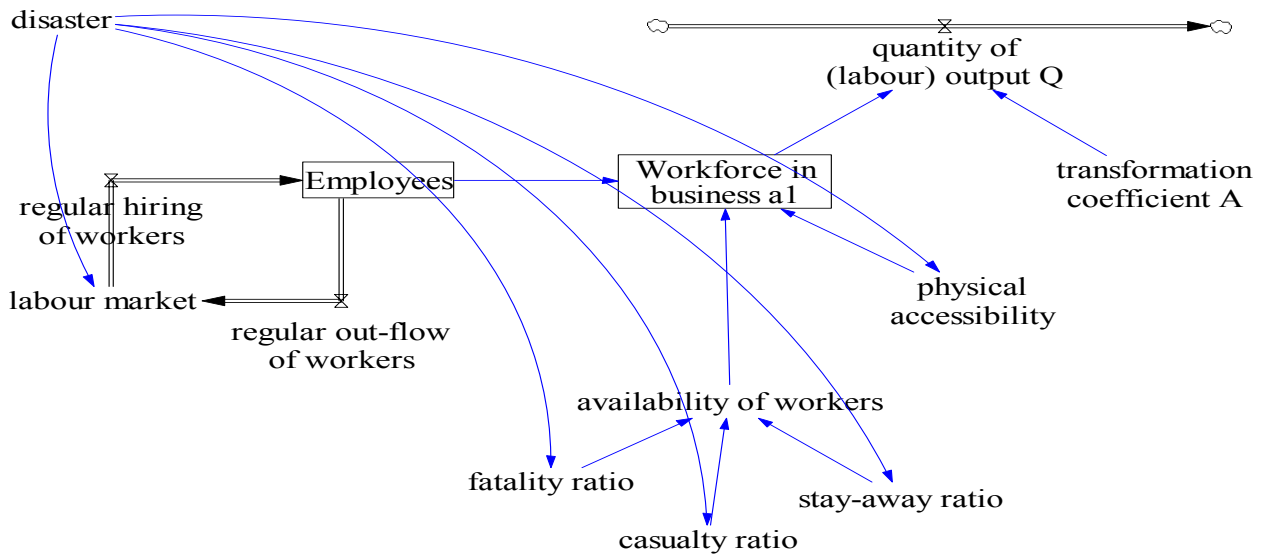


Fig. 1: Disaster impacts for the input factor of labour.

Detailed considerations have been undertaken for textile businesses because of the key importance of this branch as biggest employment sector in manufacturing and its major share of national exports. Parameter values for the variables and their functional relations were derived from historical empirical studies on business disruptions and losses after disasters (e.g., Tierney, 1994) in combination with direct loss estimates from engineering studies for a scenario earthquake in Istanbul (e.g., ARC-BU, 2002) as well as from statistical information (e.g., SIS, n.d.) and own expert assumptions. The calculations are executed in the System Dynamics software environment Vensim©, which provides the capabilities of both a time-dependent simulation of the effects and an explicit handling of uncertainties by the means of scenarios for variables with only very inaccurate data on-hand. The following figure 2 illustrates the functioning of the time-dependent simulation for the variables of the production factor labour:

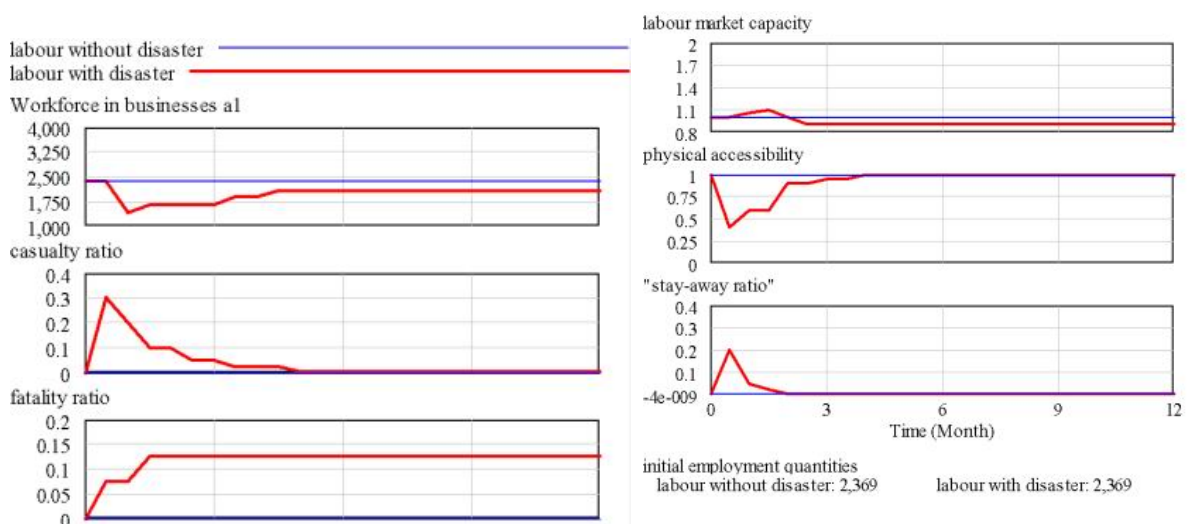


Fig. 2: Variables of production factor labour compared to the levels without disaster

The reduced availability of the labour workforce for the production of a business is stemming from the combined impact of mainly health and accessibility problems. Other important drivers of reduced production outputs within the textile branch are infrastructure disruptions which lead to a reduced availability of the materials production factor. Comprehensive results

for the city economy can be gained by repeated execution of the methodology for further sectors of high socio-economic importance or by using macro-economic knowledge on inter-industry relationships between different branches.

Macro-Economic Assessment

The IIASA CATSIM model was used for the macroeconomic analysis. CATSIM is an economic growth model and employs stochastic simulation utilizing the Monte-Carlo method to generate random catastrophe shocks to a national or state-level economy. A major purpose of CATSIM is to support public authorities to better consider disaster effects in budget and economic planning and account for *contingent liabilities* when allocating budgetary resources.

Input data for the Monte-Carlo simulation are loss-frequency distribution curves representing the probability of disaster losses on infrastructure, machinery and other assets in aggregated format. Risk as represented by these stochastic shocks is modeled as a function of the natural hazards, the elements exposed and the vulnerability of the exposed elements. CATSIM outputs are economic consequences as projections of economic growth, fiscal effects or a country's external debt situation considering the possibility of disaster events occurring; for example, CATSIM can provide an estimate of disaster effects on economic variables such as the national or regional government's budget and economic value added measured by GDP. It can also be used in *scenario* mode to study impacts of selected events, such as the scenario event of magnitude 7.5 (ARC-BU, 2002) projected to occur with high probability in the Marmara sea over the next years. In the following we focus on the stochastic modeling for the aggregate Turkish economy.

We used CATSIM to simulate fiscal and macroeconomic consequences of disasters for the whole Turkish economy and the Istanbul province. Figures 3a, b show selection of trajectories for macroeconomic and fiscal impacts in Turkey. 100 selected trajectories for GDP and the government's budget for a time horizon over the next 10 years are outlined here (out of a total of 5,000 simulated trajectories).

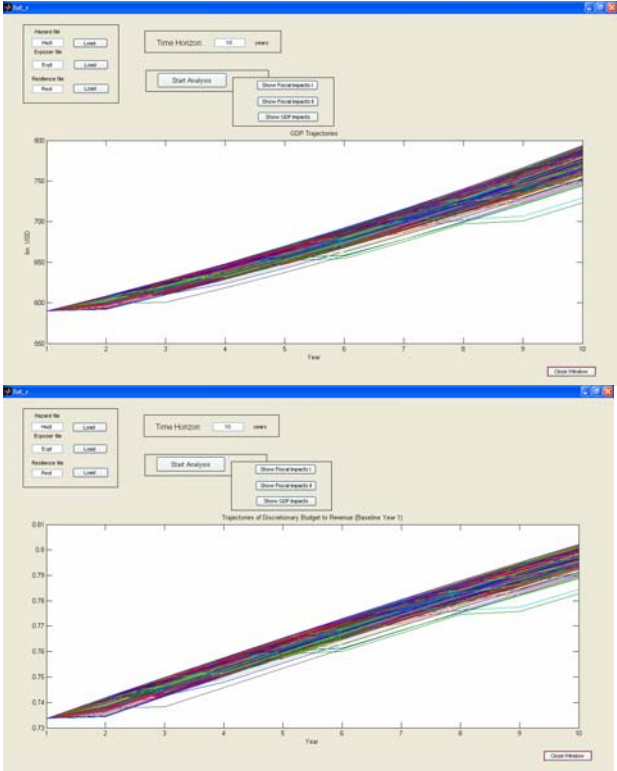


Fig. 3a, b: Selected CATSIM trajectories of macroeconomic and fiscal impacts under disaster risk in Turkey

Macroeconomic performance may be affected by disasters as they destroy assets, impair economic performance and necessitate government budget spending on relief and reconstruction (shown on the left). Without disaster events occurring, the economy would be growing over time up from ca. 600 billion USD to about 800 billion USD as expected and hoped for. However, in a number of cases disasters cause a loss of assets and income. Given the economic resilience of the economy, these events put the economy on a lower trajectory. In some cases, there is a dramatic decrease in economic activity. The graph on the right shows that while on average, budget flexibility should increase (in terms of available financial resources not committed, e.g., to debt repayment, compared to overall budget), there is some potential for disasters seriously affecting the budget.

The occurrence of such trajectories is stochastic and depends on the probability distribution of the financial losses. These trajectories do not have equal probability: the cases with economic growth proceeding as planned (the trajectories in the upper part) have a higher probability than the catastrophic cases at the bottom. Such an assessment illustrates the worst outcomes compared to the planned business-as-usual cases of economic development. Uncertainty concerning input data and assumptions such as on economic growth over the next 10 years is considerable. Furthermore, stakeholder preferences may differ substantially. Acknowledging this, CATSIM has been designed to allow potential users such as from the finance ministry or provincial authorities to get actively involved in the assessment and change input data, modify assumptions or study key variables of their choice via its graphical user interface. Given such an assessment, one application of the modeling may be to assess the potential annual relief and reconstruction requirements given disaster risk, and potentially set money aside in a government relief fund or organize insurance for public sector liabilities. A number of disaster-exposed countries have started doing so, and, for example, CATSIM informed policy development in Mexico, which resulted in the reinsurance of public sector liabilities for earthquake risk in 2006.

Conclusions

Complementing the existing loss estimations regarding direct economic effects of a scenario earthquake near Istanbul, within this project indirect effects have been studied using both a micro and a macro-economic approach of assessment. The new methodology of micro assessment uses in detail information on the availability of production factors to estimate the extent of indirect losses of potentially vulnerable branches which can then be put into the focus of mitigation measures. Though, its comprehensive assessment for all the sectors of the city economy must be considered very resource-intensive.

The simulations of the macro assessment have documented a wide range of potential trajectories of future governmental budgets. Although uncertainty is high and there exist trade-offs between different objectives, the tool can help decision-makers at the national and provincial level to quantify the financial needs for coping with the outcomes of a major disaster and to timely set up financial countermeasures.

Altogether, the two approaches broaden the basis for an improved decision-making by extending the view on the vulnerability and risk of the city of Istanbul by adding another dimension to the existing scope of loss assessments.

Acknowledgement

This work is part of the joined IMM-KOERI project “Earthquake Risk and Risk Development in the Megacity Istanbul” with the Center for Disaster Management and Risk Reduction Technology (CEDIM), a joint venture between the Helmholtz Centre Potsdam GFZ German Research Centre for Geosciences and the Karlsruhe Institute for Technology (KIT - the

Cooperation of Forschungszentrum Karlsruhe GmbH and Universität Karlsruhe (TH)). We thank GFZ and KIT for financial support.

References

- American Red Cross and Bogaziçi University (ARC-BU) (eds.) (2002). Earthquake Risk Assessment for Istanbul Metropolitan Area, Istanbul, Turkey.
- Emergency Management Australia (EMA) (ed.) (2002). Disaster Loss Assessment Guidelines – Manual 27, Dickson, Australia. Download <http://ema.ausinfo.gov.au/Media?id=1742> [09-29-2008].
- Gutenberg, E. (1951). Fundamentals of Business Administration – Vol 1: Production (in German), Berlin, Germany.
- Okuyama, Y. (2007). Economic Modelling for Disaster Impact Analysis – Past, Present, and Future. *Economic Systems Research* 19/2, pp. 115-124, June 2007.
- Okuyama, Y., and S. E. Chang (eds.) (2004). Modeling Spatial and Economic Impacts of Disasters, Berlin, Germany.
- Rose, A. (2004). Economic Principles, Issues, and Research Priorities in Hazard Loss Estimation. In *Modeling Spatial and Economic Impacts of Disasters*, Okuyama, Y., Chang, S. E. (eds.), 13-36.
- State Institute of Statistics (SIS) (ed.) (n.d.). Annual Manufacturing Industry Statistics 2001, Ankara, Turkey.
- Thieken, A. H., D. Borst, B. Guse, G. Grünthal, P. Heneka, T. Hofherr, H. Kreibich, S. M. Murshed, K. Poser, S. Tyagunov, and F. Wenzel (forthcoming). A Comparative Risk Assessment of Natural Hazards on the Regional Scale.
- Tierney, K. J. (1994). Business Vulnerability and Disruption: Data from the 1993 Midwest Floods (Draft), Paper presented at the *41st North American Meetings of the Regional Science Association International*, Niagara Falls, Ontario, November 16-20, 1994. Download <http://dspace.udel.edu:8080/dspace/bitstream/19716/596/1/PP213.pdf> [10-03-2008].